The Messenger

No. 165 – September 2016

Telescope time allocation and gender
SEPIA installed at APEX
APEX Galactic Plane surveys
Conference report “Discs in Galaxies”

Gender Systematics in Telescope Time Allocation at ESO

Ferdinando Patat[1]

[1] ESO

The results of a comprehensive statistical analysis of gender systematics in the time allocation process at ESO are presented. The sample on which the study is based includes more than 13 000 Normal and Short proposals, submitted by about 3000 principal investigators (PI) over eight years. The genders of PIs, and of the panel members of the Observing Programmes Committee (OPC), were used, together with their career level, to analyse the grade distributions and the proposal success rates. Proposals submitted by female PIs show a significantly lower probability of being allocated time. The proposal success rates (defined as number of top ranked runs over requested runs) are 16.0 ± 0.6 % and 22.0 ± 0.4 % for females and males, respectively. To a significant extent the disparity is related to different input distributions in terms of career level. The seniority of male PIs is significantly higher than that of female PIs, with only 34 % of the female PIs being professionally employed astronomers (compared to 53 % for male PIs). A small, but statistically significant, gender-dependent behaviour is measured for the OPC referees: both genders show the same systematics, but they are larger for males than females. The PI female/male fraction is very close to 30/70; although far from parity, the fraction is higher than that observed, for instance, among IAU membership.

The ESO 2020 prioritisation exercise (Primas et al., 2015) spawned a number of actions. Among them was the constitution of a Time Allocation Working Group (TAWG), which has been tasked with the review of the whole telescope time allocation process at ESO. The TAWG, chaired by the author of this article, will submit a set of recommendations to the Director for Science, to be presented to the ESO Scientific Technical Committee in October 2016. The activities of the TAWG included a wide range of statistical studies on time requests, proposal grading and possible trends in the allocation process. The results will be presented in a separate report, while this article focuses solely on the gender aspect.

Obtaining telescope time at world-leading facilities is fundamental for the well-being of an astronomer's scientific activity. Therefore, systematics in the time allocation process can have negative consequences on the career of a researcher. The present study was carried out along the lines traced by Reid (2014), who conducted a similar analysis for the Hubble Space Telescope (HST) proposal selection process. The main purpose is the quantification of gender dependent systematics and subsequent considerations in the wider context of possible correlations between the final merit attributed to a proposal and aspects that are scientifically irrelevant.

The ESO proposal review process

The proposal review process currently deployed at ESO is described in detail in Patat & Hussain (2013). Here only a brief summary will be provided. The review is performed in two steps, before and during the Observing Programmes Committee (OPC) meeting, indicated as pre- and post-OPC.

During the pre-OPC phase the proposals assigned to a given panel are read and graded by all non-conflicted panel members. Each panel is composed of six referees. The grade scale is between 1 (best) and 5 (worst), where a grade larger than 3 will not be considered for scheduling. The pre-OPC grade is entered into the database independently and secretly by each panel member. Every proposal is assigned a primary referee, who will present the case during the panel discussion and be in charge of editing the comment sent to the principal investigator (PI). No special weight is attributed to the primary referee's grade. A proposal may contain one or more runs, which are graded separately by the reviewers. The final grade of a run is computed as the average of the grades given by all non-conflicted panel members. In order to account for systematic differences between the various referees, before computing the final average the grade distributions of the reviewers are normalised to have the same average and standard deviation.

Once the pre-OPC grading is complete, the Observing Programmes Office (OPO) compiles ranked lists per telescope and applies triage, removing the bottom 30 % (by observing time). With very few exceptions (at the discretion of the panels), triaged proposals are not discussed during the OPC meeting and their fate is fully dictated by the pre-OPC grades. The surviving proposals are discussed by all non-conflicted panel members during the OPC meeting and graded (again secretly). Unlike in the pre-OPC phase, the post-OPC grades are logged anonymously in the database (meaning that the referee's identity is lost). Once all panels have completed their activities, the ranked lists per telescope are computed by OPO using the average run grade, after normalising the grade distributions of the panels to have the same average and standard deviation.

The ranked lists are finally used to schedule the various telescopes. On account of the different oversubscription rates and different demands in terms of right ascension and observing conditions, two runs having the same OPC grade may end up having different allocation outcomes.

For any given telescope, the rank class A is assigned to the top 50 % (by time) of the Service Mode (SM) runs that were allocated time, while the remaining runs are assigned to rank B. The grade at which the A/B transition occurs changes from telescope to telescope, depending on the demands and the exact time distribution of allocated runs. No priority rank is assigned to Visitor Mode (VM) runs, whose observations, once scheduled, are conducted in any case, barring adverse weather conditions. As the grading takes place by run, the statistics presented in this study refer to runs and not to proposals.

Characteristics of the proposal dataset

The data on which this study is based were extracted from the ESO proposal

database. The sample includes only Normal and Short proposals. Large Programmes, Calibration Programmes and Surveys were not included because they are not graded by the panels. Guaranteed Time Observations (GTO), Target of Opportunity (TOO) and Monitoring proposals were also excluded because of their special nature, which would introduce systematic effects in the statistics. Normal and Short programmes account for more than 85 % of the runs requested every semester.

The database contains pre- and post-OPC proposal gradings starting from Period P79 (April 2007–September 2007). However, the data are properly and consistently stored only from P82 (October 2008–March 2009). For this reason, the analysis presented here covers ESO Periods 82 to 97 (April 2016–September 2016), inclusive. This eight-year interval can be considered representative of regular operations, with the Very Large Telescope (VLT) and Very Large Telescope Interferometer (VLTI) in full activity and with practically every telescope focus occupied by an instrument. In addition, during the above period the ESO User Portal (UP) was fully functional, so that PI information could be retrieved in a consistent, homogeneous and complete way.

In Periods 82 and 83, the OPC included 12 panels. An extra panel was added to category A (Cosmology) in P84. From P84 onwards, the OPC had a stable composition of 13 panels, with six members each. The panel members serve for typically two semesters, although in order to maintain some memory, a fair number of them are asked to stay for an extra semester. The OPC-proper members (i.e., panel chairs and members-at-large) normally serve for four semesters. The full dataset includes 22 022 runs (13 420 proposals) submitted by 3017 distinct PIs (about 4.4 proposals per PI, at an average rate of ~ 840 proposals per semester). About 65 % of the proposals include one single run, while ~ 85 % of the proposals have fewer than three runs. The runs were reviewed by 527 distinct referees, who assigned 123 358 pre-OPC grades and 100 558 post-OPC grades. On average, each proposal was reviewed by 5.6 referees, with about 95 % of the proposals reviewed by 5 or 6 referees.

Career level and gender of proposers and referees

All UP subscribers can set their career level, choosing from one of the following options: Professional astronomer (hereafter AP), Teacher/Educator/Journalist, Post-doc in astronomy (PD), Student (ST), Amateur astronomer, Non-astronomer scientist, or Other. It is important to note that, like other information stored in the UP, this does not necessarily reflect the actual status at the time of proposal review or submission, and represents a snapshot relative to the last UP profile update. Therefore, there can be cases in which a user created the account when she/he was a student and then never updated the profile, although she/he may now be a post-doc or even a professional astronomer. In the extreme scenario in which no users update their career level after the creation of their UP account (for PIs most likely when they submitted their first proposal), one expects that the fractions of ST and PD scientists are overestimated, while that of AP is underestimated.

This effect would produce time trends, with the fraction of AP PIs steadily decreasing with time, which is actually what is seen in the data. This needs to be kept in mind when considering the accuracy of the results related to the career level. For our purposes, only AP, PD and ST levels are relevant, as they account for 99.0 % of PIs; the remaining categories were ignored. The overall fractions of PIs in the three classes are: 47.4 % (AP), 33.9 % (PD) and 18.7 % (ST). By construction, the OPC panel composition is heavily dominated by professional astronomers (87.7 %), while the small remaining portion is constituted by post-docs (12.3 %).

The referee and PI genders are not stored in the UP. For this reason, the gender had to be deduced through personal knowledge, from the first name in email addresses and through web search, similar to what was done by Reid (2014). For the 527 distinct referees, there is confidence that the gender classification is exact for all entries. For the ~ 3000 distinct PI classifications, the confidence level is estimated to be better than 99 %. The gender could not be determined for five PIs, who were excluded from the analysis. The final set of PIs belonging to one of the three career levels AP, PD or ST, for which gender information is available, includes 2990 scientists, who submitted 13 330 proposals.

The distributions per career level and gender are summarised in Table 1 for referees (top), PIs (middle) and submitted proposals (bottom); for proposals, career level and gender refer only to the PI. The first aspect worth noting is that the overall

Table 1. Distribution of referees (upper), PIs (middle) and proposals (lower) by career level and gender.

Referees

Career level	All		F			M			Balance	
	N	%	N	% of all	% of F	N	% of all	% of M	F	M
Astronomer	462	87.7	129	24.5	83.2	333	63.2	89.5	27.9	72.1
Post-doc	65	12.3	26	4.9	16.8	39	7.4	10.5	40.0	60.0
All	527		155	29.4		372	70.6			

Principal Investigators

Career level	All		F			M			Balance	
	N	%	N	% of all	% of F	N	% of all	% of M	F	M
Astronomer	1418	47.4	1294	9.8	33.9	1124	37.6	52.9	20.7	79.3
Post-doc	1013	33.9	366	12.2	42.3	647	21.6	30.5	36.1	63.9
Student	559	18.7	206	6.9	23.8	353	11.8	16.6	36.9	63.1
All	2990		866	29.0		2124	71.0			

Proposals

Career level	All		F			M			Balance	
	N	%	N	% of all	% of F	N	% of all	% of M	F	M
Astronomer	7516	56.4	1377	10.3	41.2	6139	46.1	61.5	18.3	81.7
Post-doc	4595	34.5	1522	11.4	45.5	3073	23.1	30.8	33.1	66.9
Student	1219	9.1	446	3.3	13.3	773	5.8	7.7	36.6	63.4
All	13 330		3345	25.1		9985	74.9			

female (F) and male (M) fractions are close to 30/70 in both the referees and the PIs division. The observed differences are within the expected Poisson uncertainties, so that the F/M proportion in the panels can be considered identical to that of the PI community. Of course, the gender fraction in the PI sample does not necessarily reflect that of the overall astronomical community, as there may be selection effects relating to gender when it comes to choosing the leader of a proposal. The magnitude of these effects could be estimated by computing the ratio by gender between the number of PIs and total applicants. This analysis, which may reveal an additional selection bias at source, is not possible at the moment as the gender of the proposal co-investigators is not available.

The second aspect, which is very important for the purposes of this analysis, is the diversity of the career level fraction by gender. In general, both for the referees and the PIs, the average professional astronomer seniority level is higher for male scientists. This difference is particularly marked for PIs, for which the number of professional astronomers is 19 % larger for M than for F applicants (see Table 1). Since, at least to some extent, the quality of a proposal is expected to grow with the PI's career level[1], it is to be expected that the depletion of professional astronomers as female PIs turns into a lower success rate. This will be discussed in more detail below. As a by-product of this analysis, one can also look at the evolution of the PI gender balance as a function of professional career level (see Table 1, last two columns). While there is no statistically significant evolution between the ST and PD levels (with a F/M balance ~ 36/64), a clear jump is seen in the AP level (~ 21/79). If the PI community appears already to be unbalanced from the career start, the situation clearly degrades in the last stage. The lack of a finer level resolution (both within the PD and the AP classes) does not allow any more refinement in the study of the career trajectory by gender.

The diversity seen in the PIs is reflected in the distribution of submitted proposals by gender and career level (Table 1, lower). The numbers are similar, but all differences tend to become more pronounced when considering the proposals. For instance, the overall gender fraction is 25/75 (*vs.* 29/71), and the AP gender fraction is 18/82 (*vs.* 21/79). In addition, the male career level distribution becomes more top-heavy (61.5 % of the proposals are submitted by senior astronomers) than for female PIs (41.2 %). The fraction of proposals submitted by female professional astronomers (41.2 %) is comparable to that of post-docs (45.5 %), while for male PIs, the AP fraction (61.5 %) is about a factor of two more than the PD fraction (30.8 %).

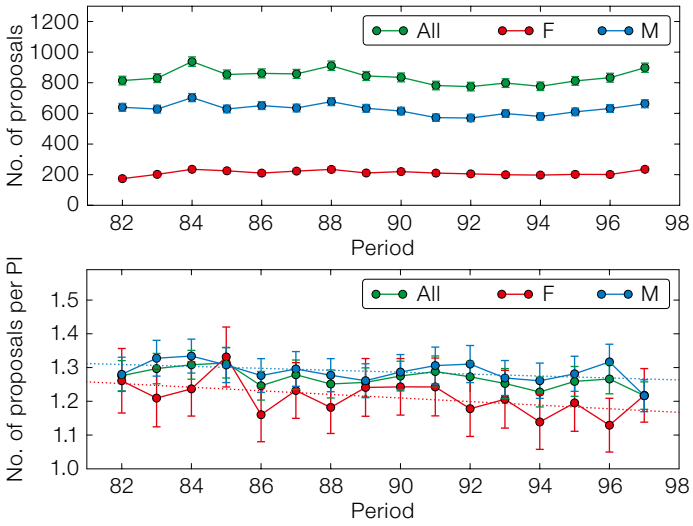

Figure 1. Trends of proposal submission over Periods 82–97. Upper panel: number of submitted proposals. Lower panel: number of proposals per PI. In this and all following plots, the error-bars indicate the Poisson noise, while the dotted lines trace a linear least squares fit to the data points.

Trends in proposal submission

The proposal submission trend by PI gender is presented in Figure 1 (upper panel). The overall average submission rate (proposals per semester) is 838.8 ± 11.5, while it is 211.4 ± 4.0 (25.2 %) and 627.3 ± 8.9 (74.8 %) for F and M PIs, respectively. The number of proposals is particularly stable for F PIs. In addition to the difference in the F and M fractions (which are directly related to the PI gender distribution, see below), it is worth noticing that the two genders differ significantly in their submission rate in terms of proposals per semester per distinct PI (Figure 1, lower panel). The overall average rate is 1.27 ± 0.01 proposals per PI, and shows a mild decrease during the period covered by this study. The submission rate for M PIs (1.29 ± 0.01) is larger than that of F PIs (1.21 ± 0.01): on average, a female PI submits ~ 8 % fewer proposals per semester.

There is some evidence for a steady decrease of the submission rate with time. The number of proposals remained roughly constant during the period under consideration (see Figure 1). This steady situation is also common to the number of distinct PIs per semester. The overall average number of PIs is 661.8 ± 9.5 (standard error of the mean), while for F and M the average is 174.5 ± 3.3 and 487.0 ± 7.5, respectively. Every semester only a fraction of all potential PIs submit a proposal[2]. The data show that, on average, every semester the list of distinct PIs includes about half of those who submitted a proposal in the previous period. This fraction is larger for M PIs (~ 55 %) than for F PIs (~ 40 %), implying that the ratio between the number of effective PIs and the number of potential PIs is smaller for F than for M scientists (for whom the opposite trend is observed).

The fraction of F PIs increased by a few percent over the eight years considered in this report, with an average value around 26 %. A closer look reveals that the Period-by-Period fraction is significantly smaller than the global sample value deduced considering all Periods together (28.8 %). This is explained by the effect described above, which is related to the different behaviour of the female astronomer community in terms of period-to-period changes in the PI set. The gender fractions within the three career levels are roughly constant in time, as illustrated in Figure 2 for the F PIs (the larger fluctuations seen for AP, and especially ST, PIs are due to the small number

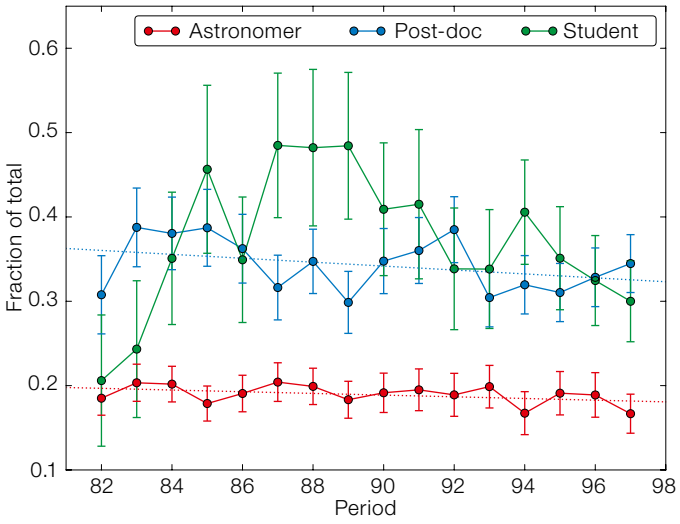

Figure 2. Evolution of the fraction of female PIs by career level.

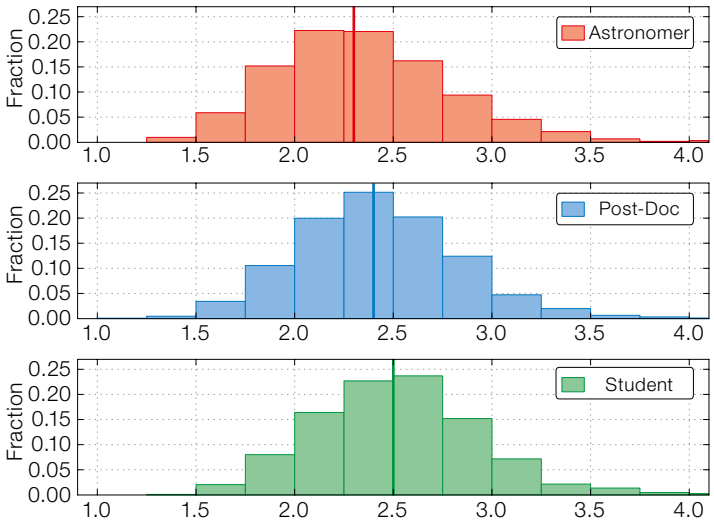

Figure 3. Pre-OPC average grade distributions by PI career level: Professional astronomer (upper), Post-doc (middle) and Student (lower). The vertical lines indicate the average values of the three distributions.

statistics. The best fit line for the ST class was omitted because the slope is characterised by a large uncertainty and is consistent with no time evolution).

Career level, gender and proposal grading

The pre-OPC average grade distributions are presented in Figure 3 for the three career levels. A first glance at the plots reveal that there are statistically significant differences, with a progressive shift of the central values towards poorer grades as one proceeds through the AP, PD and ST levels. Classical statistical tests (such as Kolmogorov-Smirnov) show that the three distributions differ at very high confidence levels (> 99.999 %). The deviations between the distributions can be robustly quantified using the differences (Δ) of their cumulative functions (Σ), which are plotted in Figure 4. The largest deviation is seen between the AP and ST distributions: the number of runs with grades better than 2.2 is 18.1 % larger for AP than for ST proposals. This difference reduces to 9.9 % when considering AP – PD distributions, and to 11.0 % when considering PD – ST distributions. In the latter case the maximum difference is attained at grade 2.4, which signals a weaker advantage of PD proposals over ST proposals (see Figure 4, red curve).

In light of these results, there is no doubt that reviewers systematically attribute different merit to proposals submitted by PIs at different career levels, with professional astronomers scoring better than post-docs, who in turn score better than students. Of course one can still ask whether the observed differences are intrinsic ("more experienced scientists write better proposals") or perceived ("this proposal was written by a senior scientist, therefore it must be good"). Irrespective of this consideration, the fact remains that there is a significant difference in the grade distributions,

Table 2. Run success rate by PI career level, rank class and gender (in percent). The values in parentheses indicate the Poisson uncertainty.

	Gender					
Career level	All		F		M	
	A+VM	A+B+VM	A+VM	A+B+VM	A+VM	A+B+VM
Astronomer	23.4 (0.4)	36.2 (0.5)	18.3 (0.9)	32.5 (1.2)	24.4 (0.5)	36.9 (0.6)
Post-doc	18.3 (0.5)	30.5 (0.6)	14.5 (0.8)	29.1 (1.1)	20.0 (0.6)	31.1 (0.8)
Student	13.2 (0.8)	25.0 (1.1)	12.9 (1.3)	26.4 (1.9)	13.5 (1.1)	24.2 (1.4)
All	20.7 (0.3)	33.3 (0.4)	16.0 (0.6)	30.5 (0.8)	22.2 (0.4)	34.2 (0.5)

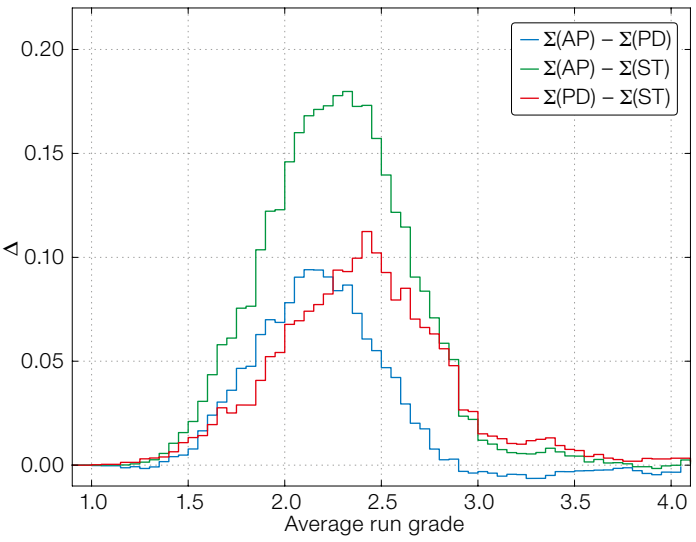

Figure 4. Differences between the cumulative functions of the pre-OPC run grade distributions.

which translates into different probabilities of obtaining telescope time. This is quantified in Table 2, which presents the success rates (scheduled runs over requested runs) by career level, rank class and gender.

The success rate of runs of rank A and VM for professional astronomers (23.4 %) is ~1.3 times larger than for post-docs (18.3 %), and ~1.8 times larger than for students (13.2 %). The statistical significance of the differences exceeds the 5σ level. Since the career level distributions of F and M PIs are different, this is expected to have an impact on the corresponding overall success rates by gender, even in the complete absence of gender effects in the review process. In this idealised case, the overall success rates by gender can be simply predicted by computing a weighted average of the success rates by career level deduced for the whole sample. The weights are the fractions of runs requested by the two genders in the three career bins (Table 1). This simple calculation leads to A+VM success rates of 19.3 % (F) and 22.1 % (M), which provide an estimate of the success rate produced by a pure difference between the career level mixtures of the two gender sets. These values can be compared to the measurements presented in the last row of Table 2 for F/M of 16.0 % and 22.2 %, respectively. While the M values are fully compatible, the F rate is smaller, signalling an additional effect. This may be explained as a combination of too coarse a career level granularity (for instance, the AP class ranges from an entry-level lecturer to a full professor) and/or genuine gender systematics in the review process.

An indication of the presence of the granularity problem comes from the fact that the advantage of M PIs does not significantly decrease when looking at single career levels. With the exception of the ST class, for which the M and F values are indistinguishable within the noise (see Table 2), the A+VM success rate ratios are 1.33 ± 0.07 and 1.38 ± 0.09 for the AP and PD levels, respectively. This leads to the legitimate suspicion that a finer classification would reveal further gradients within the coarse AP and PD classes used in this analysis. In other words, it is not unreasonable to imagine that, on average, the bin of male professional astronomers contains more high-level scientists (in terms of career advancement and opportunities) than the corresponding bin for female astronomers. This conjecture is supported by the fact that no statistically significant difference between F and M is detected in the ST bin, within which no meaningful seniority gradient is expected.

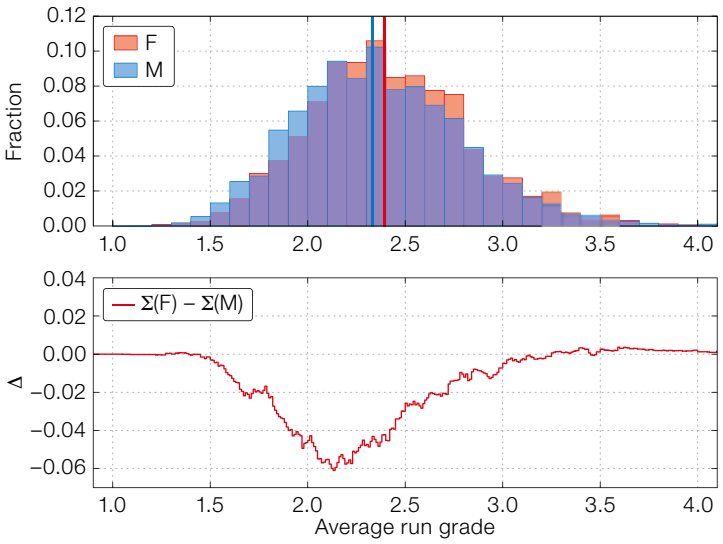

Figure 5. Upper panel: Professional astronomers and Post-doc pre-OPC run grade distributions for M (blue) and F (red) PIs. Lower panel: difference between the cumulative distribution functions (F – M).

In the absence of higher resolution (or of a better parameter), it is not possible to disentangle the career level effect from genuine gender issues in the review process. By the same line of reasoning, the demonstrated presence of a career level effect for both genders implies that the measured differences cannot be blindly and fully attributed to a systematic influence of gender in the reviewing process. The correlation between career level and success rate is by far the strongest feature among all those examined in the TAWG analysis, the blurring effects discussed above notwithstanding.

Comparison of gender effects

At face value, male PIs have a factor 1.39 ± 0.05 greater chance of getting time in the top rank classes (22.2 % *vs.* 16.0 %). The discrepancy becomes less marked when looking at the A+B+VM rates (34.2 % *vs.* 30.5 %), indicating that the disadvantage is generated by differences in the high-end tail of the grade distribution. This difference is illustrated in Figure 5, which compares the distribution of pre-OPC grades of F and M PIs in the AP and PD career levels. The divergence is clearly visible (upper panel) and quantified by the difference Δ between the two cumulative functions: the peak difference indicates that M PI runs have a 6 % excess at grades better than 2.2 (lower panel). The difference is statistically very significant, as confirmed by the Kolmogorov-Smirnov test, and the low noise level characterising the Δ function. Another indicator, at the low-end edge of the distributions, is the fraction of triaged proposals, which is 22.1 ± 0.6 % and 17.8 ± 0.3 % for F and M PIs, respectively. The difference is 4.3 ± 0.7 %, which exceeds the 6σ level.

Similar results are obtained when considering the AP and PD career levels separately, while for the ST bin the distributions are statistically indistinguishable. A similar analysis on the post-OPC data shows the same dichotomy, although with a slightly smaller amplitude, hence signalling a mild smoothing effect operated by the panel discussions. This behaviour is observed for most of the parameters studied in the TAWG analysis.

One further step in the investigation of the effect of gender systematics is the distinction between the behaviour of F *vs.* M referees when judging F or M PI proposals. Since the referee identity is lost in the post-OPC phase because of

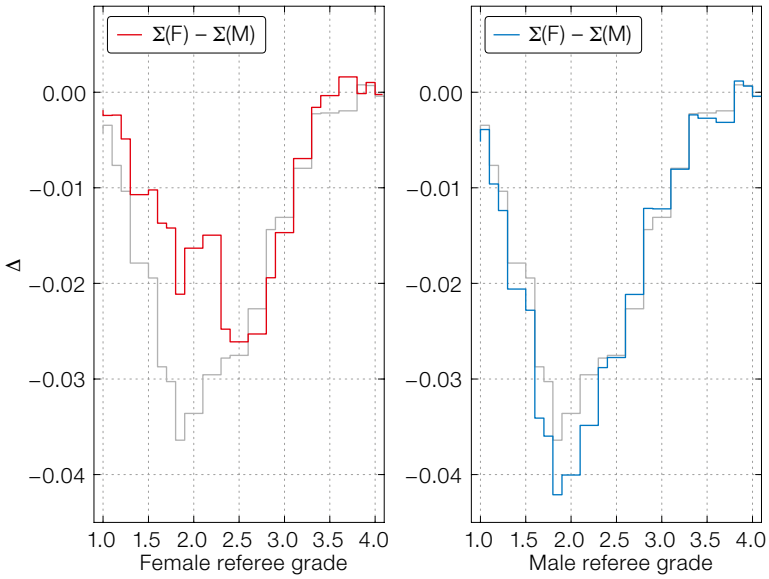

Figure 6. Difference between the cumulative functions of grade distributions (F – M) for F (left) and M (right) referees. The grey curves trace the difference for the whole pre-OPC sample, with no referee gender distinction.

Table 3. Fraction of pre-OPC grades ≤ 1.9 given by referees of given gender and career level to runs requested by PIs of given gender. All values are in percent and values in parentheses are the Poisson uncertainties.

All referees

PI	All	F	M	Δ
All		29.1 (0.3)	26.3 (0.2)	+2.8 (0.4)
F	23.5 (0.3)	28.0 (0.6)	23.5 (0.3)	+4.5 (0.7)
M	27.8 (0.2)	29.4 (0.3)	27.1 (0.2)	+2.3 (0.4)
Δ	−4.3 (0.4)	−1.4 (0.7)	−3.6 (0.4)	

AP referees

PI	All	F	M	Δ
All		29.1 (0.3)	26.3 (0.3)	+2.8 (0.4)
F	23.8 (0.3)	28.2 (0.6)	23.8 (0.3)	+4.4 (0.7)
M	27.9 (0.2)	29.4 (0.4)	27.4 (0.2)	+2.0 (0.4)
Δ	−4.1 (0.4)	−1.2 (0.7)	−3.6 (0.4)	

PD referees

PI	All	F	M	Δ
All		29.2 (0.8)	23.6 (0.5)	+5.6 (0.9)
F	21.0 (1.0)	26.9 (1.5)	21.0 (1.0)	+5.9 (1.8)
M	26.6 (0.5)	29.9 (0.9)	24.4 (0.6)	+5.5 (1.1)
Δ	−6.6 (1.1)	−3.0 (1.7)	−3.4 (1.2)	

the way the grades are collected, this analysis is only possible for the pre-OPC grades. To compare gender-specific behaviour, the pre-OPC grades for F and M referees were extracted separately. Then, from each of the two datasets, the grade distributions for F and M PIs were derived and the Δ functions were computed. These are plotted in Figure 6. In both cases (F and M referees), the proposals with female PIs are disfavoured. The effect is more pronounced for M referees, with a maximum difference of 4.2 % at grade ~ 1.8. For F referees the maximum difference is 2.6 % at grade ~ 2.5.

When considering the whole sample, the maximum difference is 3.8 % at grade 1.8 (grey line in Figure 6). The comparison between the F/M curves and the global curve gives an idea of the effect of excluding completely one of the referee genders from the panel composition. Clearly, even having an entirely F composition would not completely remove the influence of gender systematics, although it would reduce it by a factor ≈ 2. For the same reason, moving to a 50/50 balance would produce an almost unmeasurable improvement. This is in line with the results reported by Reid (2014), who concluded that "the increased diversity on the panels has not affected the success rate of proposals with female PIs."

For the sake of completeness, the same analysis was repeated on the AP and PD referee samples separately, to check whether there is any detectable gender dependency on the career level of the referee. As it turns out, there is no statistically significant difference between the two classes. This is illustrated in Table 3, which shows the fraction of pre-OPC grades ≤ 1.9 for the various gender/level referee combinations by PI gender. The limiting grade was chosen as approximately defining the first quartile, so that the values in the table can be considered as the fractions of top ranked runs. The Δ values are the differences between the various cumulative functions computed at the chosen limit grade; those reported in the rows correspond to the difference between PI genders, those in the last column to the difference between referee genders[3]. Although at face value PD referees show the largest deviation between F and M proposals (−6.6 ± 1.1 %), the Δ value is only ~ 2 standard deviations away from that derived for AP referees (−4.1 ± 0.4 %), and therefore not much significance should be attached to it.

Conclusions and actions

The average period-by-period fraction of proposals with female PIs is ~ 26 %, with a few percent increase during the time range covered by the present analysis. The overall fraction is ~ 30 %. Although this value certainly underestimates the fraction in the population of potential PIs, it can be compared to the reference statistics provided by the International Astronomical Union[4]. The values for the ESO Member States are presented in Table 4. These show large fluctuations but, on average, they are significantly smaller than the above PI fraction (only the two largest values, derived for France and Italy, provide an almost exact match): the ESO Member State IAU female membership is 18.6 % which, in turn, is larger than the overall IAU fraction (16.9 %). For comparison, Table 4 also presents the equivalent numbers for ESO PIs: with very few exceptions, the F fractions are larger than the corresponding IAU values. Therefore, although certainly far from parity, the PI community is more balanced than the IAU, which is known to suffer from a strong selection bias in its membership (see for instance Cesarsky & Walker, 2010). In his study on proposal selection at HST (covering 11 cycles

Country	Number of IAU members			IAU members		Number of ESO PIs			ESO PIs	
	F	M	Total	F	M	F	M	N	F	M
Austria	13	53	66	19.7 %	80.3 %	21	35	56	37.5 %	62.5 %
Belgium	27	119	146	18.5 %	81.5 %	20	50	70	28.6 %	71.4 %
Chile	19	100	119	16.0 %	84.0 %	54	169	223	24.2 %	75.8 %
Czech Republic	18	106	124	14.5 %	85.5 %	6	18	24	25.0 %	75.0 %
Denmark	12	73	85	14.1 %	85.9 %	13	28	41	31.7 %	68.3 %
Finland	13	67	80	16.3 %	83.8 %	6	32	38	15.8 %	84.2 %
France	219	619	838	26.1 %	73.9 %	106	261	367	28.9 %	71.1 %
Germany	82	594	676	12.1 %	87.9 %	167	367	534	31.3 %	68.7 %
Italy	174	494	668	26.0 %	74.0 %	108	163	271	39.9 %	60.1 %
Netherlands	25	202	227	11.0 %	89.0 %	45	96	141	31.9 %	68.1 %
Poland	27	132	159	17.0 %	83.0 %	6	18	24	25.0 %	75.0 %
Portugal	16	52	68	23.5 %	76.5 %	13	29	42	31.0 %	69.0 %
Spain	77	300	377	20.4 %	79.6 %	70	156	226	31.0 %	69.0 %
Sweden	20	118	138	14.5 %	85.5 %	14	34	48	29.2 %	70.8 %
Switzerland	16	120	136	11.8 %	88.2 %	26	61	87	29.9 %	70.1 %
United Kingdom	100	604	704	14.2 %	85.8 %	130	394	524	24.8 %	75.2 %
All	858	3753	4611	18.6 %	81.4 %	805	1911	2716	29.6 %	70.4 %

Table 4. IAU membership for ESO Member States and Chile (source IAU[4]), by number and percent. For comparison, the equivalent numbers for ESO PIs are also presented.

between 2001 and 2013), Reid (2014) reported a female fraction growing from 19 % to 24 %, very similar to the results presented in this paper.

Despite the pro-active attitude that characterises the OPC recruiting process, the gender fraction reached in the panels at most matches that observed in the PI distributions. This fraction decreases typically below 15 % when considering the membership of the OPC-proper, the reason being that it is more difficult to find senior female scientists willing to serve. This common problem has to do with the relatively low number of F scientists at higher career levels. Since the PI community is affected by the same imbalance, this also has a strong impact on the overall success rate by gender, as is clearly shown by the data.

Despite the coarse classification available for this study, the limitations posed by its static nature and the caveats that accompany it, the success rates shows a very marked correlation with the career level. This correlation is far stronger than any other, including that related to gender. Interestingly, this dependence is also visible in the data published by Reid (2014) for Cycles 19 and 20 (see his Figure 9), although the noise level is larger because of the smaller sample. For these reasons, any gender analysis that blindly compares F to M success rates without taking the career effect into account would mix two different issues. As a consequence, such an approach leads to a considerable overestimate of the influence of gender attributable to the proposal review process, while there certainly is an issue in the underlying population.

The fact remains that F success rates are consistently lower than M rates. Trending against time shows that this divergence is systematic (see Figure 7), with a mild indication of improvement over the time span studied. The disadvantage for female PIs is similar to that derived for HST in the Cycle range 11 to 20 (Reid, 2014, Table 1): their probability of getting time is 20–30 % lower than for their male counterparts. Although not included in the original TAWG study, an analysis of the acceptance rate of Large Programmes (LP) over the same period range (320 proposals) reveals that the discrepancy is even larger. The F fraction of submitted LPs is smaller (21.6 % *vs*. 25.1 % for Normal and Short programmes), and even more so is the acceptance rate (17.4 % *vs*. 24.7 % for M PIs), with M PIs having about 40 % greater probability of getting time through this high-impact channel.

On account of the above arguments, it is clear that this F/M difference cannot be fully attributed to the review process itself. Nevertheless, the fact that there is a significant difference between the grade distributions of F and M referees, when they rank proposals submitted by F and M PIs, confirms that, to some extent, the reviewing process does introduce extra gender differentiation, and hence cannot be fully absolved from the charge of unequal gender treatment (be it conscious or unconscious).

ESO will continue to monitor the gender fractions in the time allocation process, will consider possible actions to mitigate the measured effects and intensify its efforts to raise awareness among the OPC panel members. However, to allow for more accurate and thorough studies, the PIs and the co-Is of proposals will be asked to provide gender information in their UP profiles, together with a more robust career level indicator, like the year of PhD. This is fully in line with what is done at other inter-governmental facilities, and also outside of science.

While resolving the gender issue in the scientific environment requires a large and coordinated effort involving the whole community, addressing it in the more specific context of proposal evaluation is within ESO's reach. A number of possible counter-measures can be devised, ranging from raising the awareness of reviewers to more aggressive actions, such as making the proposals anonymous (see for instance the blind audition approach used in orchestras; Goldin & Cecilia, 2000). While the first action is certainly necessary (and some steps have already been taken at ESO, following practices already in place at other major scientific facilities), more radical solutions need to be carefully evaluated, because they can introduce other subtle effects that would be even more difficult to quantify. This delicate topic is

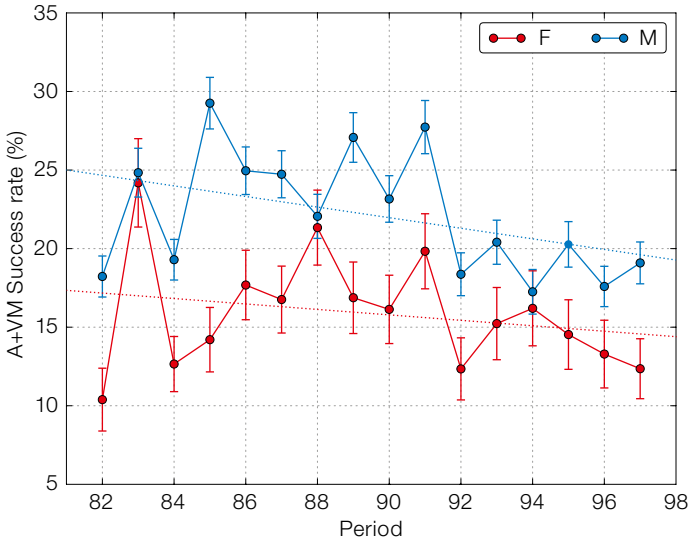

Figure 7. Success rates for proposals at rank A and in Visitor Mode by PI gender as a function of time.

discussed by Reid (2014), who examines various possibilities, all related to the level of information about the proposing team made available to the reviewers, and its possible implications. ESO may consider implementing the changes being tested at HST, which go along the lines of progressively obfuscating the applicants' identity (Reid 2016, private communication), possibly after the effects of such actions are statistically quantified.

Acknowledgements

I am very grateful to Elisabeth Hoppe, for painstakingly deducing the gender of more than 3000 scientists. Helpful discussions on gender issues in astronomy with Francesca Primas are also acknowledged.

Special thanks go to the members of the Time Allocation Working Group, for all their support and collaboration. In particular, I am grateful to Neill Reid for the very fruitful exchange of ideas on telescope time allocation matters. Finally, I wish to thank Rob Ivison and Tim de Zeeuw for suggesting the use of a seniority indicator and for kindly reviewing the manuscript, which greatly improved its quality.

References

Cesarsky, C. & Walker, H. 2010, Astronomy & Geophysics, 51, 2.33

Goldin, C. & Cecilia, R. 2000, The American Economic Review, 90, 715

Patat, F. & Hussain, G. A. J. 2013, in *Organizations, People and Strategies in Astronomy,* Vol. 2, ed. Heck, A., (Duttlenheim: Venngeist), 231

Primas, F. et al. 2015, The Messenger, 161, 5

Reid, I. N. 2014, PASP, 126, 923

Notes

[1] This correlation is less obvious than may be expected. For instance, the fact that the PI of a proposal is a student does not necessarily mean the proposal was written entirely by the student. It is plausible that the supervisor had a role, and contributed in a significant way, both in terms of content and presentation. On the other hand, it is also reasonable to expect that some supervisors, for educational purposes, leave some degree of independence to the student. In addition, the choice of the PI may be also dictated by strategic arguments within the proposing team, not necessarily and strictly related to science and/or who wrote the proposal. All these aspects contribute to blurring the possible correlation between PI career level and scientific merit of the proposal.

[2] The total number of distinct investigators (PIs and co-Is) per semester steadily evolved from ~2500 to ~3500 across the considered time span. The total number of distinct investigators exceeds 10 000; if all these are considered as potential PIs, about two thirds never submitted a proposal over the eight years covered by this study.

[3] An interesting aspect emerges from the Δ values reported in the last column of Table 3: F referees tend to be slightly more lenient than M referees, meaning that their distributions tend to be shifted towards better grades. For instance, the F distribution has a nominal rejection (the fraction of grades ≥ 3.0) that is 4.0 ± 0.4 % *vs.* 24.6 ± 0.2 %), and the number of runs with grades ≤ 1.9 is 4.8 ± 0.4 % larger than for M referees (29.1 ± 0.3 % *vs.* 24.3 ± 0.2 %).

Links

[4] IAU membership list, last updated 1 July 2016: http://www.iau.org/administration/membership/individual/distribution/

A. Russell/ESO

The Paranal Observatory just before dawn, with the Milky Way, Large and Small Magellanic Clouds all in view.

The Next Generation Transit Survey Becomes Operational at Paranal

Richard G. West[1]
Don Pollacco[1]
Peter Wheatley[1]
Michael Goad[2]
Didier Queloz[3]
Heike Rauer[4]
Christopher Watson[5]
Stéfane Udry[6]
Nigel Bannister[2]
Daniel Bayliss[6]
François Bouchy[6]
Matthew Burleigh[2]
Juan Cabrera[4]
Alex Chaushev[2]
Bruno Chazelas[6]
Michel Crausaz[6]
Szilard Csizmadia[4]
Philipp Eigmüller[4]
Anders Erikson[4]
Ludovic Genolet[6]
Ed Gillen[3]
Andrew Grange[2]
Maximilian Günther[3]
Simon Hodgkin[3]
James Kirk[1]
Grégory Lambert[7]
Tom Louden[1]
James McCormac[1]
Lionel Metrailler[6]
Marion Neveu[6]
Alexis Smith[4]
Andrew Thompson[5]
Roberto Raddi[1]
Simon R. Walker[1]
James Jenkins[8]
Andrés Jordán[9]

[1] Dept. of Physics, University of Warwick, United Kingdom
[2] Dept. of Physics and Astronomy, University of Leicester, United Kingdom
[3] Institute of Astronomy, University of Cambridge, United Kingdom
[4] Institut für Planetenforschung, Deutsches Zentrum für Luft- und Raumfahrt, Berlin, Germany
[5] Astrophysics Research Centre, Queen's University Belfast, United Kingdom
[6] Observatoire de Genève, Sauverny, Switzerland
[7] ASTELCO Systems GmbH, Martinsried, Germany
[8] Departamento de Astronomía, Universidad de Chile, Santiago, Chile
[9] Departamento de Astronomía y Astrofísica, Pontificia Universidad Católica de Chile, Santiago, Chile

A new facility dedicated to the discovery of exoplanets has commenced science operations at Paranal. The Next-Generation Transit Survey (NGTS) will deliver photometry at a precision unprecedented for a ground-based wide-field survey, enabling the discovery of dozens of transiting exoplanets of the size of Neptune or smaller around bright stars. NGTS is briefly described and the survey prospects are outlined.

Introduction

Most of our knowledge of the properties of individual exoplanets comes from those that transit their host star. Measurements of the transit lead to an estimate of the planet's radius relative to that of the star and, since its orbital inclination can be recovered from the transit shape, then its mass can be derived. Together these data provide the planet's density, which can be compared to theoretical models of its structure. Even in this new era of directly imaged planets (with high contrast imaging instruments such as the Spectro-Polarimeter High-contrast Exoplanet REsearch Instrument [SPHERE] on the Very Large Telescope, for example) and astrometric orbits from the European Space Agency (ESA) Gaia satellite, transit observations remain the only direct method to determine accurate planetary radii.

However, the detection of transiting planets is not trivial. As the transit probability diminishes rapidly with orbital period, strong selection effects favour the detection of large planets (or, strictly speaking, planets large relative to their host) with short periods. Consequently, transit surveys observe thousands of (Sun-like) stars to find just a handful of large planets. The two leading ground-based survey projects are HAT (Hungarian-made Automated Telescope[1]) and WASP (Wide Angle Search for Planets[2]), which together have discovered the majority of planets that have accurately determined masses.

The instruments used in these surveys are quite modest, but are capable of repeatedly imaging hundreds of square degrees and obtaining accurate photometry (better than 1% precision) for stars brighter than $V = 11$ mag. Each facility has the significant computer resources required to reduce the data for each star in an image and search for brightness variations. In the case of WASP the reduced data products (star brightness as a function of time) grow at a rate of several GB per night. Over ten years of operation, WASP has acquired more than 16 million images covering 30 million stars, a total of more than 0.5×10^{12} photometric data points.

The ESA space mission CoRoT (Convection, Rotation and planetary Transits) and the National Aeronautics and Space Administration (NASA) satellite Kepler (and its continuation as K2) have obtained photometry of sufficient accuracy to enable the detection of smaller, rocky planets. Given the relatively modest fields of view of these instruments, most of their planet candidates have been detected with host stars of $V > 13$ mag. Consequently, given their faintness and the expected size of the reflex motion induced in the star, confirmation and measurement of the planetary mass have generally been beyond our current observational capabilities, and just a handful of the brightest hosts with small planets have been studied.

The need for another (red) survey

In order to characterise small planets we have two options:

a) Employ an extremely wide-field satellite enabling photometry of many bright stars. Both NASA and ESA are planning such missions, respectively the Transiting Exoplanet Survey Satellite (TESS) and the PLAnetary Transits and Oscillations of stars (PLATO);
b) Remembering that the transit depth is dependent on the relative sizes of the planet and its star, observe smaller stars to detect smaller planets for a given photometric accuracy. There are several projects targeting individual M-dwarfs that have recently achieved stunning successes, such as the detection of GJ 1132b (Berta-Thompson et al. 2015) with MEarth[3] and TRAPPIST-1 (Gillon et al., 2016) with the TRAnsiting Planets and PlanetesImals Small Telescope (Jehin et al., 2011; TRAPPIST[4]). While M-dwarfs are common, they are intrinsically faint and spectroscopic

Grégory Lambert

Figure 1. Photograph of the NGTS facility at Paranal with the VLT in the background to the west.

follow up of these targets is challenging. An alternative approach is to optimise the system for the detection of planets around K-dwarfs, which are more luminous. The Next Generation Transit Survey is our attempt to realise this survey.

The scientific goal of NGTS is to discover a population of Neptune-sized planets around bright stars. In order to achieve this, a photometric precision unprecedented in wide-field ground-based surveys (better than 0.1 %) is required. NGTS has therefore been carefully designed to minimise the instrumental effects which have limited the precision of previous surveys.

NGTS has its roots in the hugely successful WASP project[2] but has been developed through two prototypes. The first was set up on La Palma in 2010 and was used to look at the potential use of deep-depleted charge-coupled device (CCD) technology for the detectors and of wider-aperture astrographs. This first prototype led to the final design which was constructed at Geneva Observatory in 2012. This second prototyping phase was then used to further optimise the design, and to develop the control software.

After discussions with ESO it was agreed to site the NGTS at Paranal Observatory. While astronomical seeing was not a prime factor, atmospheric water content and excellent photometric conditions were paramount in this decision.

The NGTS facility

NGTS[5] consists of a cluster of twelve identical telescope units, each unit comprising a 20-cm f/2.8 astrograph and a 2k × 2k deep-depleted CCD camera mounted on an independently steerable fork mount. Each unit has a field of view of approximately 3 × 3 degrees, yielding a total field of view for the whole facility of approximately 100 square degrees (roughly equivalent to that of the Kepler satellite). A photograph of the NGTS facility at Paranal is shown in Figure 1.

In general, NGTS utilises commercial off-the-shelf products which have been modified to optimise their performance. For example, the detectors are deep-depleted e2v (CCD-42) devices packaged into a camera by Andor Technology (model iKon-L). Andor manufactured the original WASP cameras so we already had a good working relationship with this company. Optimisation of these devices proved more demanding than we expected and the company expended considerable effort to produce devices suitable for the extreme accuracies we were trying to achieve. Similarly, the telescopes are H-series astrographs from Astro Systeme Austria (ASA), but fitted with a custom corrector optic designed to NGTS specifications. The NGTS enclosure was designed and fabricated by GR-PRO in the UK; it is of glass-reinforced plastic (GRP) composite construction, and has a footprint of around 10 × 15 metres.

The NGTS facility is fully robotic and operates unsupervised, following a pre-generated schedule that is prepared on a daily basis. The survey data are transferred to the NGTS Data Centre at the University of Warwick, UK, to be analysed using sophisticated automated algorithms that search for the tell-tale signatures of an exoplanet transiting its host star. Detections made by these algorithms are further vetted by automatic and manual means, and the highest quality candidates are passed for photometric and spectroscopic follow-up using larger facilities (e.g., the CORALIE spectrograph on the EULER telescope at La Silla). Processed NGTS light-curves will be made available to the community via the ESO Science Archive Facility after a proprietary period (two years for the first release, one year for subsequent releases).

First results and the future

First light at Paranal was achieved with the first NGTS telescope in January 2015 and the transit survey began with five telescopes in August 2015. The full complement of twelve telescopes became operational in February 2016 and, despite the poor weather associated with El Niño, NGTS has already acquired more than 3.5 million science images. The quality of the data produced by NGTS is exceptional, and the instrument has proven itself well capable of delivering the required sub-millimagnitude photometric precision. As an example of the step-change improvement that NGTS represents over previous ground-based surveys, Figure 2 compares the light-curve of a single transit of a known exoplanet (the "hot Jupiter" WASP-4b [Wilson et al., 2008]) taken with NGTS, with the best quality transit in the WASP survey data. The WASP data show instrumental effects that have a magnitude similar to that of the transit signal, so WASP required coverage of many transits in order to make a significant detection. NGTS on the other hand could have detected WASP-4b with a single transit.

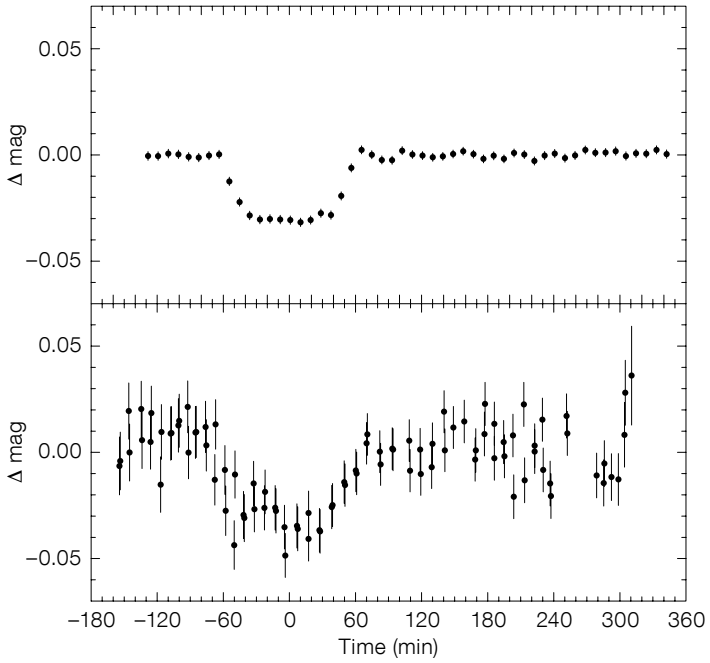

Figure 2. Light curves of single transits of the Jupiter-sized exoplanet WASP-4b measured with NGTS (upper) and WASP (lower).

A preliminary analysis of the data from the first six months of the full NGTS survey has yielded several dozen candidate planets which are we currently following up. Recent simulations based on the actual performance of NGTS have shown that the full NGTS survey can be expected to detect several super-Earths (planets with a radius less than twice that of the Earth), tens of Neptune-sized planets (2–6 Earth radii), and more than 200 planets with a radius larger than Saturn's (6–22 Earth radii). NGTS is most sensitive to planets with orbits of less than 20 days.

NGTS Consortium

The NGTS Consortium consists of the following institutes: University of Warwick, UK; Observatoire de Genève, Switzerland; Deutsches Zentrum für Luft- und Raumfahrt (DLR), Germany; University of Leicester, UK; Queen's University Belfast, UK; and the University of Cambridge, UK. The Chilean astronomical community is currently represented by the Pontificia Universidad Católica de Chile and the Universidad de Chile.

References

Berta-Thompson, Z. K. et al. 2015, Nature, 527, 204
Gillon, M. et al. 2016, Nature, 533, 221
Jehin, E. 2011, The Messenger, 145, 2
Wilson, D. M. et al. 2008, ApJ, 675, L113

Links

[1] HAT Exoplanet Surveys: https://hatsurveys.org/
[2] WASP: https://wasp-planets.net/
[3] MEarth project: https://www.cfa.harvard.edu/MEarth/Welcome.html
[4] TRAPPIST Telescope Network: http://www.orca.ulg.ac.be/TRAPPIST/Trappist_main/News.html
[5] NGTS: http://www.ngtransits.org

SEPIA — A New Instrument for the Atacama Pathfinder Experiment (APEX) Telescope

Katharina Immer[1]
Victor Belitsky[2]
Michael Olberg[2]
Carlos De Breuck[1]
John Conway[2]
Francisco Miguel Montenegro-Montes[1]
Juan-Pablo Perez-Beaupuits[1]
Karl Torstensson[1]
Bhushan Billade[2]
Elvire De Beck[2]
Andrey Ermakov[2]
Sven-Erik Ferm[2]
Mathias Fredrixon[2]
Igor Lapkin[2]
Denis Meledin[2]
Alexey Pavolotsky[2]
Magnus Strandberg[2]
Erik Sundin[2]
Vinodiran Arumugam[1]
Maud Galametz[1]
Elizabeth Humphreys[1]
Thomas Klein[1]
Joost Adema[3]
Jan Barkhof[3]
Andrey Baryshev[3,4]
Wilfried Boland[5,6]
Ronald Hesper[3]
Teunis Martien Klapwijk[7]

[1] ESO
[2] Department of Earth and Space Sciences, Chalmers University of Technology, Onsala Space Observatory, Sweden
[3] Kapteyn Astronomical Institute, University of Groningen, the Netherlands
[4] SRON Netherlands Institute for Space Research, Groningen, the Netherlands
[5] Leiden Observatory, Leiden University, the Netherlands
[6] Netherlands Research School for Astronomy, Leiden, the Netherlands
[7] Kavli Institute of Nanoscience, Delft University of Technology, the Netherlands

The Swedish-ESO PI receiver for APEX (SEPIA) was installed at the APEX telescope in 2015. This instrument currently contains ALMA Band 5 (157–212 GHz) and Band 9 (600–722 GHz) receivers. Commissioning and science verification for Band 5 have been successfully completed but are still ongoing for Band 9. The SEPIA instrument is briefly described and the commissioning of the Band 5 receiver and results from the first science observations are presented.

In 2015, the Atacama Pathfinder Experiment (APEX) telescope received a new instrument, the Swedish-ESO PI receiver for APEX. The arrival of SEPIA at APEX featured in several press releases[1,2]. More information about the instrument can be found on the APEX webpage[3]. Currently, Band 5 receivers are also being installed at antennas of the Atacama Large Millimeter/submillimeter Array (ALMA) and it is planned to offer this band for science proposals in Cycle 5 (beginning September 2017). Preparatory observations with SEPIA Band 5 at APEX to pave the way for future ALMA projects are thus possible now. ESO will organise a dedicated workshop on SEPIA and the preparatory work for ALMA Band 5 at the beginning of 2017.

Description of SEPIA

SEPIA is a single pixel heterodyne instrument that can accommodate three ALMA-like receiver cartridges. It currently contains ALMA Band 5 (157.36–211.64 GHz) and Band 9 (600–722 GHz) receivers. A Band 7 receiver (275–373 GHz) is planned to be added in early 2018. The SEPIA receiver project was realised within one year: the decision for a new instrument for APEX was taken in February–March 2014 and the installation at the telescope was performed in February 2015. Details of the instrument and its commissioning will be presented in Belitsky et al. (in prep.).

The tertiary optics to illuminate the SEPIA cartridges inside the Nasmyth cabin A of the APEX telescope were designed, constructed, and installed by the Group for Advanced Receiver Development (GARD) at Onsala Space Observatory (OSO) in Sweden. The SEPIA cryostat was also manufactured by GARD. It provides the required mechanical, cryogenic, vacuum, optical and electrical interfaces for the receiver cartridges. The control system and software were also developed by GARD at OSO. The total weight of the SEPIA instrument (including the tertiary optics and its supporting frame, the integrated turbo-pump and three cartridges) is ~315 kg. Figure 1 shows a picture of the installed SEPIA instrument.

An ALMA Band 5 pre-production cartridge (Billade et al., 2012) was refurbished by

E. Sundin/OSO

Figure 1. The SEPIA instrument installed at APEX.

GARD with full-production mixer components as well as a local oscillator (LO) system and a warm cartridge assembly, which were purchased from the National Radio Astronomy Observatory (NRAO). Band 5 is a dual-polarisation sideband-separated (2SB) receiver which covers the frequency range 157.36–211.64 GHz. Each sideband has a total bandwidth of 4 GHz. The central frequencies of the two sidebands are separated by 12 GHz, corresponding to an intermediate frequency (IF) of 4–8 GHz. At 183 GHz, the beam size is 34 arcseconds. The single-sideband noise temperature is below 55 K at all frequencies of the band. The sideband rejection ratio is > 10 dB at all frequencies and 18.5 dB on average.

During Band 5 and Band 9 observations, the SEPIA receiver is connected to the Max-Planck-Institut für Radioastronomie's eXtended bandwidth Fast Fourier Transform Spectrometer (XFFTS; Klein et al., 2012). Each sideband is recorded by two 2.5 GHz wide XFFTS units, with an overlap of 1 GHz. The back end provides a fixed number of 65 536 and 32 768 channels per sub-band of the lower and upper sideband, which yields spectral resolutions of 38 kHz and 76 kHz, respectively. The main transition of astronomical

interest in the frequency range of this receiver is the H_2O(3–2) line at 183.3 GHz. Table 1 lists the astrophysically important molecules and their transitions within Band 5.

The atmospheric transmission at APEX at the frequency of the 183 GHz line is better than 0.3 for a precipitable water vapour (PWV) of < 0.5 mm, which happens for about 50 days per year (15 % of the total observing time). At frequencies outside of the atmospheric water line (≲ 175 GHz, ≳ 192 GHz), the atmosphere is much more transparent and observations can be conducted for most of the year. Figure 2 shows the atmospheric transmission for the whole band for five different PWV values. In addition, the frequencies of the brightest transitions of various molecules (listed in Table 1) in the band are indicated.

The Band 9 cartridge was built by the Netherlands Research School for Astronomy (NOVA) instrumentation group, following the specifications of the ALMA Band 9 receivers (Baryshev et al., 2015). Band 9 is a dual-polarisation double sideband (DSB) receiver covering the frequency range 600–722 GHz, again recorded over an IF of 4–8 GHz. At 660 GHz, the beam width is 9.5 arcseconds. The DSB noise temperature is 70–125 K. Similarly to Band 5, Band 9 is connected to the XFFTS backend. It is planned to upgrade the Band 9 DSB receiver with a 2SB receiver in February/March 2017. First science verification observations have already been conducted and, as an example, Figure 3 shows the H_2O spectrum of the supergiant star AH Sco at 658 GHz (Baudry et al., in prep.).

Molecule	Transition	Frequency (GHz)	Comment
H_2O	$J_{Ka,Kc} = 3_{1,3}–2_{2,0}$	183.31	
$H_2{}^{18}O$	$J_{Ka,Kc} = 3_{1,3}–2_{2,0}$	203.41	
HCN	J = 2–1	177.26	
$H^{13}CN$	J = 2–1	172.68	
$HC^{15}N$	J = 2–1	172.11	
HNC	J = 2–1	181.32	
HCO^+	J = 2–1	178.38	
$H^{13}CO^+$	J = 2–1	173.51	
$HC^{18}O^+$	J = 2–1	170.32	
CS	J = 4–3	195.95	
^{13}CS	J = 4–3	184.98	
$C^{34}S$	J = 4–3	192.82	
N_2H^+	J = 2–1	186.34	
CH_3CN	J = 9–8	165.60	Several K-components
	J = 10–9	183.90	Several K-components
	J = 11–10	202.30	Several K-components
CH_3CCH	J = 10–9	170.90	Several K-components
	J = 11–10	187.90	Several K-components
	J = 12–11	205.00	Several K-components
CH_3OH	J = 4–3	193.50	Several lines
CCH	N = 2–1	174.70	Several lines
SiO, v = 0	J = 4–3	173.69	
SiO, v = 1	J = 4–3	172.48	
SiO, v = 2	J = 4–3	171.28	
H_2S	$J_{Ka,Kc} = 1_{1,1}–1_{0,1}$	168.76	

Table 1. Astrophysically important molecular transitions in SEPIA Band 5.

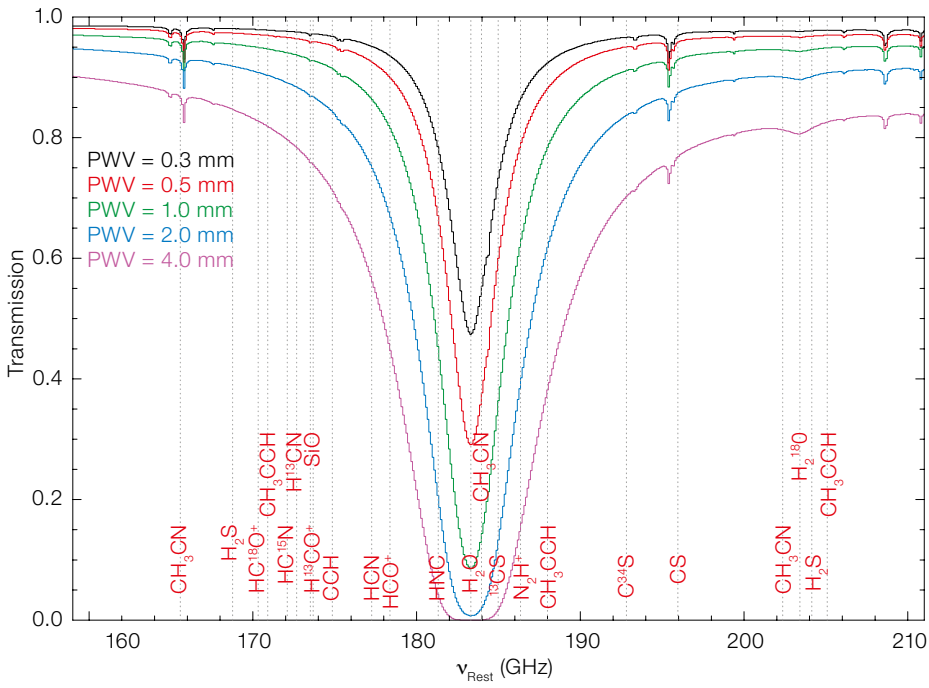

Figure 2. Atmospheric transmission in Band 5 for five different water vapour levels: PWV = 0.3 mm (black), PWV = 0.5 mm (red), PWV = 1.0 mm (green), PWV = 2.0 mm (blue), PWV = 4.0 mm (pink). The transitions of Table 1 are marked.

Commissioning

The SEPIA Band 5 receiver was installed and successfully commissioned between February and September 2015. The technical commissioning of the Band 9 receiver was performed between February and March 2016 by a joint team from GARD and NOVA. Sky commissioning of Band 9 is still ongoing.

Technical commissioning

During the technical commissioning of both SEPIA receivers, the hardware (reference LO, phase lock loop [PLL] synthesiser, IF switches, vacuum control gauge, turbo-pump, computerised control system, etc.) was installed at the telescope. The tertiary optics were aligned in the cabin and the SEPIA cryostat and the cold

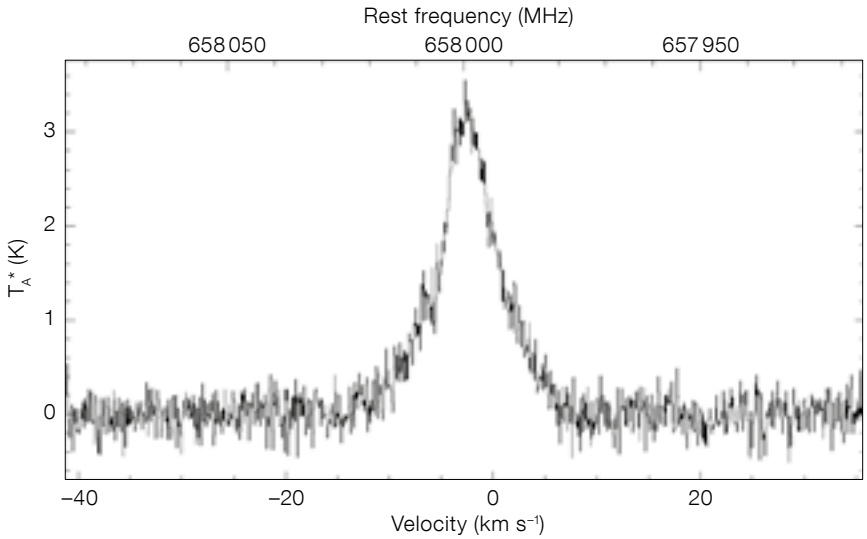

Figure 3. SEPIA Band 9 H_2O spectrum of AH Sco at 658 GHz (Baudry et al., in prep.).

head compressor installed. The integrity of the whole system was tested and the alignment of the optics was verified with small nitrogen-cooled absorbers.

Sky commissioning

A number of on-sky tests have to be conducted before a new instrument can be offered for observing time. By tuning Band 5 every 0.5 GHz, we confirmed that the whole tuning range from 157.36–211.64 GHz is accessible. Observing strong water masers as part of the Science Verification, Humphreys et al. (in prep), determined the sideband suppression level to be 17.7 dB by comparing the water line in the upper sideband to its ghost line in the lower sideband. From a preliminary analysis of planet observations (for Jupiter, Uranus and Mars), we determined an average main beam efficiency η_{mb} = 0.68 at 208 GHz, corresponding to a Jy/K conversion factor of 38. A more detailed analysis, examining the frequency dependence over the entire band, will be published in Belitsky et al. (in prep), and the resulting values will be given on the APEX webpage[3].

Pointing and focus observations at APEX are conducted towards compact sources with either strong continuum or line emission. For the other APEX heterodyne instruments, these observations are often done in the main transitions of the CO molecule. Since the Band 5 frequency range does not contain a CO transition (Table 1), we had to find sources that emit strongly in other molecular transitions. We chose evolved stars that are bright in HCN or SiO. After testing their quality as pointing sources, we constructed a pointing catalogue which covers the whole local sidereal time (LST) range. The positions of the sources are plotted in Figure 4. The pointing sources are being used to compile a good pointing model for Band 5 (more details will be provided in Belitsky et al., in prep.). With this receiver, pointing accuracies of 2.5 arcseonds are achieved.

Recalibration of Band 5 data

The online calibration of spectral line observations at the APEX telescope is based on SKY-HOT-COLD calibration scans immediately before the spectral line data are taken. During these scans, observations of blank sky, a hot load at ambient temperature and a cold load at liquid nitrogen temperature are conducted. From the HOT and COLD signal, the online calibrator determines the receiver temperature. From the SKY phase, it calculates the sky temperature, correcting for spillover and forward efficiency. Based on the elevation of the SKY observations and a sophisticated atmospheric model (ATM: Pardo et al., 2001), the opacity in image and signal band is determined.

In the online calibration, only one opacity value is calculated for the whole 2.5 GHz sub-band. This is sufficient if the atmospheric opacity is reasonably flat. However, in Band 5, due to the water absorption of the atmosphere, this approach

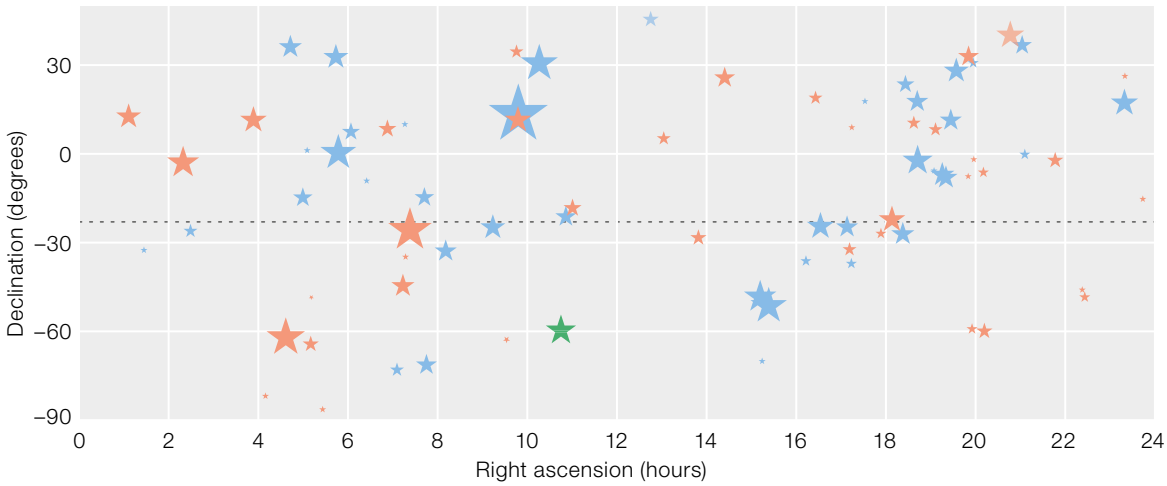

Figure 4. Local Siderial Time (LST) distribution of Band 5 pointing sources (HCN [blue], SiO [red] and continuum [green]). The size of each symbol is proportional to the logarithm of the integrated flux (K km s^{-1}). The dotted line indicates the latitude of the APEX telescope.

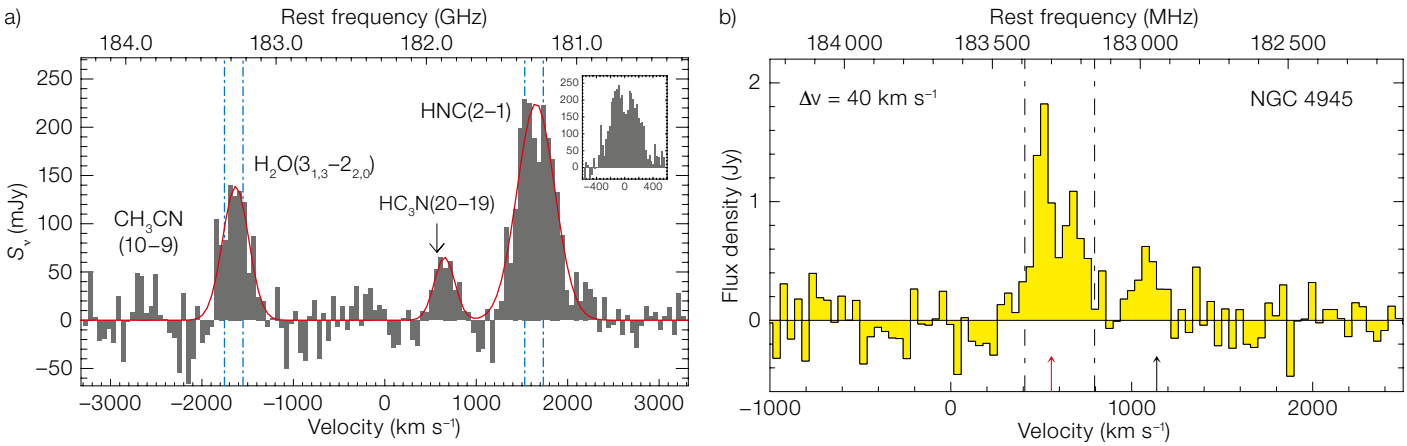

Figure 5. (a) 183 GHz H_2O emission detected towards Arp 220 (from Galametz et al. 2016). Other molecular lines are detected, such as HNC and HC_3N which trace the dense gas. The inset shows HNC double-peak profile at a 25 km s^{-1} resolution. (b) 183 GHz water maser emission from the nearby galaxy NGC 4945 (from Humphreys et al., 2016). The data were binned to 40 km s^{-1} resolution. The red arrow indicates the approximate galactic systemic velocity of 556 km s^{-1}.

is insufficient for observations close to 183.3 GHz. This type of data needs to be recalibrated offline at the telescope. In the offline calibration, opacity values are determined in chunks of 128 channels (the resolution of the atmospheric model). The online calibrated data underestimate the emission around 183 GHz by up to 30 %. The goal is to upgrade the online calibration for SEPIA Band 5 (and later Band 9) observations to provide such optimally calibrated data.

Science with SEPIA Band 5

Nine ESO[4] and five OSO[5] projects were submitted and observed for science verification of Band 5. The instrument has been offered for regular projects since ESO and OSO Period 96. Twenty-nine ESO proposals and 25 OSO proposals (including two Director's Discretionary Time proposals in Period 95) have been accepted until now. For ESO, these proposals represent a third of all APEX proposals during Periods 96–98. Since the installation of Band 5, the instrument has been used for almost 1000 hours.

Many different molecules have transitions in the SEPIA Band 5 frequency range (Table 1). One of the main science drivers for an ALMA Band 5 receiver at APEX was the possibility of observing the 183.3 GHz water line. Interstellar water emission was first detected by Cheung et al. (1969) and since then the Herschel Space Observatory has shown that gaseous water is widespread in molecular clouds in our Galaxy (van Dishoeck et al., 2011). With APEX, surveys for both maser and thermal water emission towards a large number of sources are feasible.

The water molecule is an important tracer of the energetic processes which take place during the formation of low- and high-mass stars. In combination with the lower optical depth $H_2{}^{18}O$ transition at 203.4 GHz, the observations probe the water content even in the inner parts of hot molecular cores, complementing space-based water observations (for example, from Herschel). The 183.3 GHz line has also been detected in the O-rich circumstellar envelopes of several evolved stars with mass-loss rates exceeding 10^{-6} $M_\odot$/yr (González-Alfonso et al., 1998, 1999). Observations of this transition with APEX will thus allow the study of the water abundance in evolved stars. In addition, the degree of the linear polarisation of the 183.3 GHz water maser emission can be determined from dual-polarisation observations with Band 5 (Humphreys et al., in prep.).

Beyond the Galaxy, water maser observations will provide information about the water content of nearby ($z < 0.1$) galaxies, as well as the high temperature and density regions of active galactic nuclei (AGN). In the Seyfert 2 galaxy NGC 4945, 183.3 GHz H_2O megamaser emission was detected for the first time with SEPIA Band 5 (Humphreys et al. 2016; see Figure 5b); the strongest extragalactic submillimetre water maser detected to date. The emission seems to be dominated by that from the AGN central engine.

Galametz et al. (2016) (Figure 5a) recently detected water (183.3 GHz) and the methanol (4–3) group (193.5 GHz) in the ultra-luminous infrared galaxy Arp 220. No time variations were observed in the megamaser water line compared to previous observations, supporting arguments against an AGN nuclear origin for the line.

The J = 2–1 transitions of the nitrogen-bearing species HCN, HNC, and N_2H^+, as well as HCO^+, are available in the SEPIA Band 5 frequency range. Their isotopologues $H^{13}CN$, $HC^{15}N$, $H^{13}CO^+$, and $HC^{18}O^+$ are observable in one frequency setting, as are HCN and HCO^+. These transitions serve as low-energy complements to the higher J-lines which are covered by other APEX bands, probing colder/lower density material. In evolved stars, simultaneous observations of HCN and SiO allow the determination of the HCN/SiO intensity ratio which is indicative of the star's chemical type (Olofsson et al., 1998).

The symmetric top molecules CH_3CN and CH_3CCH have several K-ladders in the band. Also, the methanol J = 4–3 line forest around 193.5 GHz, and the set of lines of CCH(2–1) around 174.7 GHz, are accessible with SEPIA Band 5. All these transitions are excellent temperature tracers of the denser molecular gas. They are more

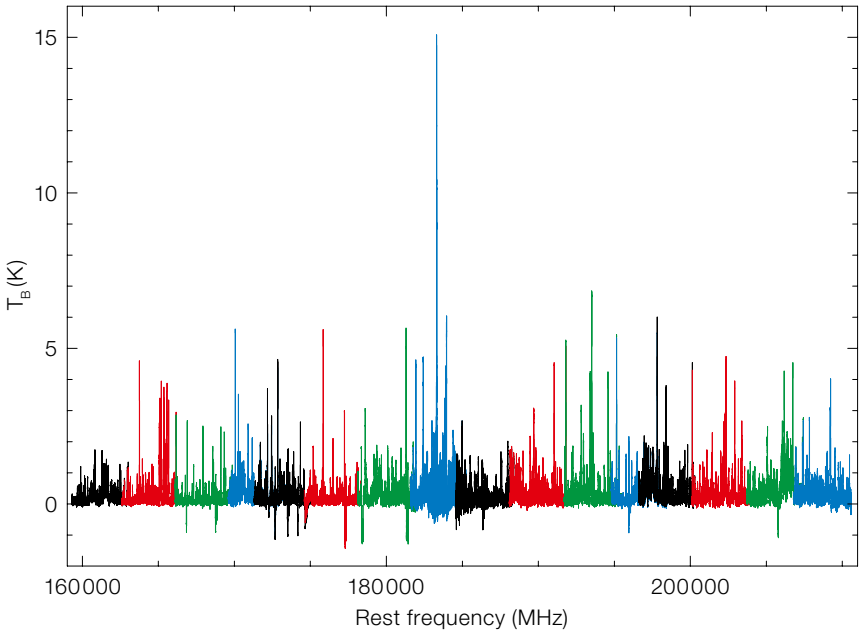

Figure 6. Spectral line survey of Sgr B2. The eight different frequency tunings are marked in black, red, green, and blue. The strongest emission line is the H_2O transition at 183.3 GHz. Absorption lines, such as of HCN, HNC, and HCO^+, are also detected. From Immer et al. in prep.

sensitive to lower temperatures than the corresponding transitions in other APEX bands. Molinari et al. (2016) observed CH_3CCH(12–11) towards 51 dense clumps and determined their gas temperatures.

For all sources at $z > 0.615$, at least one CO transition falls within the frequency range of the SEPIA Band 5 receiver. This allows observations of high-J CO transitions in bright submillimetre galaxies in order to investigate their CO spectral line energy distributions or confirm their redshifts. Strandet et al. (2016), who studied the redshift distribution of SPT sources, used the SEPIA CO observations of two sources to confirm their redshifts. In addition to CO, detecting [C II] in highly redshifted sources ($z > 8.9$) is challenging for APEX, but could be extremely rewarding.

Due to the instantaneous bandwidth of 8 GHz, the whole frequency range of SEPIA Band 5 can be covered with only eight frequency tunings with several 100 MHz overlap. An ESO Science Verification project observed the frequency range 159.2–210.7 GHz towards the high-mass star forming complex Sgr B2 (Figure 6), proving once again the line-richness of this source and illustrating the large number of transitions that can be detected in SEPIA Band 5 (Immer et al., in prep.).

Acknowledgements

We thank the APEX team for conducting the commissioning, Science Verification and regular observations with SEPIA Band 5. We are grateful to Palle Møller (ESO) who contributed significantly during the ESO Science Verification phase.

References

Baryshev, A. M. et al. 2015, A&A, 577, A129
Billade, B. et al. 2012, IEEE Trans. Terahertz Science and Technology, 2, 208
Cheung, A. C. et al. 1969, Nature, 221, 626
Galametz, M. et al. 2016, MNRAS, 462, 36
González-Alfonso, E. et al. 1998, A&A, 334, 1016
González-Alfonso, E. et al. 1999, ApJ, 525, 845
Humphreys, E. M. L. et al. 2016, arXiv:1608.00258
Klein, B. et al. 2012, A&A, 542, 3
Molinari, S. et al. 2016, ApJL, 826, 8
Olofsson, H. et al. 1998, A&A, 329, 1059
Pardo, J. R. et al. 2001, IEEE Trans. on Antennas and Propagation, 49, 1683
Strandet, M. L. et al. 2016, ApJ, 822, 80
van Dishoeck, E. et al. 2011, PASP, 123, 138

Links

[1] OSO SEPIA press release: http://www.chalmers.se/en/centres/oso/news/Pages/apex-sepia-alma-band-5-water-space.aspx
[2] ESO SEPIA press release: https://www.eso.org/sci/publications/announcements/sciann15015.html
[3] SEPIA webpage: http://www.apex-telescope.org/instruments/pi/sepia/
[4] ESO Science Verification: http://www.eso.org/sci/activities/apexsv/sepia/sepia-band-5.html
[5] OSO Science Verification: http://www.chalmers.se/en/centres/oso/Documents/APEX%20Observed%20projects/APEX-SepiaScienceVerification_Apr-Jul-2015_P95.pdf

C. Durán/ESO

Long exposure photograph of the APEX telescope during night-time observing.

Part of the APEX Telescope Large Area Survey of the Galaxy (ATLASGAL) image of the Galactic Plane around longitude +6 degrees. The Plane crosses the middle of the field: just below the Plane to the left is the H II region M20 (NGC 6514) and at lower latitude, the complex filamentary feature is the nebula M8 (NGC 6523). See Release eso1606 for more images.

ESO/APEX/ATLASGAL consortium/NASA/GLIMPSE consortium/ESA/Planck

Globular Clusters and the Milky Way Connected by Chemistry

Bruno Dias[1]
Ivo Saviane[1]
Beatriz Barbuy[2]
Enrico V. Held[3]
Gary Da Costa[4]
Sergio Ortolani[5,3]
Marco Gullieuszik[3]

[1] ESO
[2] Instituto de Astronomia, Geofísica e Ciências Atmosféricas, Universidade de São Paulo, Brazil
[3] INAF, Osservatorio Astronomico di Padova, Italy
[4] Research School of Astronomy & Astrophysics, Australian National University, Australia
[5] Dipartimento di Fisica e Astronomia, Università di Padova, Italy

There are two ways to study galaxy formation and evolution: one is to observe a large number of galaxies at a variety of redshifts, the other is to observe in detail just a few nearby galaxies. The precision achievable by the latter method enables the galactic history, including the formation and early evolution, to be studied. Globular clusters provide targets for the second method. We show how the chemical content of Milky Way globular clusters can be used to place them on a timeline charting the history of our Galaxy. The results suggest that different α-elements trace different processes of Milky Way chemical evolution.

The seminal work of Eggen, Lynden-Bell & Sandage (1962) was the first to use stars as tracers of the history of the Milky Way. They found that older metal-poor stars have more elliptical orbits while younger metal-rich stars move in circular paths. They concluded that the proto-Milky Way had collapsed by the time of the formation of the first stars and a few hundred million years later the collapsed gas achieved circular motion and formed new stars. This was the beginning of the field now called galactic archaeology.

Another important step was provided by Searle & Zinn (1978), who found no trace of a radial metallicity gradient for the halo globular clusters, and suggested that halo globular clusters formed in protogalactic fragments that were accreted to build the Milky Way halo, after the collapse of the Bulge. Since then many works have been devoted to the use of globular clusters in the study of galactic archaeology. In particular, with the advent of telescopes in space, and larger ground-based telescopes, such studies are able to spatially resolve stars in these clusters and also to obtain spectra of individual stars, even for the most distant clusters. Saviane et al. (2012) present a summary of this work. Figure 1 illustrates the current capacity to observe individual stars in clusters in a broad context.

Digging into the clusters

Almost 40 years after the work of Searle & Zinn, it is legitimate to ask what there is left to study. In many investigations that followed Searle & Zinn, astronomers observed the integrated light of all the globular cluster stars, which can be contaminated by non-cluster members and does not provide information on, for example, any star-to-star chemical abundance variations. Nowadays it is well known that stars in most globular clusters are split into at least two generations, evident from variations in the abundances of light-elements such as Na, O, Mg, Al, C, N. Further, we now know that bright horizontal branch stars can be bluer or redder depending on their He abundance. The current challenge is to find a model that connects the variations in Na, O, Mg, Al, C and N with the variation in He. Age and total metallicity also play a role in determining horizontal branch morphology (see reviews by Gratton et al., 2004, 2012). Therefore, in order to understand the formation of stars in globular clusters, it is clearly important to derive chemical abundances of individual cluster stars.

However, only about 60% of Milky Way globular clusters (of which 157 are currently known [Harris, 1996]) have had their metallicities derived on a homogeneous scale based on consistently obtained integrated or resolved spectroscopy. But only ~ 50% of these determinations are based on spectroscopy of individual

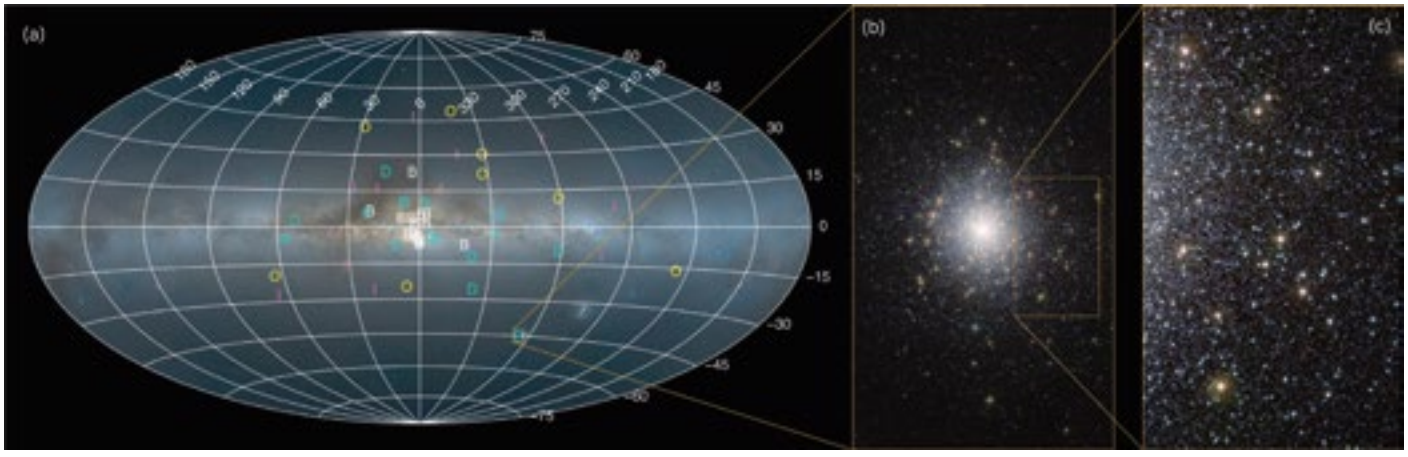

Figure 1. (a) All-sky view centred on the Milky Way Plane in an Aitoff projection from Mellinger (2009) with a Galactic coordinate grid. The globular clusters studied here are identified by letters according to their populations, namely (B)ulge, (D)isc, (I)nner halo, and (O)uter halo. (b) Zoomed-in image of the globular cluster 47 Tucanae (near-infrared image taken with VISTA: ESO image eso1302a), which can be seen with the naked eye in a dark sky. (c) Detail from the same image as (b) of an outer region of 47 Tucanae, showing its brightest bluer and redder stars; the latter stars were analysed in this work.

stars (Carretta et al., 2009). Furthermore, high-resolution spectroscopic metallicities are available for only ~ 25 % of them (Pritzl et al., 2005). Not only is this number of clusters low but the sample is biased, given that it includes only a few metal-rich Bulge clusters.

We selected 51 globular clusters that represent well the Milky Way Bulge, Disc, and Halo populations, and which cover the full range of metallicity, total mass, distance and reddening values, in order to increase the statistics and generate an unbiased sample. In particular, the cluster red giants in half of our sample are very faint owing to substantial foreground dust or large distances, and are therefore poorly studied (Dias et al., 2016). The present work increases to ~ 70 % the fraction of clusters with known spectroscopic metallicity derived on the same scale.

High-resolution spectroscopic observations would be too time-consuming if devoted to the sample of about 800 red giant stars in 51 globular clusters that we have studied, especially for the fainter targets. We instead used a lower resolution (R ~ 2000) spectrograph, which consequently allows higher signal-to-noise ratios to be achieved with lower integration times. This approach also enables us to observe more targets and have a more complete sample, including fainter targets. For the analysis we were able to apply full-spectrum fitting that is intrinsically reddening-free (Dias et al., 2015). The method has the advantage that it can be applied to red giants in extragalactic globular clusters in the future.

FORS2 data

The FOcal Reducer / low dispersion Spectrograph (FORS2) in its medium-resolution and multi-object mode (Appenzeller et al., 1998) is consequently more suitable for our purposes than the Fibre Large Array Multi Element Spectrograph (FLAMES) facility (Pasquini et al., 2002) combined with the Ultra-violet Visible Echelle Spectrograph (UVES). The first question that arises is: are we losing precision in the determination of chemical abundances with this choice? We were able to derive metallicities from FORS2 spectra in very good agreement with UVES metallicities

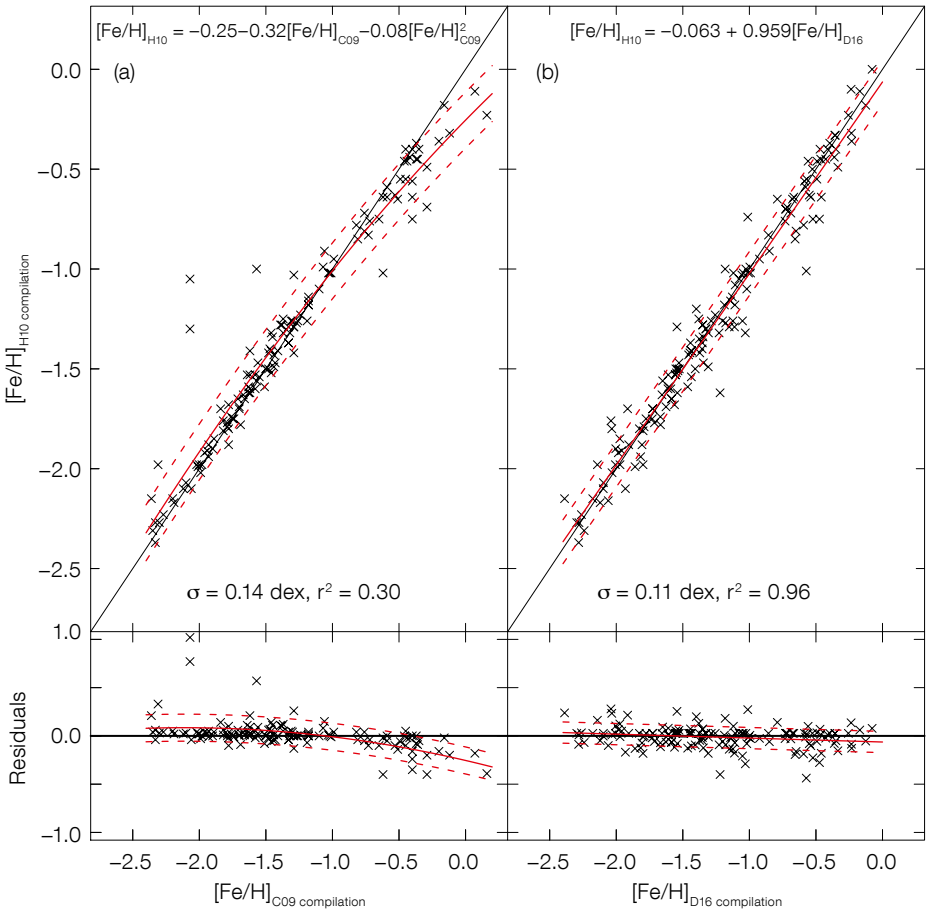

Figure 2. (a) Comparison of metallicities of 132 clusters common to the metallicity scales of Carretta et al. (2009) and Harris (1996), C09 and H10 respectively. The best fit and 1σ limits are shown by red continuous and dotted lines, respectively. (b) The same as (a) but for 151 clusters common to our abundance scale (Dias et al., 2016a) and that of Harris (1996). Details of the fits are given in each panel.

for the globular clusters in common: the root mean square of the differences is within 0.08dex and presents no trend with abundance. Therefore there is no need to re-calibrate our FORS2 results (Dias et al., 2016).

Carretta et al. (2009) applied their metallicity scale, based on UVES data, to all previous sets of cluster metallicity and averaged them. Their scale is limited in the metal-rich tail because they did not observe clusters in this regime. Harris (1996) produced a compilation of cluster metallicities based on spectroscopy and photometry, and made an effort to put them all on a homogeneous scale, similarly to Carretta et al. We followed the same steps, with the advantage that we have 51 clusters in our sample (compared to 19 for Carretta et al.) as references for scaling previous work. Importantly, our clusters cover the full metallicity range: the catalogue of globular cluster abundances can be downloaded[1]. Figure 2 shows good agreement between our compilation of abundances and those from Harris, with a mild linear trend that should be applied to the Harris (1996) values. The comparison with Carretta et al. confirms the discrepancy for the metal-rich clusters as expected, and reveals a few outliers. We have increased the fraction of clusters with known (spectroscopic and photometric) metallicities from 84 % (Carretta et al.) to 97 % of the total Milky Way globular cluster sample, improving coverage of the metal-rich tail.

Field versus cluster stars

It has been known for quite some time that the ratio of α-elements over iron [α/Fe]

is larger at the beginning of a galaxy's life, as a result of early chemical enrichment by core-collapse supernovae. Some time later, estimated to be around 0.5 to 2 Gyr, thermonuclear type Ia supernovae produce large amounts of iron, which causes [α/Fe] to decrease. The time when the second event starts to be important is a key piece of information for understanding the efficiency of star formation in a galaxy. In the case of the Milky Way, the chemistry of field stars indicates a timescale of about a billion years as indicated by the depletion in [α/Fe] (e.g., Matteucci & Recchi, 2001). Nevertheless, not all α-elements are expected to behave in the same way. For example, the lighter element magnesium is produced in hydrostatic phases of massive star evolution, whereas the heavier elements calcium and titanium result from explosive nucleosynthesis (see, for example, McWilliam, 2016). If we compare the nucleosynthesis yields from core-collapse and thermonuclear supernovae, the contrast of [Mg/Fe] between the two episodes is larger than the contrast of [Ca/Fe] and [Ti/Fe] (Pagel, 1997).

This difference is noticeable in field star distributions, but globular clusters seem to have a constant [Mg/Fe] and [<Mg,Ca,Ti>/Fe] ratio for any given metallicity, despite their age range of a few billion years (see the literature compilation by Pritzl et al., 2005). A possible reason for the disparity is that the thermonuclear supernovae that affected field stars did not occur before all stars in globular clusters were formed. Our homogenous abundances for 51 clusters suggest the different trends of [Mg/Fe] and [<Mg,Ca,Ti>/Fe], as expected.

It is important to point out that many of the α-elements are electron donors, and their excess adds electrons, and therefore H^- opacity. Besides the true α-elements, Al behaves as an α-element in the Galactic Bulge, being an important electron donor. Such effects have to be taken into account when computing abundances in stellar atmospheres, as done in Coelho et al. (2005) whose approach we adopted. Possibly the high dispersion of α-element abundances from Pritzl's compilation was hiding trends that are now revealed by our results with lower dispersion (see Figure 3). Our

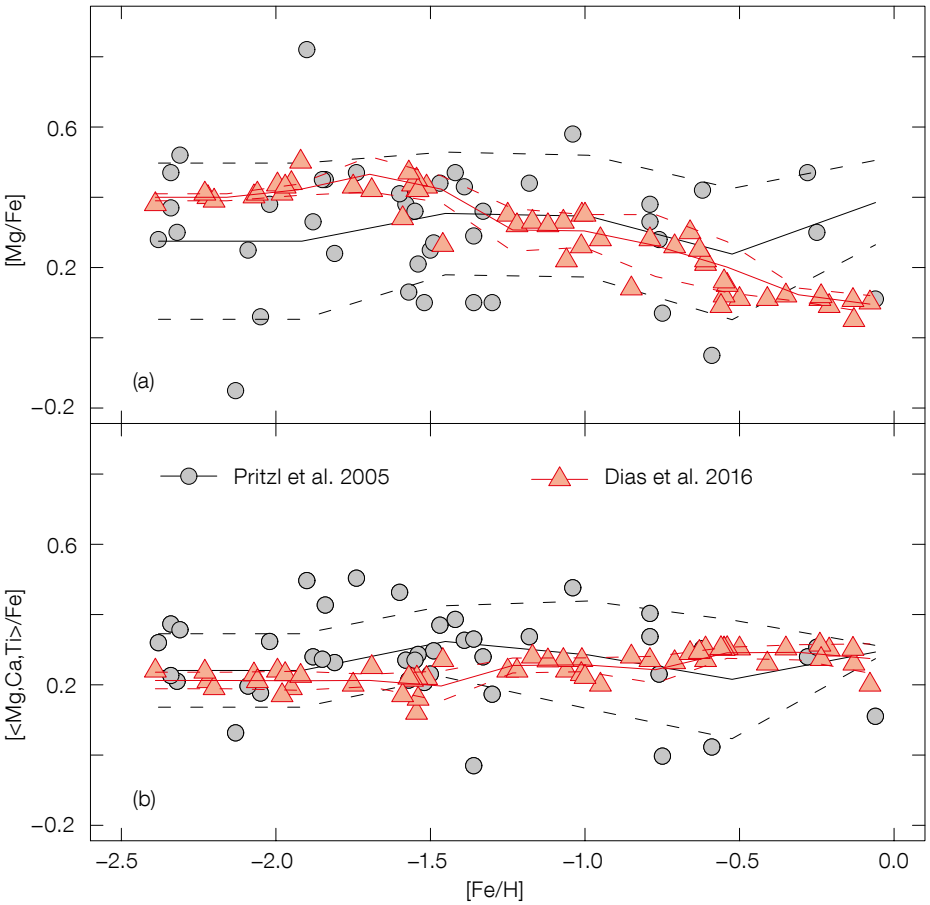

Figure 3. (a) Distribution of enhancement of magnesium versus total metallicity for globular clusters from Pritzl et al. (2005) in grey (with the fit shown by a black line and the 1σ error bands by dashed lines), contrasted with our results (Dias et al., 2016) in pink (with fit and error bounds as red solid and dashed lines, respectively). (b) Same as (a) but for the average of enhancements of three α-elements: magnesium, calcium, and titanium.

contrasting results beg the question: is chemical enrichment by supernovae for field and cluster stars correlated?

Extragalactic globular clusters

Since our strategy of employing low-resolution spectroscopy has succeeded for faint stars in distant and highly reddened Milky Way clusters, we can certainly follow the same steps to observe red giants in nearby galaxies to understand their formation and early evolution using a similar array of techniques. In the era of extremely large telescopes, this strategy can be extended to many nearby galaxies.

References

Appenzeller, I. et al. 1998, The Messenger, 94, 1
Carretta, E. et al. 2009, A&A, 508, 695
Dias, B. et al. 2015, A&A, 573, 13
Dias, B. et al. 2016, A&A, 590, 9
Eggen, O. J., Lynden-Bell, D. & Sandage, A. R. 1962, ApJ, 136, 748
Gratton, R., Sneden, C. & Carretta, E. 2004, ARA&A, 42, 385
Gratton, R., Carretta, E. & Bragaglia, A. 2012, A&ARv, 20, 50
Harris, W. E. 1996, AJ, 112, 1487 (2010 edition)
Matteucci, F. & Recchi, S. 2001, ApJ, 558, 351
McWilliam, A. 2016, PASA, submitted, arXiv:1607.05299
Mellinger, A. 2009, PASP, 121, 1180
Pagel, B. E. J. 1997, *Nucleosynthesis and Chemical Evolution of Galaxies*, CUP
Pasquini, L. et al. 2002, The Messenger, 110, 1
Pritzl, B. J., Venn, K. A. & Irwin, M. 2005, AJ, 130, 2140
Saviane, I., Held, E. V. & Da Costa, G. S. et al. 2012, The Messenger, 149, 23
Searle, L. & Zinn, R. 1978, ApJ, 225, 3

Links

[1] Access to catalogue of abundances: http://www.sc.eso.org/~bdias/catalogues.html

Connecting the Dots: MUSE Unveils the Destructive Effect of Massive Stars

Anna Faye McLeod[1]
Adam Ginsburg[1]
Pamela Klaassen[2]
Joseph Mottram[3]
Suzanne Ramsay[1]
Leonardo Testi[1,4]

[1] ESO
[2] UK Astronomy Technology Centre, Edinburgh, United Kingdom
[3] Max-Planck-Institut für Astronomie, Heidelberg, Germany
[4] INAF Osservatorio di Arcetri, Florence, Italy

Throughout their entire lives, massive stars have a substantial impact on their surroundings, such as via protostellar outflows, stellar winds, ionising radiation and supernovae. Conceptually this is well understood, but the exact role of feedback mechanisms on the global star formation process and the stellar environment, as well as their dependence on the properties of the star-forming regions, are yet to be understood in detail. Observational quantification of the various feedback mechanisms is needed to precisely understand how high mass stars interact with and shape their environment, and which feedback mechanisms dominate under given conditions. We analysed the photo-evaporative effect of ionising radiation from massive stars on their surrounding molecular clouds using MUSE integral field data. This allowed us to determine the mass-loss rate of pillar-like structures (due to photo-evaporation) in different environments, and relate it to the ionising power of nearby massive stars. The resulting correlation is the first observational quantification of the destructive effect of ionising radiation from massive stars.

Pillar-like structures are a ubiquitous feature of massive star-forming regions. The ionising radiation from young and nearby high mass stars is not only responsible for the inflation of H II regions, but also for shaping, compressing and destroying the surrounding molecular clouds. Whether these pillar-like structures form from pre-existing dense structures within the clouds, which are then exposed by stellar feedback, or via gas compression and subsequent instabilities (for example, Gritschneder et al., 2010; Tremblin et al., 2012) is still debated. However, these structures, which typically point back into the HII region towards the feedback-driving massive stars, are seen in both observations and simulations of massive star-forming regions. They are found to lose mass as the ionising radiation to which they are exposed gradually destroys them. This process happens via photo-evaporation, in which the surface layer of the pillar material (composed of dust and molecular gas) is ionised and heated and as a consequence streams away from the pillar surface in a so-called photo-evaporative flow (Hester et al., 1996). This phenomenon was already described with analytical models some twenty years ago (Bertoldi, 1989; Lefloch & Lazareff, 1994), but a quantitative observational test of such models has been lacking so far.

Previous observations of the Pillars of Creation in M16 (McLeod et al., 2015) with the Multi Unit Spectroscopic Explorer (MUSE) demonstrated that the instrument is ideal for the determination of the mass-loss rate from cloud structures due to photo-evaporation, as the simultaneous optical imaging and spectroscopy yield information on both the morphology and kinematics of the ionised evaporating material. The analysis of the M16 pillars was not, however, sufficient to achieve the ultimate goal of determining the connection between the ionising stars and the mass-loss rate due to photo-evaporation. What is needed is a systematic study of pillar-like structures in different star-forming regions, which are subject to different ionising fluxes and are found in different Galactic environments. We obtained such a sample by combining the M16 dataset with MUSE observations of other pillars in the Milky Way — in NGC 3603 and the Carina Nebula Complex. The full analysis is presented in McLeod et al. (2016).

The sample

In order to sample photo-evaporating pillar-like structures in different environments, we combine MUSE data of three different star-forming regions. These regions differ in terms of their massive star content, as well as location within the Galaxy. All of the observed pillars show ionisation fronts at their tips as they are exposed to the radiation from the nearby massive stars (or star clusters).

The M16 pillars are shown in Figure 1 and lie at ~ 2 pc projected distance south-west of the massive star cluster NGC 6611, which contains about 13 O-type stars (Evans et al., 2005). M16 is situated at a distance of about 2 kpc from the Sun. These pillars can be divided into four different structures with different inclinations towards the observer and different distances along the line of sight. By estimating the mass of the photo-evaporative flow from the sulphur emission, we find these structures to have an expected remaining lifetime of about 3 Myr (McLeod et al., 2015).

At a distance of about 6.9 kpc, NGC 3603 is one of the most massive star-forming regions in the Galaxy, and contains over 30 O-type stars (Melena et al., 2008) in a centrally condensed region surrounded by a bright nebula. There are two parsec-scale pillars about 1 pc away from the central cluster. The south-east pillar was observed with MUSE during Science Verification with a single pointing (Figure 2).

The Carina Nebula Complex (CNC), at a distance of 2.3 kpc, is a very rich and well studied star-forming region, which contains several massive young star clusters and is therefore an ideal region for the analysis of feedback from massive stars. We selected four regions containing pillar-like structures from the recent census presented in Hartigan et al. (2015) in the vicinity of the three main clusters of the CNC (Trumpler [Tr] 14, 15 and 16), in order to sample different conditions in the same region.

With about 10 and 18 O-type stars respectively, the younger clusters Tr 14 and 16 are more massive and more luminous than Tr 15, which boasts only 6 O-stars. Of the four regions, shown in Figure 3, R18 lies about 7 pc north-east of Tr 15, R37 about 4.1 pc north-east of Tr 16, and R44 and R45 are located at > 10 pc east of Tr 14 and Tr 16 respectively. This configuration greatly complicates the determination of the main

Figure 1. MUSE RGB composite of the emission of the pillars in M16 (red = [S II], green = Hα, blue = [O III]) from nine pointings covering an area 3 × 3 arcminutes. See McLeod et al. (2015) and ESO Photo Release eso1518.

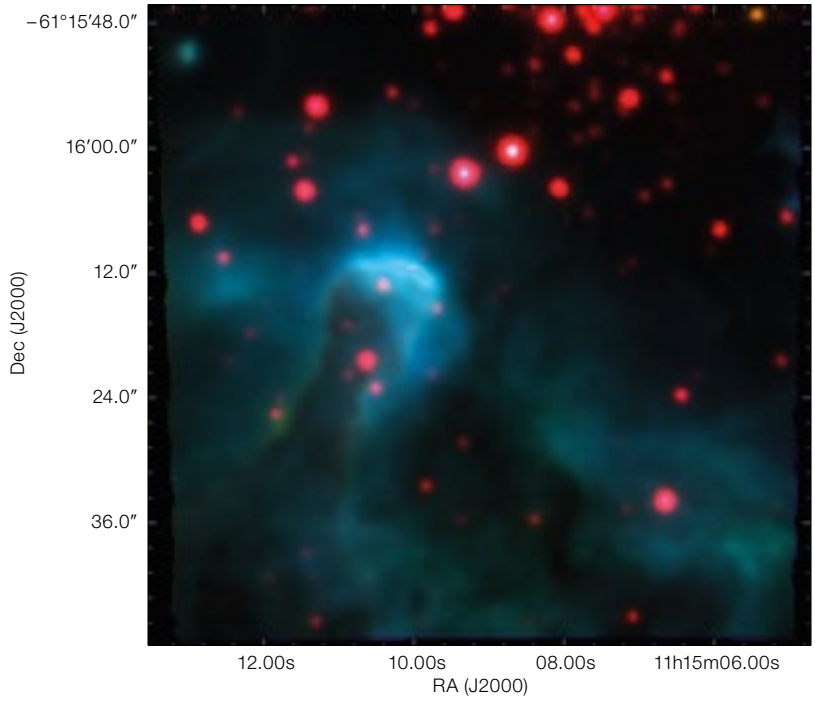

Figure 2. MUSE RGB composite of the pillar in NGC 3603 (same colour coding as Figure 1). The field is 1 × 1 arcminutes (single MUSE pointing).

ionising source for each pillar. However, as discussed below, the identification of the main ionising sources responsible for the photo-evaporation of the single pillars is of great importance and can be tackled by carefully analysing the spatial orientation of the pillars and the locations of their main ionisation fronts.

The sample of photo-evaporating ionised pillars thus consists of a total of ten objects in three different star forming regions, probing a broad range of radiation field conditions. Furthermore, the six pillars in the CNC are found around different massive clusters, therefore sampling different conditions within the same region.

Ionisation from nearby massive stars

The number of ionising photons reaching each pillar can be estimated from assumptions about which stars or star clusters are responsible for the feedback. Furthermore, we assume that the O-type stars dominate in terms of ionising photon flux, and therefore we do not consider the B-type stars. To determine the number of O-stars in each region we refer to population studies from the literature (see below) and convert the spectral types of the known O-stars to a photon flux Q_0 according to Martins et al. (2005). The isotropically emitted photon flux then needs to be scaled to the distance of the feedback-affected pillars, as well as the size of their exposed tips. For this step, we determine the solid angle subtended by the pillar tips with respect to the ionising sources, under the assumption that the pillar tips can be approximated as spherical caps.

In the case of NGC 3603 and M16, which host only one massive cluster each, we assume that the pillars are subject to the combined flux from all the O-stars in the

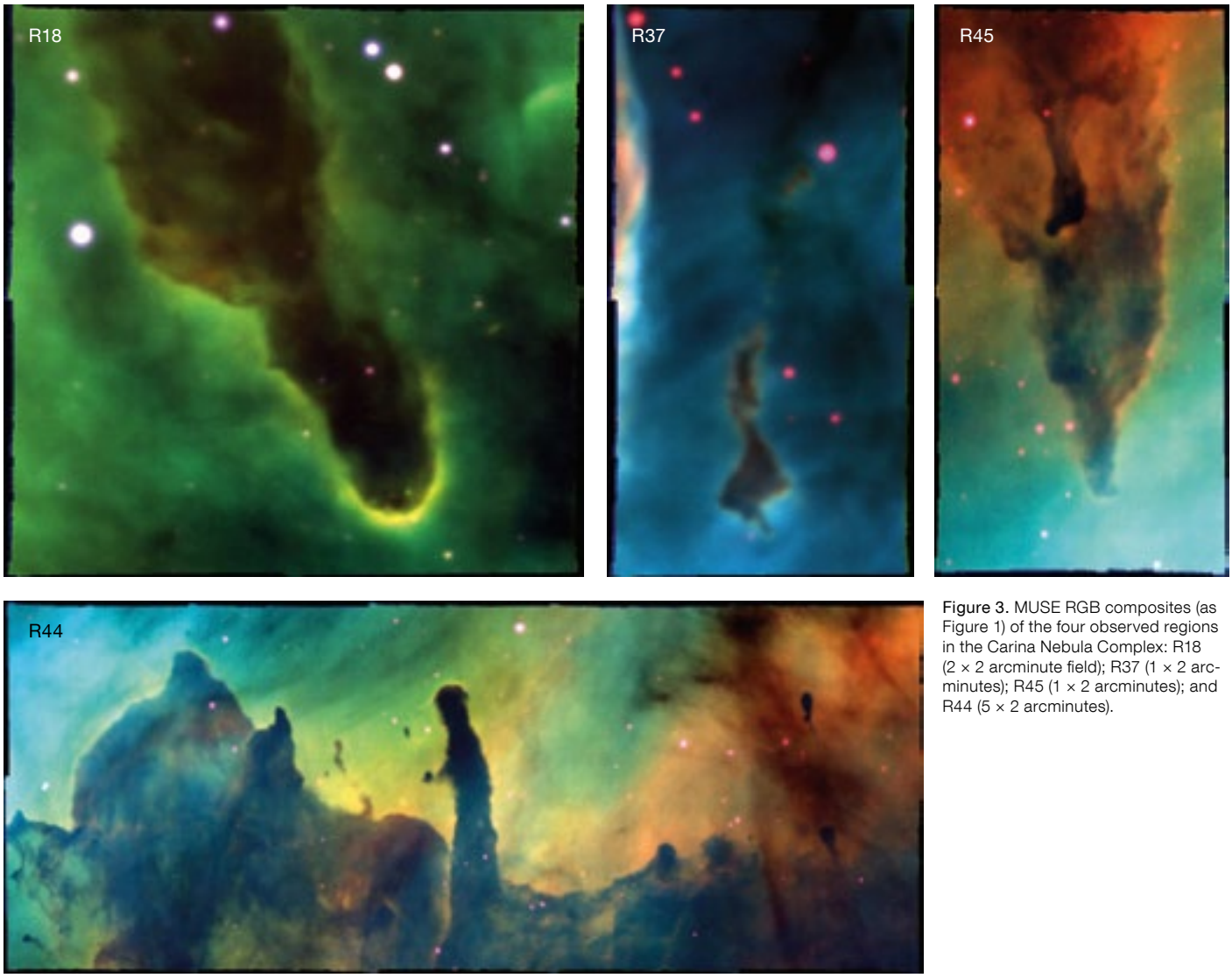

Figure 3. MUSE RGB composites (as Figure 1) of the four observed regions in the Carina Nebula Complex: R18 (2 × 2 arcminute field); R37 (1 × 2 arcminutes); R45 (1 × 2 arcminutes); and R44 (5 × 2 arcminutes).

nearby cluster. For the 33 O-type stars in NGC 3603 (Melena et al., 2008) we estimate log Q_0 ~ 50.98 s^{-1}, while for the 13 O-stars of NGC 6611 (Evans et al., 2005) we calculate log Q_0 ~ 49.87 s^{-1}. We then scale the photon flux Q_0 to the projected distance and size of the ionised pillar tips as described above to obtain the photon flux at the respective pillar tips, $Q_{0,pil}$. Values of $Q_{0,pil}$ can be found in Table 3 of McLeod et al. (2016).

For the pillars in the CNC, where multiple ionising star clusters are present within a few tens of parsecs of each other in the same star-forming region, particular care needs to be taken when determining which O-type stars affect which pillars. We combine the relative projected distances of each pillar in Carina with its orientation and ionisation structure (thus assuming that the orientation of the main pillar body is indicative of the origin of the incident radiation) to determine the ionising sources. The pillar in region 18 (R18 in Figure 3) is closest (~ 7 pc) to Tr 15 and points directly back towards the central coordinates of this cluster; we therefore considered the combined flux of the Tr 15 O-stars.

The globule in R37 is just 4.1 pc north of Tr 16, but points instead at two massive stars away from the cluster centre. These two, an O4 and a Wolf-Rayet star, have a combined photon flux of log Q_0 ~ 50.18 s^{-1}. The pillars in both R44 and R45 lie east of Tr 14 and Tr 16, but their orientation and ionisation fronts do not coincide with direct feedback from either of these clusters. Rather, the pillars in these two regions point in the direction of an O6 and an O9.5 star, which have a combined photon flux of log Q_0 ~ 49.02 s^{-1}.

Computing the mass-loss rate and connecting the dots

Next, we compute the mass-loss rate due to photo-evaporation using the expression given in Smith et al. (2004), which relates the radius of curvature r of the pillar cap, the proton mass m_H, the matter density N_H and the velocity of the ionised photo-evaporative flow $\mathbf{v}$. In order to compute N_H, we exploit the

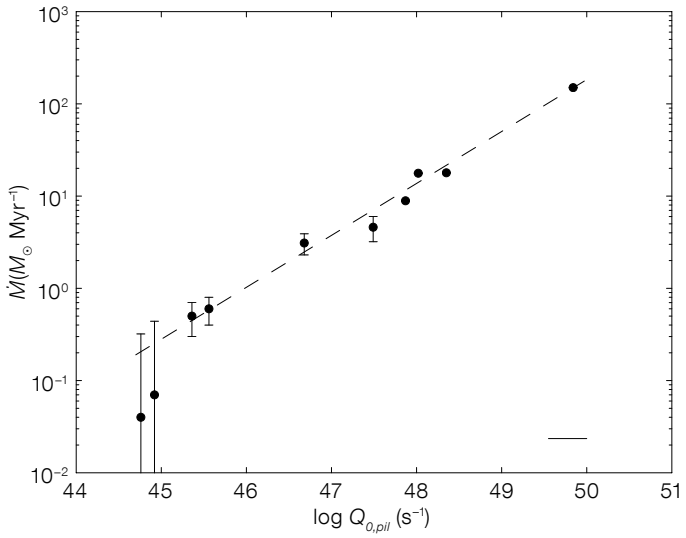

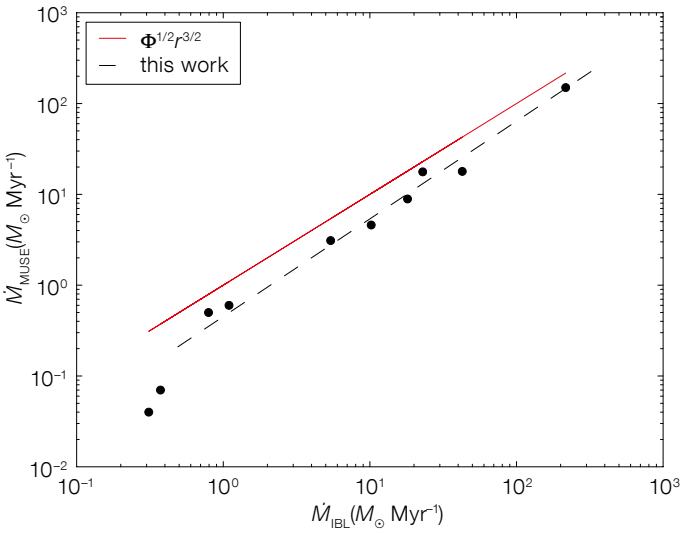

Figure 4. Left: The observed correlation between the ionising photon flux incident at the pillar tips ($Q_{0,pil}$) and the mass loss rate due to photo-evaporation. The dashed line indicates the best fit power law with index p = 0.56 ± 0.02, while the horizontal line indicates the average uncertainty in log $Q_{0,pil}$. Right: The empirically determined correlation (dashed line, this work) compared with the model by Lefloch & Lazareff (1994), indicated by the red line. Here, Φ is the ionising photon flux $Q_{0,pil}$ as scaled in the analytical model. and $\dot{M}_{IBL}$ the mass loss rate of the ionisation boundary layer (IBL).

MUSE coverage of the sulphur doublet [S II] 6717,6731 Å to produce maps of the electron density N_e (see McLeod et al., 2015), and by converting the value of N_e extracted from a circular aperture at the ionised pillar tips according to $N_e \sim 0.7\ N_H$ (Sankrit & Hester, 2000). The velocity of the ionised photo-evaporative flow is obtained by fitting the stacked spectrum[1] of the main emission lines within ~ 500 Å of the Hα line with a Gaussian fitting routine on a pixel-by-pixel basis, resulting in a velocity map for each region. In the velocity maps (see McLeod et al., 2016), the pillars are clearly distinguishable from the ambient matter, as they appear blueshifted with respect to the latter. The reason for this is that the photo-evaporative flow is normal to the surface of the pillars.

By relating the mass-loss rate computed for each individual pillar to the incident ionising photon flux $Q_{0,pil}$, we obtain a tight correlation between the two as shown in Figure 4 (left panel), which is best fitted with a power law of index p = 0.56. This is the first observational test of the analytical models describing photo-evaporation in ionised nebulae (Bertoldi, 1989; Lefloch & Lazareff, 1994), and indicates that objects that are subject to a lower ionising photon flux show lower mass-loss rates and therefore, if they have the same mass, have longer expected lifetimes.

We further compare our empirical result with the theoretical mass-loss rate derived in Lefloch & Lazareff (1994) and

Figure 5. The dependence of the electron density N_e on the ionising photon flux $Q_{0,pil}$ (left panel) and the projected distance, d, to the main ionising sources (right panel).

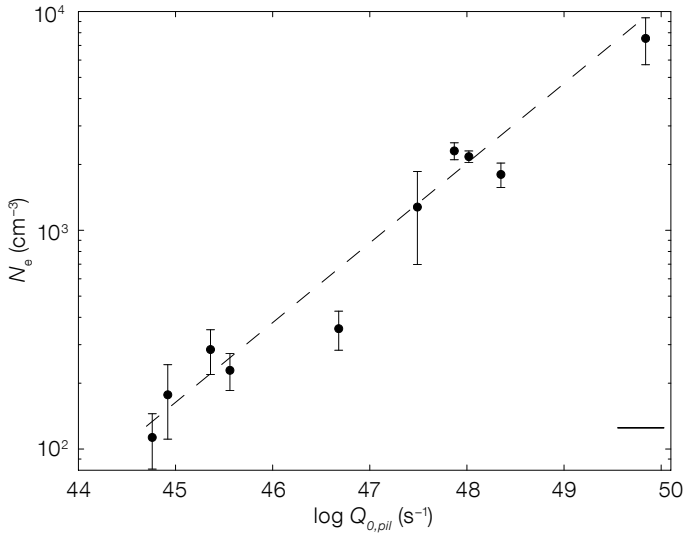

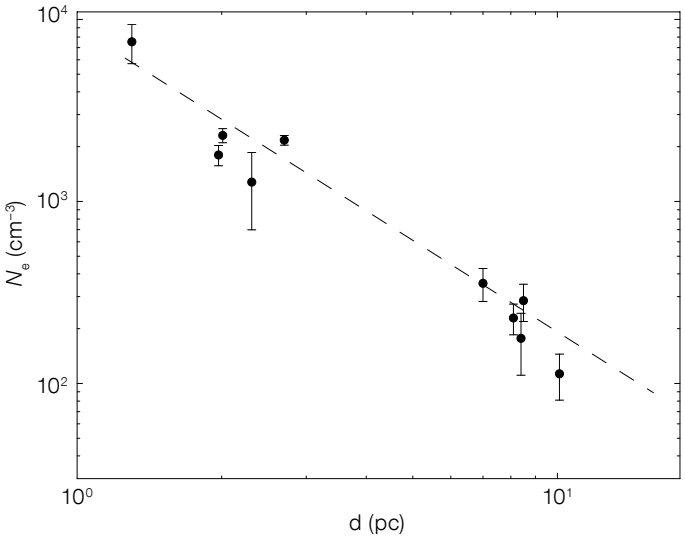

find very good agreement between the observations and the model, in which the mass-loss rate is proportional to $(Q_{0,pil})^{1/2}$ and $r^{3/2}$. The comparison with the model is shown in the right panel of Figure 4, where the mass-loss rates measured with MUSE are plotted against the values found for the so-called ionisation boundary layer (IBL). In the IBL picture, not all of the incident photons lead to ionisation at the pillar tip, as some of them are absorbed in the photo-evaporative flow to compensate recombination. The model and the observations differ by a factor of about two, which can be partly explained by the geometry of the pillar tips assumed for the computation of the mass-loss rate. This intuitively simple picture is, however, further complicated by the empirical dependence of the electron density (used to compute the mass-loss rate) on both the distance and the incident photon flux, as shown in Fig. 5. This dependence is not described by the models with which we compare our findings, and will require further investigation in order to fully disentangle the various dependencies.

These results deliver the first observational quantification of the effect of ionisation from massive stars which can be used to test models of feedback from such stars. This is a crucial step, as feedback from massive star formation represents, to date, one of the main uncertainties in galaxy evolution models, and observational constraints are needed in order to properly understand them and model the important physical mechanisms. The integral field spectrograph MUSE offers the possibility of performing simultaneous morphological and kinematical surveys of feedback-driven structures across different star forming regions. This approach not only yields uniform datasets from the same instrument, but also drastically improves on observations which can be expensive in terms of the necessary telescope time. Furthermore, MUSE also offers the possibility of both analysing the feedback-driven gas and identifying and classifying the feedback-driving massive stars. On account of these advantages, MUSE is an ideal instrument to trace feedback in massive star-forming regions.

References

Bertoldi, F. 1989, ApJ, 346, 735
Evans, C. J. et al. 2005, A&A, 437, 467
Gritschneder, M. et al. 2010, ApJ, 723, 971
Hartigan, P. et al. 2015, AJ, 149, 101
Hester, J. J. et al. 1996, AJ, 111, 2349
Lefloch, B. & Lazareff, B. 1994, A&A, 289, 559
Martins, F. et al. 2005, A&A, 436, 1049
McLeod, A. F. et al. 2015, MNRAS, 450, 1057
McLeod, A. F. et al. 2016, MNRAS, in press, arXiv:1608.00005
Melena, N. W. et al. 2008, AJ, 135, 878
Sankrit, R. & Hester, J. J. 2000, AJ, 535, 847
Smith, N. et al. 2010, MNRAS, 405, 1153
Tremblin, P. et al. 2012, A&A, 538, A31

Notes

[1] This is a necessary step, as the MUSE line spread function is undersampled and we therefore obtain a better sampled spectrum. Specifically, the lines used for this fit are Hα, [S II] 6717,6731 Å, [N II] 6548,6584 Å, [O I] 6300,6363 Å and He I 6678 Å.

ESO/G. Beccari

Wide field colour composite image, formed from broad-band filters (*B*, *V*, *I*) and narrow-band Hα, of the NGC 3603 Galactic star forming region taken with the MPG/ESO Wide Field Imager (WFI). Release eso1425 gives more information.

From ATLASGAL to SEDIGISM: Towards a Complete 3D View of the Dense Galactic Interstellar Medium

Frédéric Schuller[1]
James Urquhart[2,1]
Leonardo Bronfman[3]
Timea Csengeri[1]
Sylvain Bontemps[4]
Ana Duarte-Cabral[5]
Andrea Giannetti[1]
Adam Ginsburg[6]
Thomas Henning[7]
Katharina Immer[6]
Silvia Leurini[1]
Michael Mattern[1]
Karl Menten[1]
Sergio Molinari[8]
Erik Muller[9]
Alvaro Sánchez-Monge[10]
Eugenio Schisano[8]
Sümeyye Suri[10]
Leonardo Testi[6]
Ke Wang[6]
Friedrich Wyrowski[1]
Annie Zavagno[11]

[1] Max-Planck-Institut für Radioastronomie, Bonn, Germany
[2] Centre for Astrophysics and Planetary Science, University of Kent, United Kingdom
[3] University of Chile, Departamento de Astronomía, Chile
[4] Laboratoire d'Astrophysique de Bordeaux, University of Bordeaux, France
[5] School of Physics, University of Exeter, United Kingdom
[6] ESO
[7] Max-Planck-Institut für Astronomie, Heidelberg, Germany
[8] INAF, Istituto di Astrofisica e Planetologia Spaziali, Rome, Italy
[9] National Astronomical Observatory of Japan, Tokyo, Japan
[10] University of Cologne, I. Physikalisches Institut, Germany
[11] Laboratoire d'Astrophysique de Marseille, France

The ATLASGAL survey has provided the first unbiased view of the inner Galactic Plane at sub-millimetre wavelengths. This is the largest ground-based survey of its kind to date, covering 420 square degrees at a wavelength of 870 µm. The reduced data, consisting of images and a catalogue of > 10^4 compact sources, are available from the ESO Science Archive Facility through the Phase 3 infrastructure. The extremely rich statistics of this survey initiated several follow-up projects, including spectroscopic observations to explore molecular complexity and high angular resolution imaging with the Atacama Large Millimeter/submillimeter Array (ALMA), aimed at resolving individual protostars. The most extensive follow-up project is SEDIGISM, a 3D mapping of the dense interstellar medium over a large fraction of the inner Galaxy. Some notable results of these surveys are highlighted.

The ATLASGAL survey

Many large-scale imaging surveys of the Galactic Plane have recently been conducted. In particular, the Spitzer and Herschel space observatories have delivered an unprecedented view of the Galaxy in the near- to far-infrared range. Nevertheless, the global structure of the Milky Way (number of arms, position of the central bar) is still poorly constrained. Moreover, the life-cycle of interstellar matter is not yet understood in detail. We have made use of the high sensitivity sub-millimetre instruments installed at the Atacama Pathfinder EXperiment (APEX) telescope to conduct several large programmes, aimed at mapping the dense interstellar medium (ISM) on the scale of hundreds of square degrees.

ATLASGAL, the APEX Telescope Large Area Survey of the GALaxy (Schuller et al., 2009), mapped 420 square degrees of the inner Galaxy in sub-millimetre continuum emission. Observations started immediately after the successful commissioning of the Large APEX BOlometer CAmera (LABOCA; Siringo et al., 2009), in 2007. Data were collected until 2010. In total, this project used 420 hours of telescope time, shared between ESO, Max-Planck and Chilean time.

The LABOCA data were reduced using the dedicated bolometer analysis (BoA) software; details can be found in Schuller et al. (2009). The most critical step in the processing of ground-based sub-millimetre continuum data is the removal of the sky emission, which is several orders of magnitude brighter than even the brightest astronomical source. Since uniform, extended astronomical emission on spatial scales comparable to the instrument field of view mimics the variations in sky emission, it is also filtered out during the sky removal process. Thus, uniform emission on scales larger than a few arcminutes cannot be properly recovered at this stage. However, the lost information on the distribution of diffuse emission can be recovered by combining the ground-based data with maps observed from space; this is discussed in more detail later.

The astrometric accuracy of the ATLASGAL maps is better than 4 arcseconds, as derived from the dispersion of the offsets measured on reference pointing sources. The uncertainty of the flux density calibration is estimated to be lower than 15 %. The root mean square (rms) noise level measured in the emission maps is generally in the range 50–80 mJy/beam, but varies between maps due to weather conditions and the number of times a given area was covered; these variations are illustrated in Figure 1.

The continuum emission measured at 870 µm mostly originates from thermal dust emission, which is almost always

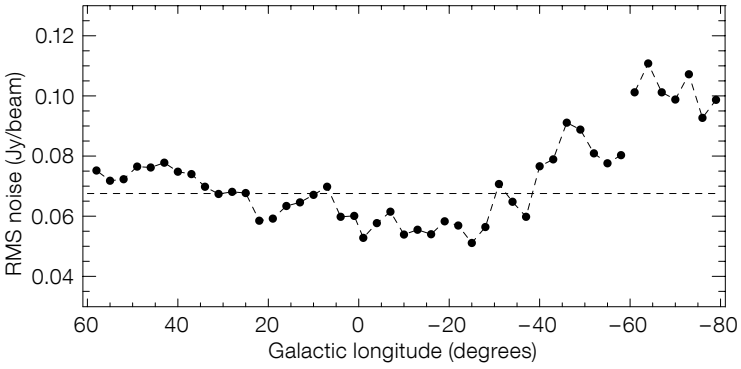

Figure 1. Variation of the RMS noise level with Galactic longitude for the ATLASGAL survey. The average value (68 mJy/beam) is indicated by the horizontal dashed line.

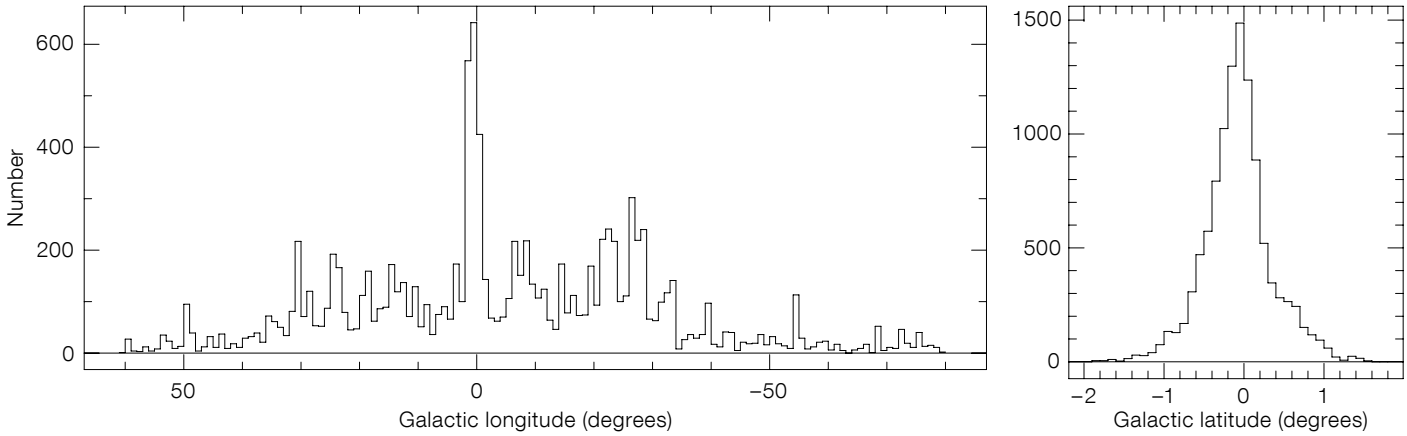

Figure 2. Distributions of ATLASGAL compact sources in Galactic longitude (left) and Galactic latitude (right).

optically thin in the sub-millimetre regime. Therefore, the measured flux density can be directly converted to a total column density along the line of sight. Using typical dust properties and a temperature of 20 K, the ATLASGAL 5-σ sensitivity (250 mJy/beam) corresponds to an H_2 column density of ~ 1 × 10^{22} cm^{-2}, equivalent to 10 magnitudes of visual extinction. When distances are known, the integrated flux densities can also be converted to masses: the ATLASGAL survey is sensitive to cold cores with masses below 1 $M_\odot$ at 500 pc, and can detect all cores more massive than ~ 100 $M_\odot$ at the distance of the Galactic Centre. It is complete across the inner Galaxy to dense clumps more massive than 1000 $M_\odot$.

After completion of a Large Programme like ATLASGAL, the legacy survey data products are ingested into the Phase 3 infrastructure of the ESO Science Archive Facility to make them available to the scientific community[1]. We adapted the headers of the ATLASGAL images and the catalogue files to conform to the ESO standards. The files were then uploaded to the ESO archive in January 2016. The weight maps, source masks and catalogue files are all included in the archive. A press release[2] announced the completion of the ATLASGAL survey and the availability of the data products. The data can also be retrieved from the dedicated server hosted at MPIfR[3], where cut-out images and complementary data at other wavelengths are also available.

Compact sources

Two compact source catalogues have been extracted from the data: the Compact Source Catalogue (CSC) was built using the SExtractor program (see Contreras et al., 2013 and Urquhart et al., 2014a for details); the GaussClump Source Catalogue (GCSC; Csengeri et al., 2014) was generated by running the GAUSSCLUMPS algorithm on modified versions of the images, where emission extended on scales larger Than ~ 100 arcseconds has been filtered out using a wavelet decomposition. Therefore, the GCSC is better suited for characterising compact sources, even those embedded within diffuse interstellar material, while the CSC provides a better estimate of the total emission along any given line of sight, and it also contains more extended clumps. The total number of sources is 10 861 in the GCSC, and 10 163 in the CSC.

The distribution of all CSC sources in Galactic coordinates is shown in Figure 2. The distribution in Galactic longitude shows a strong peak towards the Galactic Centre, while the median of the latitude distribution is at −0.08°, significantly below the Galactic mid-plane. The distributions of integrated fluxes from both catalogues are shown in Figure 3. On average, fluxes from the GCSC are lower than those measured on CSC sources, which can be explained by the filtering of extended emission performed on the images before the extraction of the GCSC sources.

The ATLASGAL CSC catalogue has been cross-matched with a number of surveys that have specifically searched for young massive embedded stars, for example the Red MSX Source (RMS) survey, the 5 GHz VLA CORNISH survey, and the methanol multi-beam (MMB) survey. This has produced a large and representative

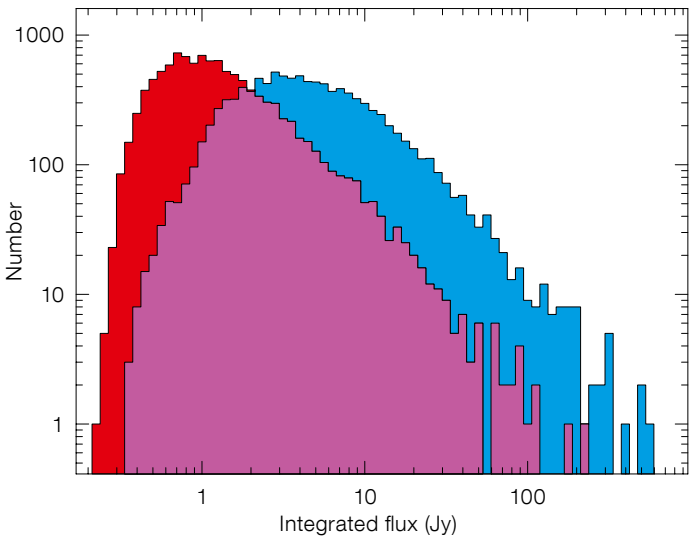

Figure 3. Distribution of integrated fluxes for all ATLASGAL compact sources extracted with GAUSSCLUMPS (in red) and SExtractor (in blue).

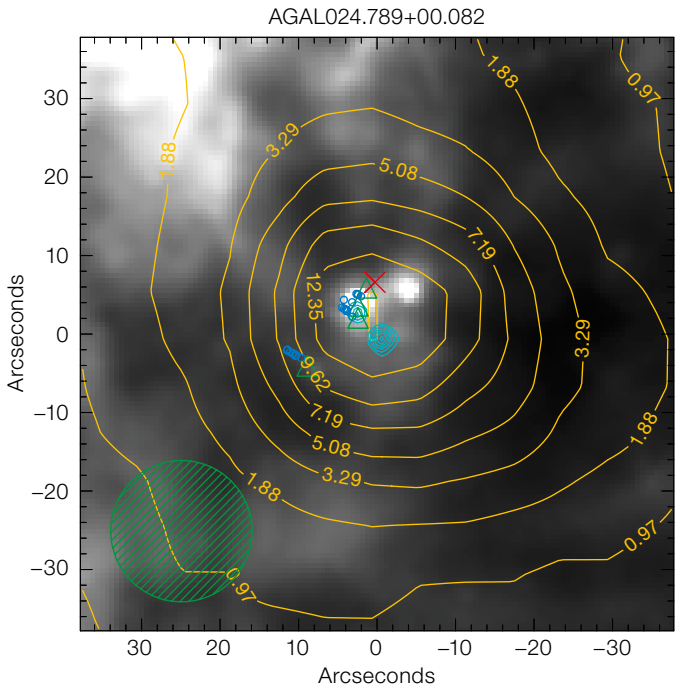

Figure 4. A typical example of a massive star-formation region hosting multiple evolutionary stages. The greyscale image is the 8 μm emission map from Spitzer, while the yellow and cyan contours trace the ATLASGAL 870 μm dust and 5 GHz radio continuum emission, respectively. The contour labels give the sub-millimetre flux in Jy. The blue circles, green triangles and red cross mark the positions of water masers, methanol masers, and the massive young stellar object, respectively. The LABOCA beam is shown with a dashed circle in the lower-left corner.

sample of massive star-forming (MSF) clumps, ideal to study the properties of the embedded objects and their natal environments (Urquhart et al., 2014b). In total, we have identified ~ 1300 MSF clumps that cover the important stages of the formation of massive stars: from the formation of the protostar traced by the association with methanol masers; through the mid-infrared bright massive young stellar object (MYSO) stage; to the arrival on the main sequence and the formation of an H II region. Approximately a third of these MSF clumps are associated with two or more different evolutionary stages, illustrating the complexity of some of these regions (see Figure 4 for an example).

A comparison with less active clumps reveals that high mass star formation is strongly correlated with the regions of highest column density in spherical, centrally condensed clumps with masses ≥ 1000 $M_{\odot}$. We find no significant differences, however, between the samples of methanol masers, MYSOs and H II regions in the structure of the clumps or the relative locations of the embedded stars with respect to the peak column density within the clumps. This suggests that massive stars tend to form towards the centre of their host clumps and that the structure of the clump is set before the onset of star formation and changes little as the embedded object evolves towards the main sequence (see Urquhart et al., 2014b for more details).

Analysis of the physical properties of the clumps does reveal systematic increases in the temperatures, luminosities and the amount of turbulence present in the gas as a function of evolution of the embedded objects, indicating that feedback from the embedded stars is having an impact on their local environment. We also find a strong linear correlation between the clump mass and the bolometric luminosity, with the most massive stars forming in the most massive clumps. Comparing the luminosities of the embedded compact H II regions and MYSOs to the expected cluster luminosity, we find they are underluminous, indicating that the lower mass companions have yet to form and suggesting a scenario where the high mass stars in a cluster form first.

Extended emission

As a blind survey, ATLASGAL provides a unique dataset from which to compile an unbiased catalogue of filamentary structures throughout the Galaxy. Li et al. (2016) used the survey images to identify filament candidates in the Galactic Plane through their continuum emission at 870 μm. They identified more than 500 filamentary structures, with lengths between ~ 2 and 20 pc. High-mass star formation seems to be ongoing within 20 % of these filaments, preferentially within the ones with the largest mass-to-length ratios. Moreover, these filaments are predominantly aligned with the Galactic Plane, and associated with the spiral arms. This seems to indicate a direct link between star formation activity and large scale Galactic structure.

On even larger scales, combining ATLASGAL with data from space-based telescopes allows us to recover the extended emission that is filtered out by the processing of ground-based observations. We used the data from the Planck HFI instrument to build maps tracing the distribution of cold dust in the Galactic Plane with an excellent spatial dynamic range, and with an angular resolution ~ 2 times better than the space-based data (Csengeri et al., 2016a). This comparison allowed us to estimate the dense gas fraction in the Galactic Plane; we find an average value of ~ 2 % for the Galaxy. Using simple but realistic assumptions, we could also convert the total flux density measured in the maps to a total mass of molecular gas in the inner Galaxy, finding ~ 1 × 10^9 $M_{\odot}$, consistent with previous estimates based on CO emission maps (see Heyer & Dame, 2015 for a recent review). Finally, from the total mass and the dense gas fraction, we can estimate an average Galactic star formation rate of ~ 1.3 $M_{\odot}$yr^{-1}.

Resolving massive clumps with ALMA

In order to better understand the origin of high-mass stars and rich clusters, the earliest phases of star formation need to be characterised in detail. The rich statistics of massive clumps provided by ATLASGAL have allowed us to define a sample of the youngest massive clumps in the inner Galactic Plane. These are the best targets for follow-up observations at sub-arcsecond resolution with ALMA to reveal their protostellar content.

Altogether 46 massive clumps were targeted, where precursors of O-type stars are expected to form. Preliminary results indeed confirm that these massive clumps are associated with the earliest stages of high-mass protostars, and reveal a sample of the most massive dense cores

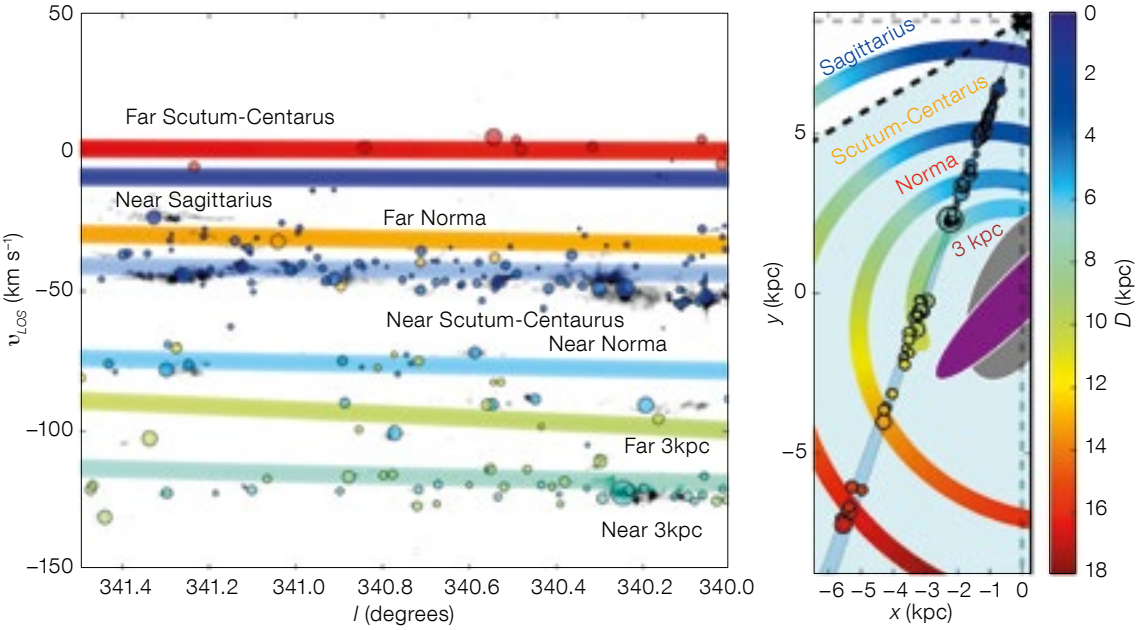

Figure 5. Left: longitude-velocity plot of the peak ^{13}CO(2–1) intensity in the science demonstration field (greyscale), overlaid with the positions of the molecular clouds extracted with SCIMES. The size of each dot is proportional to the computed mass of the cloud, and the colour indicates the assigned heliocentric distances (see the colour bar to the right). The positions of the spiral arms from an ad hoc model are also shown. Right: Top-down view of the Galaxy showing the SEDIGISM coverage (in turquoise), the different spiral arms, and the extracted molecular clouds (colours and sizes as in the left panel).

and protostars known to date (Csengeri et al., in prep.).

Spectroscopic follow-ups

Continuum observations can be affected by line-of-sight projection effects, which make it difficult to determine whether a detected structure is a single, coherent object. Spectroscopic follow-up observations are crucial to measure (local standard of rest) radial velocities (v_{lsr}) of objects detected in the continuum, and to determine their kinematic distances, essential for computing the masses and physical sizes of the clumps. Therefore, an extensive programme of follow-up observations in ammonia lines was started; such observations have the advantage of providing gas temperatures in the clumps, by combining the information about the simultaneously observed (1,1) and (2,2) ammonia inversion transitions. More than 1000 sources have been observed with the Effelsberg and Parkes telescopes (Wienen et al., 2012, 2015). Distances were determined based on the measured velocities and the analysis of archival HI data to resolve the distance ambiguities. The measured temperatures and line-widths track the evolution of the clumps. In addition, using the Herschel Space Observatory, water absorption lines from diffuse line-of-sight clouds towards ATLASGAL clumps were used to determine distances to infrared-dark clouds (Giannetti et al., 2015), leading to the surprising result that a fraction of those are situated in the far distance, and are therefore more massive than originally estimated.

Further spectroscopic follow-ups consist of millimetre line surveys of a few hundred clumps with the IRAM 30-metre, Mopra and APEX telescopes. Giannetti et al. (2014) analysed the CO isotopologue lines from these surveys to determine CO column densities and to study, in conjunction with the ATLASGAL dust column densities, the gas depletion in the clumps. This study revealed that CO depletion in high-mass clumps seems to behave as in the low-mass regime, with less evolved clumps showing larger values for the depletion than their more evolved counterparts, and increasing for denser sources. Finally, SiO, which is usually associated with shocks and traces ongoing star formation deeply embedded in the clumps, was found in a large fraction of the clumps (Csengeri et al., 2016b).

The SEDIGISM survey

Molecular line data not only provide a way to determine distances, but also deliver strong constraints on the gas excitation, chemical abundances, and the properties of interstellar turbulence. In order to complement existing molecular line surveys, such as the Galactic Ring Survey (Jackson et al., 2006) in the northern hemisphere, and older surveys at low angular resolution, we have undertaken the SEDIGISM survey (Structure, Excitation, and Dynamics of the Inner Galactic InterStellar Medium). It covers 78 square degrees of the southern Galactic Plane: $-60 \leq \ell \leq +18$ degrees, with $|b| \leq 0.5$ degrees, at 30 arcsecond resolution. The data cover the frequency range from 217 to 221 GHz, at 0.1 km s^{-1} resolution, which includes the ^{13}CO(2–1) and C^{18}O(2–1) lines. These lines are usually optically thin in the Galactic ISM, making them ideal tools to trace the cold, dense interstellar medium. The observations started in 2013, and were completed by the end of 2015. A dedicated reduction pipeline has been developed and the systematic processing of this prodigious amount of data (over 10^7 independent spectra) is ongoing.

Molecular clouds and giant complexes

Molecular line emission is crucial to reveal the 3D distribution of the gas in the Galaxy, and essential to link the compact dense gas clumps seen in the dust continuum emission of ATLASGAL to the large scales of giant molecular clouds and complexes that host them. In order to identify giant molecular clouds (GMCs), we have used the SCIMES algorithm (Colombo et al., 2015) on the ^{13}CO(2–1) data cube towards a science demonstration field, covering 1.5 square degrees.

We extracted a total of 182 molecular clouds, of which 58 are large complexes showing sub-structure. We have derived their kinematic distances using the Galactic rotation model of Brand & Blitz (1993), along with standard methods for resolving the ambiguity between near and far distances (e.g. the existence of H I self-absorption, infrared [IR] dark clouds, and parallax measurements in the literature). The distance distribution of these 182 molecular clouds traces the spiral structure of the Galaxy, providing an accurate view of the position of the near Scutum-Centaurus arm, the near and far Norma arm, and the near and far 3 kpc arm (Figure 5).

Having determined the distances to all the clouds, we estimated their physical properties: size, mass, surface density and virial parameter. We find that most clouds in our sample are stable, with a median virial parameter of ~ 2. We observe a trend of decreasing virial parameters with increasing cloud masses. A similar trend is observed for the dense clumps (as traced by ATLASGAL) embedded in the clouds. This indicates that the most massive clouds and clumps are the most gravitationally unstable, i.e. the most likely to collapse and form stars. Within the science demonstration field, we also find that 18 dense clumps (within 12 molecular clouds) are associated with high-mass star formation (HMSF) tracers; these tend to be among the most massive and unstable dense clumps and clouds of our sample (see Figure 6), and they are preferentially located within the spiral arms.

Although these are still preliminary results, based on ~ 2 % of the survey data, they demonstrate the potential of the full SEDIGISM survey as a high angular resolution spectral line survey to provide a detailed yet global view of the distribution of molecular clouds and star formation in the inner Milky Way.

Filamentary structures

The SEDIGISM data are perfectly suited for confirming the nature of filament candidates, and for separating structures overlapping along the line of sight, because the ^{13}CO(2–1) and C^{18}O(2–1) lines are excited in relatively low density gas, but are less affected by high opacities than lines from the main ^{12}CO isotopologue.

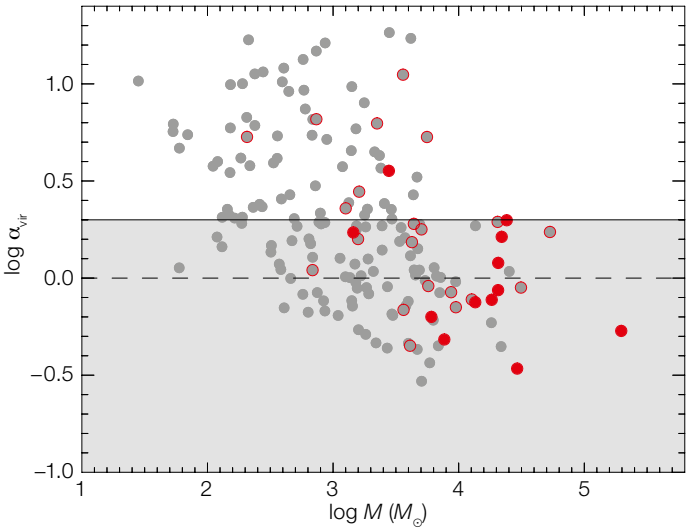

Figure 6. Virial parameter (α_{vir}) as a function of GMC mass. GMCs associated with high mass star formation (HMSF) tracers are indicated with red filled circles. GMCs with an ATLASGAL match but no HMSF tracer are shown as grey circles with a red outline. Grey shading indicates the region where clouds are unstable and likely to be collapsing.

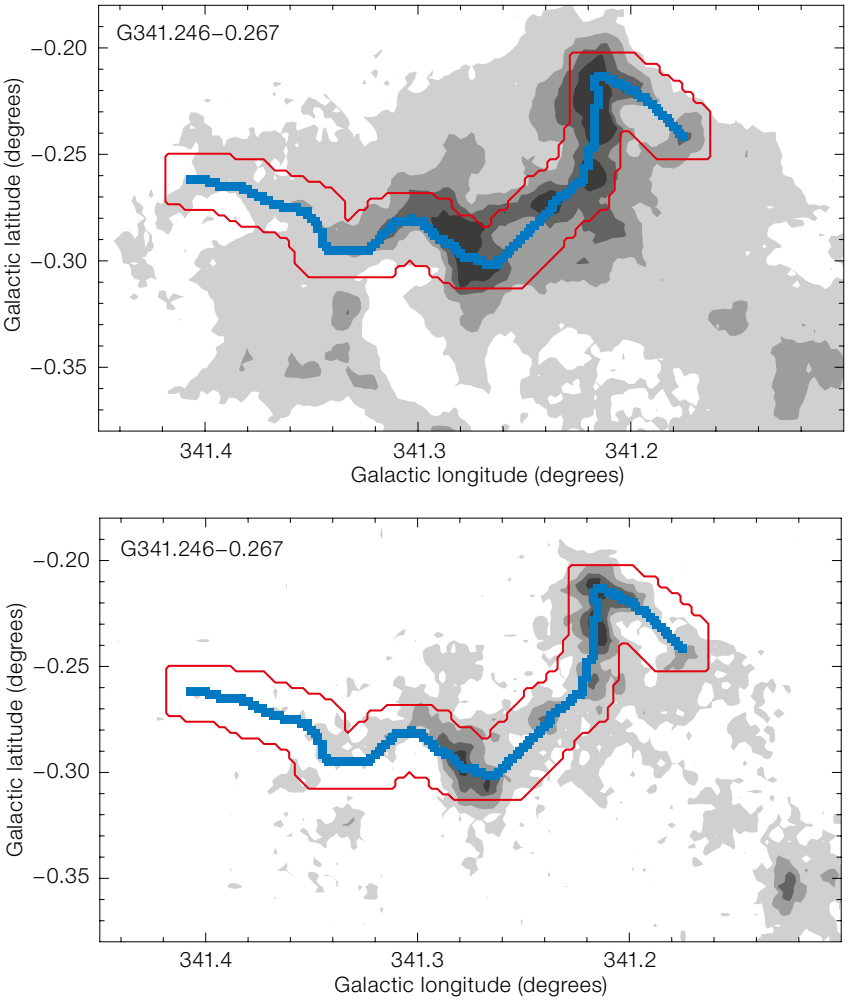

Figure 7. Emission maps of ^{13}CO(2–1) (upper) and C^{18}O(2–1) (lower) towards G341.246–0.267, integrated over the velocity range –48 to –41 km s^{-1}. The solid blue line marks the main spine of the filament identified on the ATLASGAL data. The thin red line marks the dilation box used to compute the length and the mass of the filament.

Moreover, molecular line data allow us to derive the distances and physical properties of the filaments: mass, size, velocity dispersion and line-to-mass ratio.

In Figure 7, we show the ^{13}CO(2–1) and C^{18}O(2–1) data for G341.246–00.267, one of the filament candidates extracted from ATLASGAL by Li et al. (2016). Using the SEDIGISM data, we first verified the coherence in velocity of the filament candidate. We analysed the velocity structure and compared the morphology of the molecular line emission with that of the dust to verify their association. For G341.246–00.267, we found a coherent structure at a central velocity of –44.6 km s^{-1}, with an emission line full width at half maximum (FWHM) of 3.6 km s^{-1}.

To estimate the mass of the filament, we integrated the ^{13}CO column density over the extent of the filament, both spatially and in velocity (see Figure 7). In order to compute column densities, we used a ^{13}CO(2–1)-to-H_2 X-factor that we derived from comparing the SEDIGISM data with a column density map built from Hi-GAL (Molinari et al. 2010). We found that $X^{13}CO(2–1) \approx 1 \times 10^{21}$ cm^{-2} (K km s^{-1})$^{-1}$ (see Schuller et al., 2016 for details). We then computed the mass of the filament by converting the H_2 column densities to total gas mass, using standard factors for the Galactic ISM. This results in a mass of 22.4×10^3 $M_\odot$ for G341.246–00.267, located at a distance of 3.6 kpc.

The gravitational stability of a filament can be inferred by comparing its mass per unit length, (M/l) with the virial mass per unit length given by twice the ratio of the 1-dimensional velocity dispersion squared of the average molecular gas and the gravitational constant, *G*. For the 21.3-pc-long filament G341.246–00.267, we measured a mass per unit length of 1050 $M_\odot$ pc^{-1}, or about twice the virial mass per unit length, which is 510 $M_\odot$ pc^{-1}. Therefore, the filament is critical and is likely to undergo radial collapse. However, our measurements of masses include several uncertainties: the X^{13}CO(2–1) factor has an uncertainty of at least a factor of two; additionally, opacity effects were not taken into account, which can lead to an underestimate of the true column density in the densest parts of the filament.

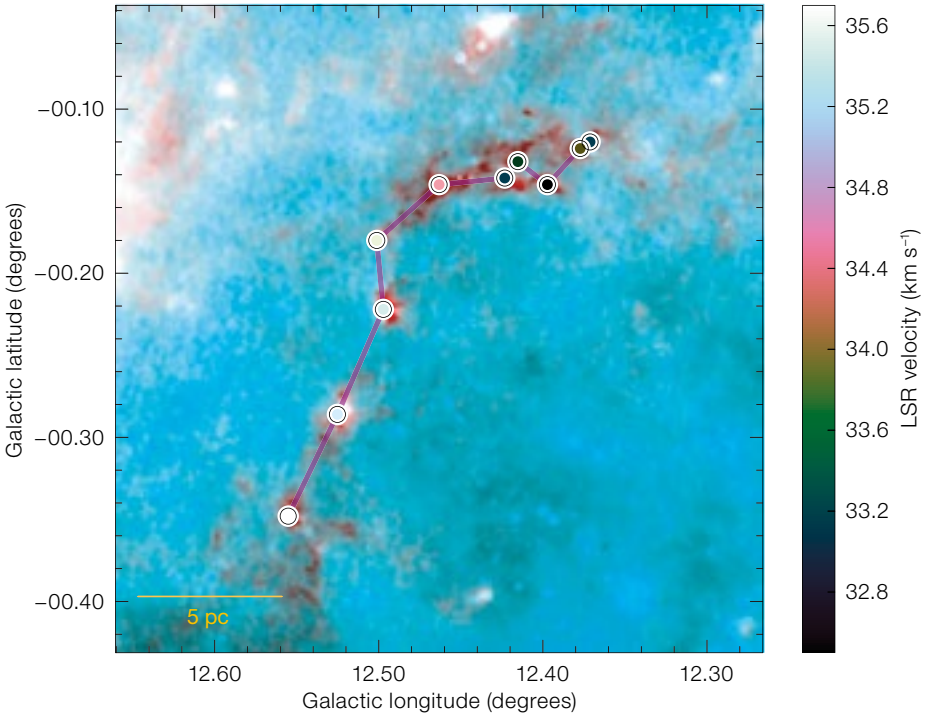

Figure 8. A two-colour view of an example filament identified by Wang et al. (2016). Cyan shows the Spitzer 24 µm emission on a logarithmic scale, and red shows the ATLASGAL + Planck 870 µm emission on a linear scale. The circles depict dense BGPS sources with fill colour coded velocity as shown by the colour bar. The filament is outlined by the connected BGPS sources (purple line).

The SEDIGISM data are likely to include many more filaments than those identified in the continuum images. The velocity information contained in spectroscopic datasets automatically solves the problem of blending of unrelated structures along the line of sight, which severely affects continuum surveys. We have used the DisPerSE algorithm (Sousbie, 2011) to directly search for filamentary structures in the ^{13}CO(2–1) data-cube for the science demonstration field. We identified 145 different velocity-coherent structures; 33 of them have an aspect ratio larger than five, making them the best filament candidates. While some of these filaments are also identified in the ATLASGAL continuum images, DisPerSE is sensitive to different structures, and in some cases it reveals that the filaments identified in the continuum are composed of several sub-structures. The typical lengths and widths of the filaments identified in the ^{13}CO data are 4.7–14.1 pc and 1.3–3.8 pc, respectively.

Recent studies have revealed some very long filaments in the Milky Way (e.g., Wang et al., 2015), with lengths up to ~ 100 pc. They are on the upper end of the filamentary hierarchy of the Galactic ISM. Their association with respect to the Galactic structure and their role in star formation are of great interest from both observational and theoretical points of view.

With SEDIGISM adding velocity information to the > 10^4 targets in the ATLASGAL compact source catalogue, the combined 3D position-position-velocity (PPV) catalogue will provide a valuable tool for extracting large-scale velocity-coherent filaments. Wang et al. (2016) have developed a new method to automate the filament-finding process from such 3D discrete data point collections. The method is based on a customised minimum spanning tree algorithm, which connects physically related voxels in PPV space (Figure 8). Applying this method to the Bolocam Galactic Plane Survey (BGPS) spectroscopic catalogue, Wang et al. (2016) have made the first census of the longest filaments in the northern Galactic Plane, where they identified 54 large-scale filaments, with masses in the range ~ 10^3 to 10^5 $M_\odot$, and lengths up to ~ 300 pc. The filaments concentrate along major spiral arms and are widely

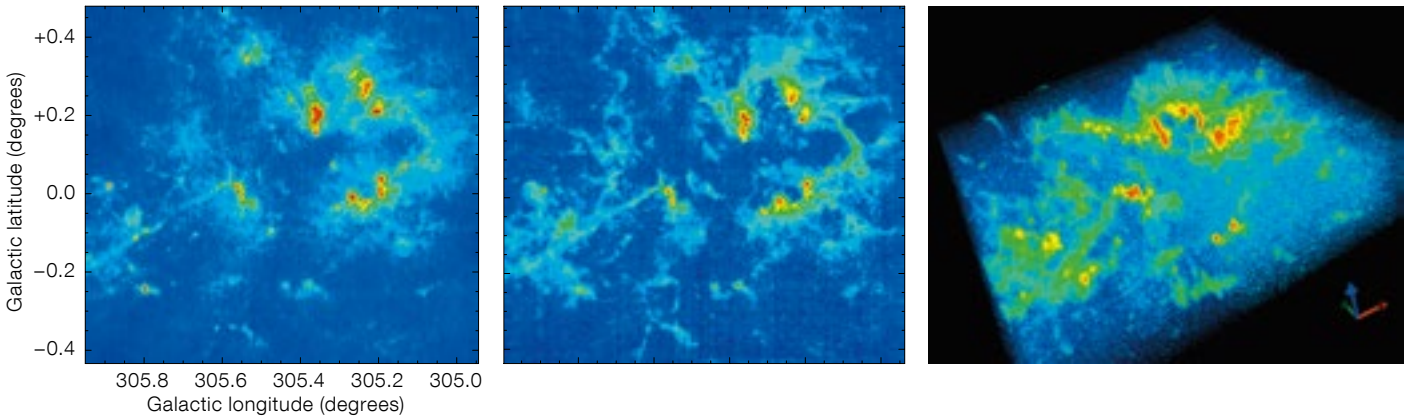

Figure 9. The G305 star-forming complex, as seen with ATLASGAL combined with Planck data (left). The middle panel shows the integrated ^{13}CO(2–1) emission observed with SEDIGISM, and the right panel shows a 3D rendering of the datacube, produced with the GLnemo2[4] interactive visualisation software.

distributed across the Galactic Disc, with 50% located within ± 20 pc of the Galactic mid-plane. 27 % of the filaments seem to run in the centre of spiral arms, and may form the "bones" of the Galactic structure. On the order of 1 % of the molecular ISM appears to be confined in large filaments. Statistically, the formation of massive stars seems to happen preferentially in large filaments.

Applying the same method to the ATLASGAL+SEDIGISM 3D source catalogue will allow us to complete the census of large filaments in the inner Galaxy, and to deliver a comprehensive filament catalogue, useful for a quantitative comparison with models of the Galactic spiral structure and numerical simulations.

Triggered star formation

Star formation is often observed at the edges of ionised (H II) regions. Recent statistical studies (for example Kendrew et al., 2016) have shown that these regions have a clear impact on their surroundings by promoting star formation. However, many questions remain about how this constructive feedback occurs. Studying the relation between the molecular material that surrounds H II regions and the young sources observed at their edges may help to answer some of the questions.

Molecular material is observed at the edges of H II regions distributed in a shell. The 2D or 3D distribution of this material is still debated (e.g. Beaumont & Williams, 2010). The 3D visualisation of molecular surveys offers a unique opportunity to make progress in this field, since it becomes possible to visualise the distribution of the different components (molecular, ionised, young sources and cores) along the line of sight and to investigate their relationship.

Figure 9 shows the distribution of the ^{13}CO(2–1) emission over the Galactic H II region G305. Seen face-on (middle panel), the CO emission surrounds the ionised gas. The molecular emission is highly structured with a large number of dense cores. These cores represent the potential sites of high-mass star formation. In 3D (right panel), the spatial distribution is revealed, spanning a range of more than 20 km s^{-1} in velocity. This example shows that the distribution of the densest material and clumps is strongly non-isotropic, suggesting that the interaction between the ionised gas and the surrounding medium can be more efficient under specific conditions. Studying star formation around H II regions with 3D visualisation offers new perspectives in the study of contaminants along the line of sight, since molecular clumps not associated with ionised regions can easily be separated. The SEDIGISM survey, covering a total area of 78 square degrees, thus provides highly valuable data to conduct this kind of study on a large number of Galactic star-forming complexes.

The SEDIGISM survey will deliver an important legacy dataset for understanding the kinematic structure of the dense gas in our Galaxy. Our early work has shown the wide variety of science advancements possible, even with data covering only a tiny fragment of the Galactic Plane. The full survey will greatly improve our current view of Galactic structure and star formation.

Acknowledgements

APEX is a collaboration between the Max-Planck-Institut für Radioastronomie, ESO and the Onsala Space Observatory.

References

Beaumont, C. N. & Williams, J. P. 2010, ApJ, 709, 791
Brand, J. & Blitz, L. 1993, A&A, 275, 67
Colombo, D. et al. 2015, MNRAS, 454, 2067
Contreras, Y. et al. 2013, A&A, 549, A45
Csengeri, T. et al. 2014, A&A, 565, A75
Csengeri, T. et al. 2016a, A&A, 585, A104
Csengeri, T. et al. 2016b, A&A, 586, A149
Giannetti, A. et al. 2014, A&A, 570, A65
Giannetti, A. et al. 2015, A&A, 580, L7
Heyer, M. & Dame, T. M. 2015, ARA&A, 53, 583
Jackson, J. M. et al. 2006, ApJS, 163, 145
Kendrew, S. et al. 2016, ApJ, 825, 142
Li, G.-X. et al. 2016, A&A, 591, A5
Molinari, S. et al. 2010, A&A, 518, L100
Schuller, F. et al. 2009, A&A, 504, 415
Schuller, F. et al. 2016, submitted to A&A
Siringo, G. et al. 2009, A&A, 497, 945
Sousbie, T. 2011, MNRAS, 414, 350
Urquhart, J. et al. 2014a, A&A, 568, A41
Urquhart, J. et al. 2014b, MNRAS, 443, 1555
Wang, K. et al. 2015, MNRAS, 450, 4043
Wang, K. et al. 2016, ApJS, in press, arXiv:1607.06452
Wienen, M. et al. 2012, A&A, 544, A146
Wienen, M. et al. 2015, A&A, 579, A91

Links

[1] Access to ATLASAGAL Phase 3 data release: http://archive.eso.org/wdb/wdb/adp/phase3_main/form?phase3_collection=ATLASGAL&release_tag=1
[2] ESO Press Release: http://www.eso.org/public/news/eso1606/
[3] ATLASGAL webpage: http://atlasgal.mpifr-bonn.mpg.de
[4] GLnemo2 interactive visualization 3D program for N-body snapshots: http://projets.lam.fr/projects/glnemo2

Ultra-deep *K*-band Imaging of the Hubble Frontier Fields

Gabriel B. Brammer[1]
Danilo Marchesini[2]
Ivo Labbé[3]
Lee Spitler[4,5]
Daniel Lange-Vagle[1,2]
Elizabeth A. Barker[1]
Masayuki Tanaka[6]
Adriano Fontana[7]
Audrey Galametz[8]
Anna Ferré-Mateu[9]
Tadayuki Kodama[6]
Britt Lundgren[10]
Nicholas Martis[2]
Adam Muzzin[11]
Mauro Stefanon[3]
Sune Toft[12]
Arjen van der Wel[13]
Benedetta Vulcani[14]
Katherine E. Whitaker[15,16]

[1] Space Telescope Science Institute, Baltimore, USA
[2] Physics and Astronomy Department, Tufts University, Medford, USA
[3] Leiden Observatory, Leiden University, the Netherlands
[4] Department of Physics & Astronomy, Macquarie University, Sydney, Australia
[5] Australian Astronomical Observatory, North Ryde, Australia
[6] National Astronomical Observatory of Japan, Tokyo, Japan
[7] INAF, Osservatorio Astronomico di Roma, Monteporzio, Italy
[8] Max-Planck-Institut für extraterrestrische Physik, Garching, Germany
[9] Subaru Telescope, Hilo, USA
[10] Department of Astronomy, University of Wisconsin, Madison, USA
[11] Kavli Institute for Cosmology, Cambridge University, United Kingdom
[12] Dark Cosmology Centre, Niels Bohr Institute, University of Copenhagen, Denmark
[13] Max-Planck-Institut für Astronomie Heidelberg, Germany
[14] School of Physics, University of Melbourne, Australia
[15] Department of Astronomy, University of Massachusetts Amherst, USA
[16] Hubble Fellow

We have recently completed a deep near-infrared imaging survey with the High Acuity Wide Field *K*-band Imager (HAWK-I), nicknamed KIFF (*Ks*-band Imaging of the Frontier Fields). KIFF provides ultra-deep images of six fields around massive galaxy clusters that have also recently been observed with the Hubble and Spitzer Space Telescopes as part of the Frontier Fields programme. Each of the KIFF mosaics is among the deepest *Ks*-band images ever obtained, and, with a boost from strong gravitational lensing by the galaxy clusters, they will be used to reveal the stellar populations of galaxies seen only a few hundred million years after the Big Bang. Fully reduced images are made available to the community through the Phase 3 infrastructure of the ESO Science Archive Facility.

Context: Deep near-infrared extragalactic imaging surveys

During the last two decades, near-infrared (NIR) imaging has taken its place at the forefront of studies of galaxy formation and evolution, enabling transformational advances in our understanding of galaxy populations at early cosmic times. Detections of galaxies in the *K*-band (2.2 μm) have provided the first opportunity to construct a comprehensive picture of the population of galaxies in the early Universe. The *K*-band has enabled the discovery of galaxies at $z > 2$ that are faint at observed optical (rest-frame ultraviolet [UV]) wavelengths, owing to their evolved stellar populations and/or significant amount of dust extinction (for example, Franx et al., 2003; Labbé et al., 2003).

In fact, these galaxies, which dominate the high-mass end of the high-*z* galaxy population, were previously missed by rest-frame UV selection techniques, such as *U*-dropout galaxies (for example, van Dokkum et al., 2006). Imaging in the *K*-band allows for direct sampling of rest-frame wavelengths longer than the Balmer break out to $z \approx 5$. Sampling the rest-frame optical wavelength regime is critical for high-*z* studies, as it is significantly less affected by dust obscuration and is a better probe of the galaxy stellar mass compared to the rest-frame UV, which is more sensitive to unobscured star formation (for example, Fontana et al., 2006).

The next Frontier

The latest effort to further our knowledge of galaxy formation and evolution is the Hubble Space Telescope (HST) Frontier Fields (HFF) programme[1] (Lotz et al., 2016). The HFF programme is a multi-cycle Hubble programme consisting of 840 orbits of Director's Discretionary (DD) time that is imaging six deep fields centred on strong lensing galaxy clusters in parallel with six deep blank fields (Figure 1). The primary science goals of the twelve HFF fields are to: 1) reveal the population of galaxies at $z = 5–10$ that are intrinsically 10–50 times fainter than any presently known; 2) solidify our understanding of the stellar masses and star formation histories of faint galaxies; 3) provide the first statistically meaningful morphological characterisation of star-forming galaxies at $z > 5$; and 4) find $z > 8$ galaxies magnified by the cluster lensing, with some bright enough to be accessible to spectroscopic follow-up. Alongside the HST observations, the Spitzer Space Telescope has devoted 1000 hours of DD time to imaging the HFF fields at 3.6 μm and 4.5 μm with the InfraRed Array Camera (IRAC).

Whereas the main goal of the HFF is to explore the galaxy population in the first billion years of cosmic history, this dataset, unique in its combination of surveyed area, multi-wavelength coverage and depth, is also well suited for studies of galaxy evolution across most of the age of the Universe, down to, and including, the redshifts of the targeted galaxy clusters ($z \approx 0.3–0.5$).

KIFF: A synergy between the VLT and space-based observatories

The space-based HFF data alone, however, are not sufficient to robustly characterise red galaxies at $z \gtrsim 3$ because the near-infrared H_{160}-band of the HST Wide Field Camera 3 IR channel (WRF3/IR) lies on the UV side of the rest-frame optical Balmer/4000 Å break at these redshifts. This mismatch results in sub-optimal accuracies in the assignment of the photometric redshifts and stellar population properties (e.g., stellar mass and rest-frame optical colour; Muzzin et al., 2009). Very deep *K*-band imaging is required to

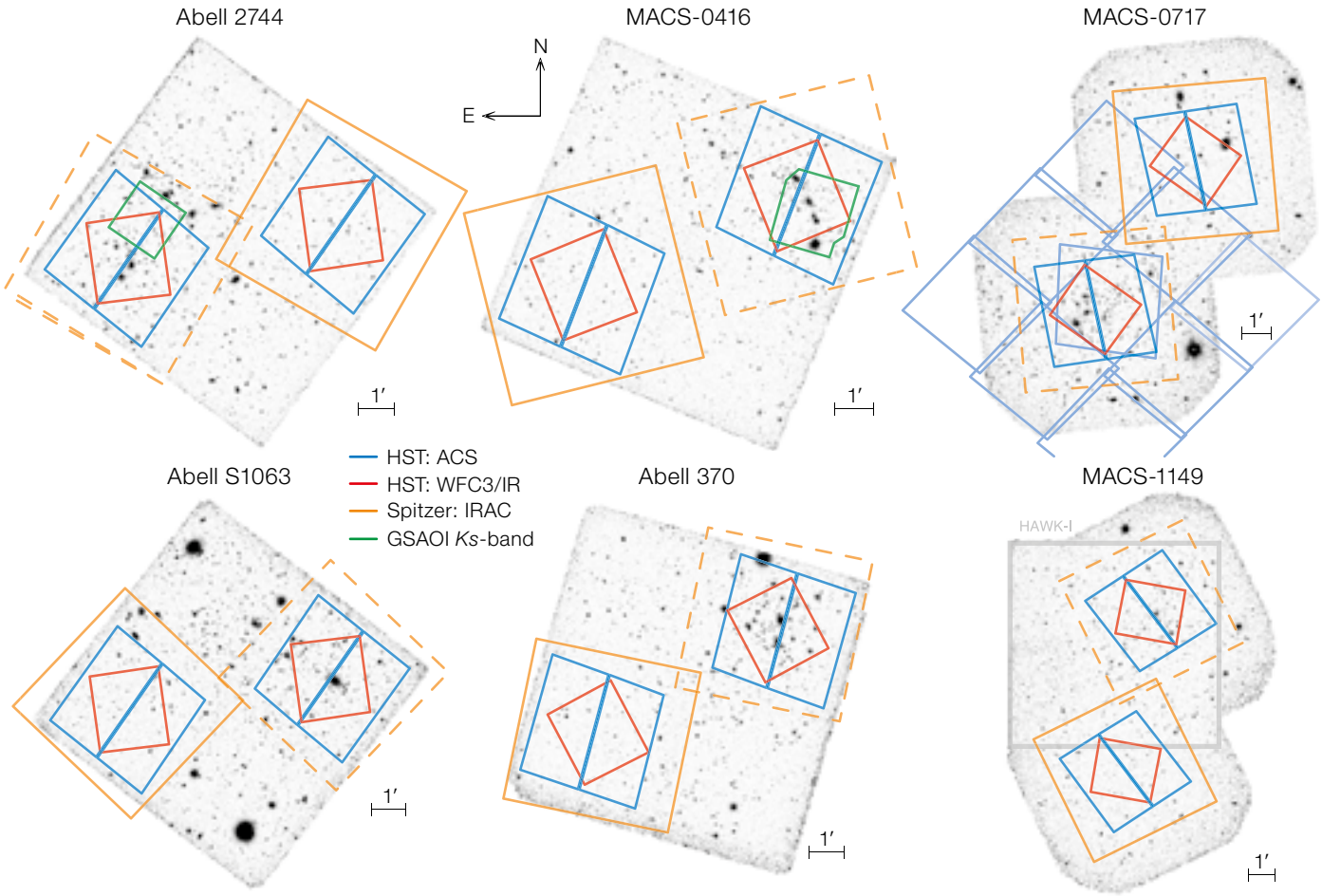

Figure 1. The layout of the imaging data in the Frontier Fields clusters: HAWK-I and MOSFIRE images with HST cluster and parallel fields (Advanced Camera for Surveys [ACS] in blue, WFC3/IR in red, Spitzer IRAC in orange) and additional Gemini South Adaptive Optics Imager (GSAOI) in green (Schirmer et al., 2015). From Brammer et al. (2016).

significantly improve the precision of both photometric redshifts and derived stellar population properties. Moreover, at $z > 8$–9, the *K*-band data help to constrain the Lyman-break redshifts (for example, Bouwens et al., 2013) and increase the wavelength lever arm for measuring the redshift evolution of the rest-frame UV slopes (i.e., the dust content and/or metallicity) of the first galaxies (Bouwens et al., 2013).

In order to resolve this issue of the lack of deep *K*-band data over the HFF, we executed the KIFF programme[2] to image four of the HFF clusters in the *Ks*-band (filter centred at 2.15 µm, width 0.32 µm) using the HAWK-I imager mounted on Unit Telescope 4 of the Very Large Telescope (VLT) to a depth comparable to that of the HST data. Coverage of two of the HFF clusters not visible from Paranal was obtained with the Multi-Object Spectrometer for Infra-Red Exploration (MOSFIRE) mounted on the Keck I telescope at Mauna Kea. Table 1 lists the six pointings with summary details of the observations and their depth and image quality.

Table 1. KIFF observations of the Hubble Frontier Fields.

Field	Cluster Redshift	R.A.	Dec.	Instrument	Exp. time (hours)	Depth (AB mag)	FWHM (arcsec)
Abell 2744	0.31	00:14:21	–30:23:50	HAWK-I	29.3	26.0	0.39
MACS-0416	0.40	04:16:09	–24:04:28	HAWK-I	25.8	26.0	0.36
Abell S1063	0.35	22:49:01	–44:32:13	HAWK-I	27.9	26.0	0.39
Abell 370	0.38	02:40:03	–01:36:23	HAWK-I	28.3	26.0	0.35
MACS-0717	0.55	07:17:34	+37:44:49	MOSFIRE	8.1	25.3	0.49
MACS-1149	0.54	11:49:36	+22:23:58	MOSFIRE+HAWK-I	15.6	25.1	0.54

The *Ks*-band data

HAWK-I images of the four southern HFF clusters were obtained in Service Mode in Periods 92 (2013–2014) and 95 (2015–2016). Reaching depths approaching those of the HST and Spitzer images requires long integrations in the *Ks*-band: each of the HAWK-I fields was observed for more than 25 hours on-source. The large 7 × 7 arcminute field of view of the HAWK-I instrument is perfectly suited to covering the two deep Hubble pointings in each field, and this instantly improves the observing efficiency of this

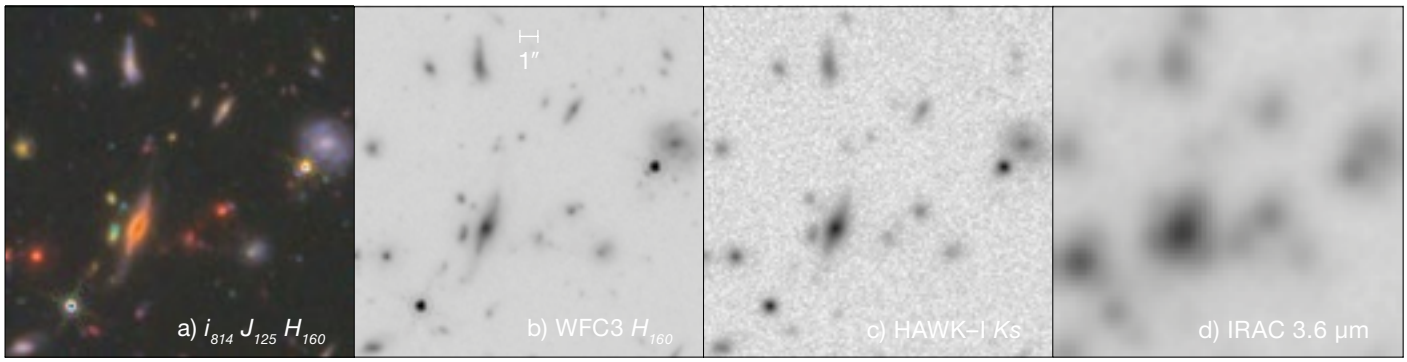

Figure 2. A 20 × 20 arcsecond cutout from the MACS-0416 parallel field (see Figure 1, upper centre, east field) as an example of the Hubble Frontier Fields imaging. (a) HST colour composite from I_{814}-, J_{125}- and H_{160}-band images. (b) The near-infrared HST H_{160} image (greyscale). (c) The HAWK-I *Ks*-band image. (d) Spitzer IRAC 3.6 µm image. From Brammer et al. (2016).

programme by a factor of two over comparable instruments with smaller fields of view (MOSFIRE, for example, requires two pointings). Figure 1 shows the layout of the HAWK-I mosaics and the accompanying deep Hubble and Spitzer data. The deep KIFF mosaics cover a combined area of 490 square arcminutes.

The depth of the *Ks*-band images and their utility, in concert with the Hubble images at bluer wavelengths, are very sensitive to the image quality achieved. Our Service Mode constraints required very good seeing and transparency conditions, and it is a testament to the excellent observing efficiency and outstanding sky conditions at the VLT and Cerro Paranal that these conditions were met within single observing periods for such long total integrations per field. The final image quality of the HAWK-I mosaics is superb — better than 0.4 arcseconds (point source full width half maximum [FWHM]) for all cases and reaching just 0.35 arcseconds in the Abell 370 field. The final depth of the deep HAWK-I mosaics reaches an AB magnitude of 26.0 (5σ for point sources), competitive with the deepest *Ks*-band images previously obtained (see the HUGS project; Fontana et al., 2014a, 2014b).

An example comparison of the KIFF *Ks*-band and space-based Frontier Fields imaging is illustrated in Figure 2, showing just a small cutout of the MACS-0416 "parallel" field (the full KIFF coverage is some 4400 times larger than the 20 × 20 arcsecond area shown). The deep optical and near-infrared Hubble imaging provide spectacular spatially resolved information on physical scales of just ~1 kpc (Figure 2a). However, there are many red galaxies clearly visible in the cutout that are predominantly at redshifts $z > 2$, where even the reddest WFC3/IR filter, H_{160} (Figure 2b), only probes rest-frame UV wavelengths and is therefore most sensitive to young, UV-bright star-forming galaxies. The KIFF imaging (Figure 2c) bridges the gap between Hubble and Spitzer and provides high-fidelity rest-frame optical images of galaxies at $z > 2$.

Improved constraints on the redshifts and intrinsic properties of distant galaxies

To explore the quantitative constraints provided by the deep *Ks*-band imaging, we have computed photometric redshifts and derived rest-frame colours and mass-

Figure 3. a) Difference in derived rest-frame *U–V* colours of Hubble Frontier Fields galaxies with and without including the *Ks*-band photometry. Points are colour-coded by their mass-to-light ratio. The selected galaxy whose SED is shown in (b) is indicated by a red star. b) Spectral energy distribution (SED) of the selected galaxy. The SED fits, with the *Ks*-band photometry excluded (grey line) and included (blue line), are shown. c) Photometric redshift probability distribution for the selected galaxy. The effect of including the HAWK-I *Ks*-band photometry alters the redshift distribution to that shown in blue (compared to the grey curve), now favouring an evolved stellar population at $z \sim 3.5$. From Brammer et al. (2016).

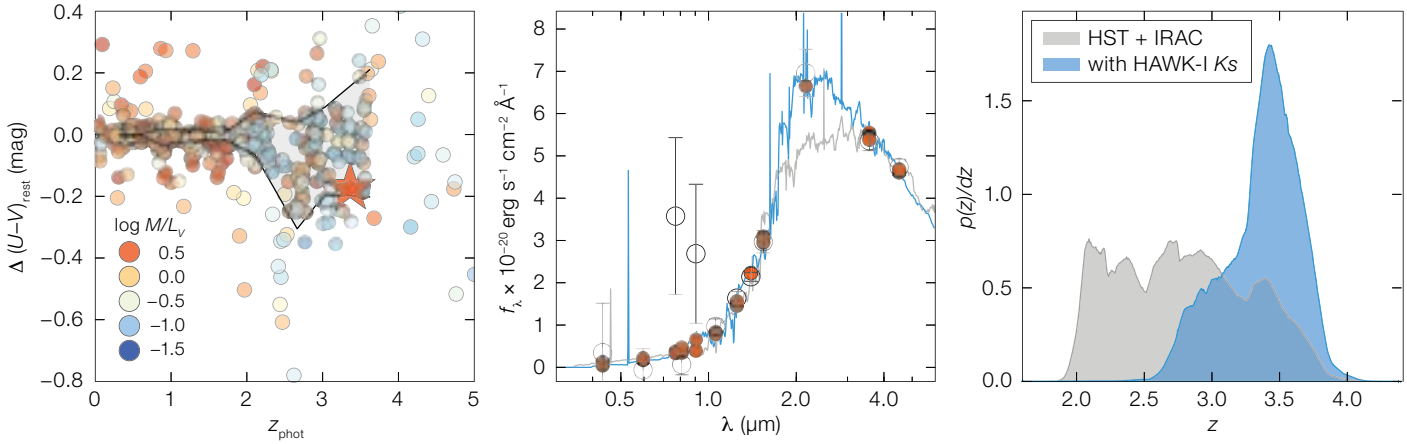

to-light ratios for photometric catalogues with and without the *Ks*-band photometry included. The left panel of Figure 3 shows the difference in the rest-frame *U*–*V* colours, which probes the strength of the Balmer/4000 Å break, and is a proxy for the age and mass-to-light ratio of the underlying stellar population. The scatter in the *U*–*V* colours with and without including the *Ks*-band information is low at $z < 2$, where the fit is constrained predominantly by the deep HST photometry. At $z > 2$, however, as the rest-frame *V*-band is redshifted beyond the near-infrared H_{160} filter, the scatter increases dramatically, reaching $\sigma > 0.1$ magnitudes at $z \sim 3$. This is much larger than the photometric uncertainties in the adjacent space-based photometric bands would suggest, as all of these galaxies with *H* mag. ~26 are detected in the deep WFC3 and IRAC images at >> 10σ.

The right two panels of Figure 3 show a single galaxy that illustrates how these systematic effects are not trivial and will likely result in biases in the interpretation of the galaxy population properties derived from the HST and IRAC observations alone. The spectral energy distribution (SED) shown rises steadily through the reddest WFC3/IR bands and then shows a sharp break with bright detections in the IRAC bands. The *Ks*-band measurement at 2.15 μm reduces the range of allowed photometric redshifts by a factor of two by pinpointing a strong Balmer break at z ~ 3.4. Even though the measured H_{160}–*Ks* colour is redder than that inferred from the HST + IRAC photometry alone, the final rest-frame *U*–*V* colour is actually bluer as a result of the higher preferred redshift. Evolved galaxies at $z > 3$, such as the one shown in Figure 3b, are an intriguing population deserving of detailed study in their own right, and the combined Frontier Fields Hubble + *Ks* + IRAC dataset is ideally suited to this purpose.

Public data release

Following the public release of the rich treasure trove of Hubble and Spitzer HFF data, we have made the final science and inverse variance mosaics of all six KIFF fields publicly available via the ESO Phase 3 data products interface[3]. For a complete presentation of the KIFF observations, analyses, and data products, see Brammer et al. (2016).

References

Bouwens, R. J. et al. 2013, ApJL, 765, L16
Brammer, G. B. et al. 2016, ApJS, in press, arXiv:1606.07450
Franx, M. et al. 2003, ApJL, 587, L79
Labbé, I. et al. 2005, ApJL, 624, L81
Lotz, J. M. et al. 2016, ApJ, submitted, arXiv:1605.06567
Fontana, A. et al. 2006, A&A, 459, 745
Fontana, A. et al. 2014, A&A, 570, A11
Fontana, A. et al. 2014b, The Messenger, 155, 42
Muzzin, A. et al. 2009, ApJ, 701, 1839
van Dokkum, P. G. et al. 2006, ApJL, 638, L59

Links

[1] Frontier Fields web page at STScI: http://www.stsci.edu/hst/campaigns/frontier-fields/
[2] KIFF news and updates: https://github.com/gbrammer/HAWKI-FF
[3] KIFF Phase 3 data release: http://archive.eso.org/wdb/wdb/adp/phase3_main/form?phase3_collection=092.A-0472&release_tag=1

ESO & D. Coe (STScI)/J. Merten (Heidelberg/Bologna)

FORS1 image (6.7 × 6.7 arcminutes) of the merging galaxy cluster Abell 2744, one of the clusters selected for study in the Frontier Fields programme. This colour image is formed from *V*-, *R*- and *I*-band images; see Release eso1120 for more details.

Signing of the agreement between ESO and a consortium led by the Leibniz-Institut für Astrophysik Potsdam, to build the 4-metre Multi-Object Spectroscopic Telescope (4MOST) instrument, on 23 August 2016. See Announcement eso16055.

AIP/ESO

The Foreign Minister of the Netherlands, HE Bert Koenders, visited Paranal in July 2016 and is seen here in the VLT Control Room. See Announcement ann16048.

ESO/J. C. Muñoz-Mateos

Report on the ESO/MPA/MPE/Excellence Cluster/LMU and TUM Munich Joint Conference

Discs in Galaxies

held at ESO Headquarters, Garching, Germany, 11–15 July 2016

Richard Ellis[1]

[1] ESO

The annual Munich Joint Astronomy Conference brought together observers and theorists studying the full range of cosmic environments and epochs where discs play a role in shaping the structural assembly history of galaxies. Considerable progress is being made in interpreting the past history of the Milky Way and Andromeda through massive stellar imaging and spectroscopic campaigns. This is being augmented with interferometric studies of gaseous discs in nearby galaxies with exquisite angular resolution. Integral field spectrographs are providing resolved data for star-forming and quiescent galaxies to redshifts of three. This explosion of new data is being interpreted with high resolution numerical simulations in order to understand the physical processes which govern the stability, formation and disruption of early discs, and how star formation is regulated in the context of various feedback processes. Selected highlights of the progress reported at the conference are presented.

Stellar and gaseous discs represent a fundamental feature of the Hubble sequence of galaxies, acknowledged in 1994 by Allan Sandage when he remarked that the sequence represents "a true order among the galaxies, not one imposed by the classifier". The modern view now emphasises a continuity in the disc properties of host galaxies from gas-rich, rotationally-supported, thin spirals to dynamically hotter early-type galaxies. Decades ago many astronomers considered that galaxies evolved in isolation with their resulting stellar populations and kinematic properties established via their formation processes. Now we realise that galaxies interact both with one another and with their environment, so that key components, such as stellar discs, can be both assembled and destroyed as the systems evolve. Explaining the physical origin, time evolution and structural properties of discs clearly underpins our understanding of galaxies, which are the visible fabric of the Universe.

There is a veritable explosion of new observational data relating to the properties of discs from detailed chemical and kinematic studies of stellar components of the Milky Way, through a new generation of integral field spectrographs gathering resolved data on thousands of intermediate redshift galaxies, to impressive progress on the earliest star-forming systems. These observations extend beyond the familiar optical and near-infrared region to include gaseous structures probed by radio and sub-millimetre interferometers. This observational progress is mirrored by high resolution numerical simulations of evolving gas-rich galaxies as well as analytic studies of the stability of their discs.

This year's Munich Joint Conference held at ESO focused on addressing the role that discs play in the history of galaxy assembly. Over 130 registered participants from all over the globe participated in a lively four day programme addressing key topical issues. The programme (available online[1]) was assembled with input from an experienced Scientific Organising Committee aided by its local members Andi Burkert, Eric Emsellem, Guinevere Kauffmann, Linda Tacconi and myself.

Galactic discs: fundamentals

The conference was structured around four interlocking themes. In the first theme, concerned with the fundamental properties of disc galaxies, Bruce Elmegreen and Mark Krumholz tackled two long-standing fundamental questions. Since 1959 it has been known that the stellar distribution in disc galaxies is exponential along the major axis without any obvious "edge". What is the origin of this "exponential profile" which extends out to ten scale lengths? Deviations are seen at large radii which appear to correlate with Hubble type. Simulations of gaseous halos aligned in various ways with the dark matter can reproduce some of the trends, most likely through a combination of the redistribution of angular momentum, torques and the relationship between star formation and gas density. However, bars, spiral arms and interactions appear to affect the profiles in ways that are not yet understood. Higher order trends are seen when examining profiles in various colours, but these arise from age gradients rather than features in the mass distribution, consistent with old stars having migrated to the outer parts. Whereas various dynamical processes can move stars radially inwards and outwards, understanding why this continues to preserve the exponential profile is a puzzle.

The second question relates to the origin of turbulence in gaseous discs. Typical discs have a dispersion of 6 km s^{-1} in warm H I gas, which is much larger than can be accounted for by thermal motions. Since turbulence decays on ~10 Myr timescales, its sustenance requires an energy source. Supernovae offer a potential continuous source of energy input, providing that the timescale of renewed star formation is about 3 Gyr, but simulations indicate many problems, particularly in regard to maintaining turbulence in outer discs. Gravity-driven turbulence is an alternative: turbulence transports angular momentum outward and mass inward; the decay of turbulence is balanced by inward accretion. In this picture, since mass inflow decreases with cosmic time, velocity dispersions should be higher in early galaxies, as observed.

The results of several new disc surveys were presented including BlueDisk (Guinevere Kauffmann), the EMIR Multi-line Probe of the ISM Regulating Galaxy Evolution (EMPIRE) by Frank Bigiel, the Hubble Legacy ExtraGalactic Ultra-violet Survey (LEGUS) by Dimitrios Gouliermis and the Westerbork Hydrogen Accretion in LOcal GAlaxieS (HALOGAS) by Guyla Józsa. Eva Schinnerer reviewed how millimetre interferometry is tracing molecular gas in nearby galaxies with exquisite (40 pc) resolution (Figure 1), enabling detailed studies of how star-formation is regulated and of environmental dependencies relating to the stellar surface density and the presence of spiral structure. Surprisingly, there is no simple spatial trend in activity as expected from star formation triggered by a spiral pattern. Kathryn Kreckel illustrated how the combination of the Atacama Millimeter/submillimeter Array (ALMA) and the Multi Unit Spectroscopic Explorer (MUSE) on the Very Large Telescope will revolutionise such *in situ* studies. Extra-planar molecular gas is also seen in M51 and inferred from CO and H I line widths in

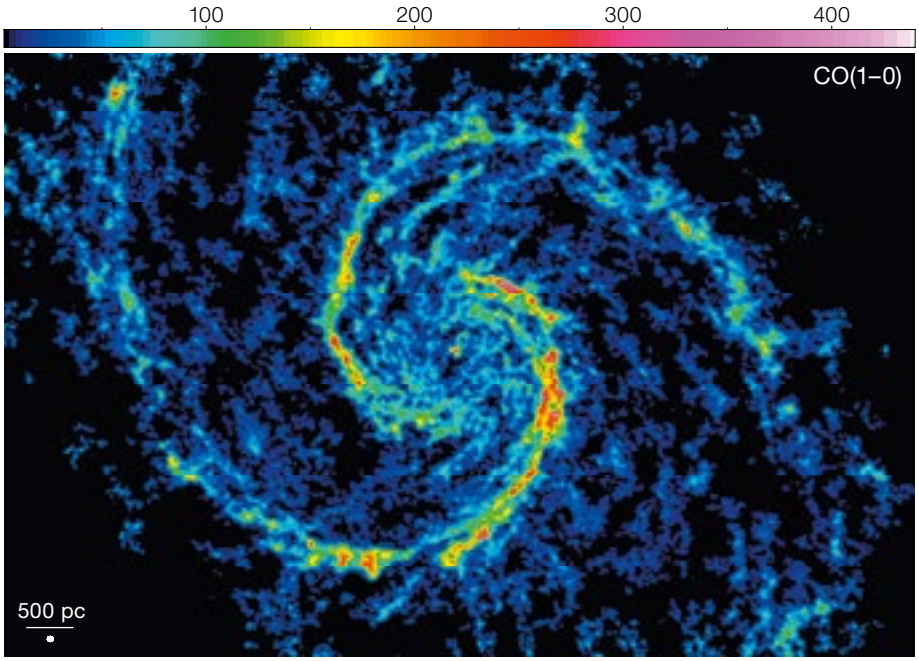

Figure 1. Plateau de Bure Interferometer (PdBI) image of CO molecular gas in M51 with a spatial resolution of 40 pc (from Schinnerer et al., 2013). Such data are probing the formation and timescales of giant molecular clouds in the presence of spiral arms in the disc. The colour bar shows CO integrated intensity.

other nearby galaxies, implying dense gas can be expelled from the thin disc via stellar feedback.

Niv Drory presented the first results from the SDSS-IV MaNGA (Mapping Nearby Galaxies at Apache Point Observatory [APO]) survey — an integral field spectroscopic survey of 10 000 galaxies for which about 30 % of the data is now in hand; Figure 2 shows a few examples. Spatially resolved spectroscopy for such a large sample is a major advance and both interesting and puzzling results are emerging. The most intriguing result (presented by Jorge Barrera-Ballesteros) concerns a mass-metallicity relation derived from the localised mass density within a galaxy, that is just as tight as that determined from integrated measures. Does this indicate that some global scaling relations are governed by localised physics? Each conference theme was followed by a panel discussion, and this MaNGA result was the source of intense debate!

Emergence of early discs

The second theme concerned the emergence of early discs in high redshift galaxies. Reinhard Genzel reviewed the formation and evolution of massive star-forming galaxies, demonstrating the remarkable progress being made with integral field spectrographs such as the *K*-band Multi Object Spectrograph (KMOS), the Spectrograph for INtegral Field Observations in the Near Infrared (SINFONI) and the OH-Suppressing Infra-Red Imaging Spectrograph (OSIRIS). Resolved kinematics is now available for several hundred galaxies in the range $1 < z < 3$ with ordered rotation evident in about 70 %. The gaseous velocity dispersion increases with redshift but is not correlated with the density of star formation, suggesting that it is gravitationally driven. ALMA will permit such studies to be extended beyond z ~ 3. By stacking the kinematic data, Philipp Lang demonstrated that outer rotation curves turn down at large radii, indicating a high baryon fraction and significant pressure support in the outer parts.

Higher spatial resolution spectroscopic data can be achieved using adaptive optics and by exploiting the magnification boost of gravitational lensing. Tucker Jones and Nicha Leethochawalit demonstrated how it is possible to probe Milky Way progenitors at z ~ 2 and systems with stellar masses less than $10^9\,M_\odot$. Whereas strong metal gradients are seen in nearby spirals, these are largely absent at z ~ 2, suggestive of gas mixing from strong feedback processes. Perhaps the most surprising result from high redshift was the discovery (presented by Drew Newman) that several massive compact quiescent galaxies have rotating discs. If these are progenitors of today’s non-rotating massive ellipticals, these discs must subsequently be destroyed, for example by minor mergers.

High redshift galaxies appear clumpy in form and although initially suggestive of widespread merging, the regular kinematics indicates that the clumps more likely represent instabilities. Avishai Dekel reviewed how adaptive mesh refinement simulations incorporating cold inflowing gas can address the build up of angular momentum. When interpreted in terms of a low Toomre parameter *Q* this naturally leads to violent instabilities. Frédéric Bournaud demonstrated that the largest clumps can survive for ~ 400 Myr and launch their own outflows. They may migrate to the nucleus, initially establishing metal gradients which are eventually disrupted by feedback. Ken-ichi Tadaki showed that dense cores can be found in z ~ 2 ALMA sources, perhaps indicative of bulge formation. Robert Feldmann offered a different perspective in his FIRE (Feedback In Realistic Environments) simulations. He argued that the Toomre instability criterion may not apply in asymmetric thick discs which are not isothermal. In the efficient feedback used in these simulations, such clumps would be transient and not contribute to bulge formation.

In the subsequent panel discussion there was a lively debate about the utility of pursuing various challenging observations (e.g., metal gradients in z ~ 2 galaxies) given the apparent ability of theorists to reproduce such observations in a wide variety of very different physical situations! It was unclear whether the community has reached a consensus on when thin discs in Milky Way-like galaxies emerged. Susan Kassin presented an update on the mass-dependent fraction of galaxies with various emission line rotational velocities, *V,* and internal dis-

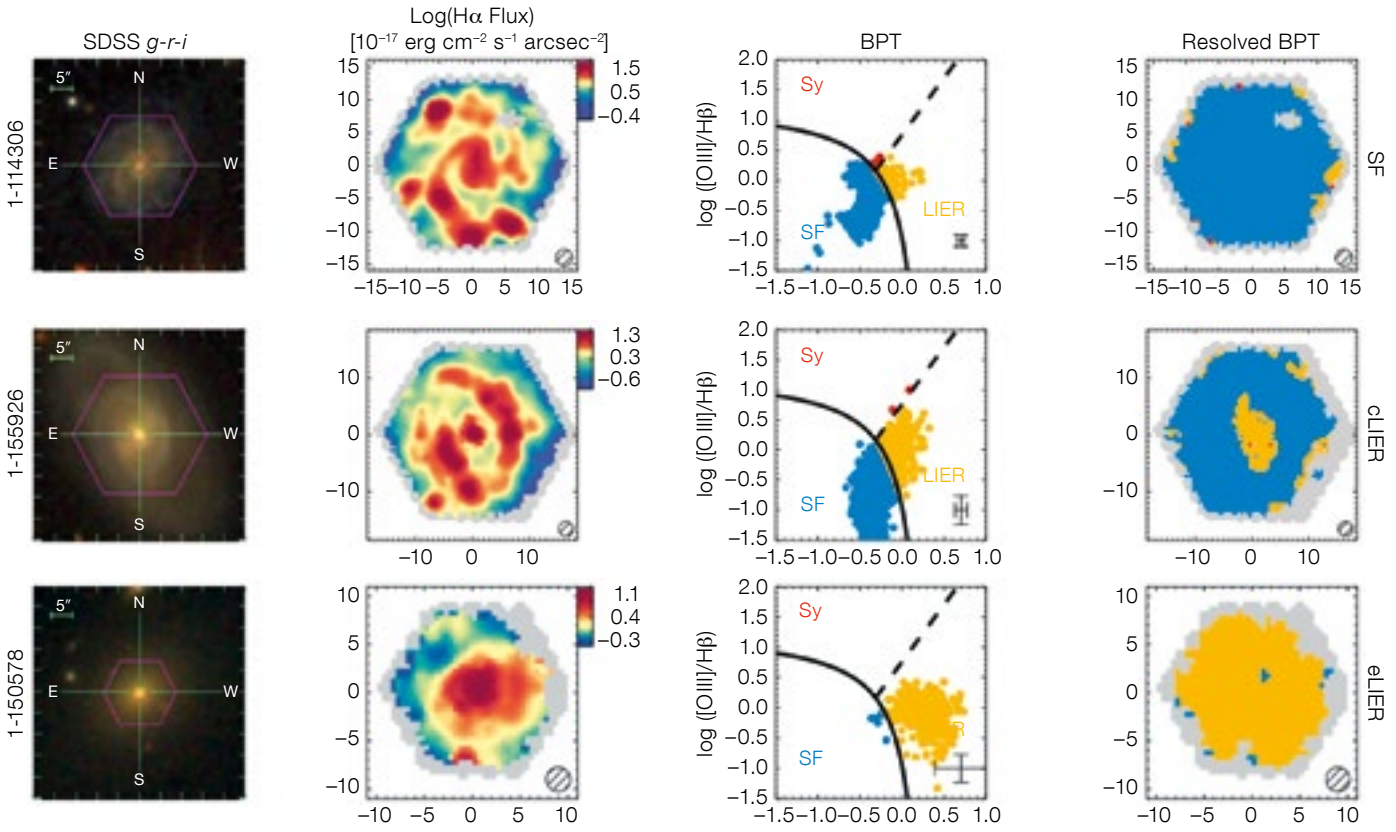

Figure 2. Spatially resolved excitation maps for a few *i*-band selected galaxies from the MaNGA survey. From Belfiore et al. (2016).

persions, σ. By z ~ 1, about 70 % of disc galaxies with masses greater than 10^{10} $M_{\odot}$ have $V/\sigma > 3$.

The Milky Way and Local Group

The third major theme of the conference addressed the progress being made in understanding discs in the context of the Milky Way and nearby galaxies, through detailed measures of stellar velocities, ages and abundances. Jo Bovy summarised the key parameters of the Milky Way Disc as well as the mass budget in the Solar Neighbourhood. The Gaia satellite is providing 6D phase space data which will be augmented with abundance data from many associated spectroscopic surveys. The APO Galactic Evolution Experiment (APOGEE) has been particularly effective in extending radius-dependent studies of the high α-element/Fe sequence as a probe of early disc evolution. The star formation rate and gas in/outflow rate have been similar across the entire Disc in its first 4 Gyr (Figure 3). Disc evolution appears to have been very quiescent over the past 10 Gyr with no large fraction of stars accreted by mergers. The migration of stars is a critical factor in understanding the metal-rich tail in the Disc.

There appears to be a smooth transition in composition (but not in angular momentum) between the thin, and so-called "thick", Disc, whereas the flaring of the low α/Fe population is consistent with radial migration. Although no flaring is seen in the high-α/Fe population, the Disc formed inside-out and was likely turbulent in its early phase. Stellar ages give an additional perspective to those based on chemical abundances, but reliable ages have always been a challenge. Gerry Gilmore introduced a potentially powerful method exploiting the [C/N] abundance ratio applicable for red giants, demonstrating that the thick Disc is likely old.

Julianne Dalcanton presented results from the Hubble Space Telescope (HST) M31 Treasury Survey; the data comprise an impressive 12 834 images taken at 414 positions, with photometric measures from six filters of the Advanced Camera for Surveys (ACS) and the Wide Field Camera 3 (WFC3) infrared channel for 117 million stars (Figure 4). Detailed colour-magnitude diagrams to AB ~ 26 mag. enable reconstruction of the star formation history with a spatial resolution of 20 pc. These data demonstrate that features such as the 10 kiloparsec star-forming ring existed several dynamical times ago. The resolved stellar populations can also be used to predict the lower resolution ultra-violet GALaxy evolution EXplorer (GALEX) satellite map of M31; in fact the GALEX signal is stronger than predicted, enabling a detailed map of the dust distribution derived from its extinction (rather than emission). Although morphologically similar, the dust masses/emissivities derived from the Spitzer Space Telescope are too high by a factor of ~ 2.5.

Whether the Milky Way (and M31) are "typical" is an important question that was addressed by both Risa Wechsler and Jeff Newman. The Milky Way appears to be a fairly representative "green valley"

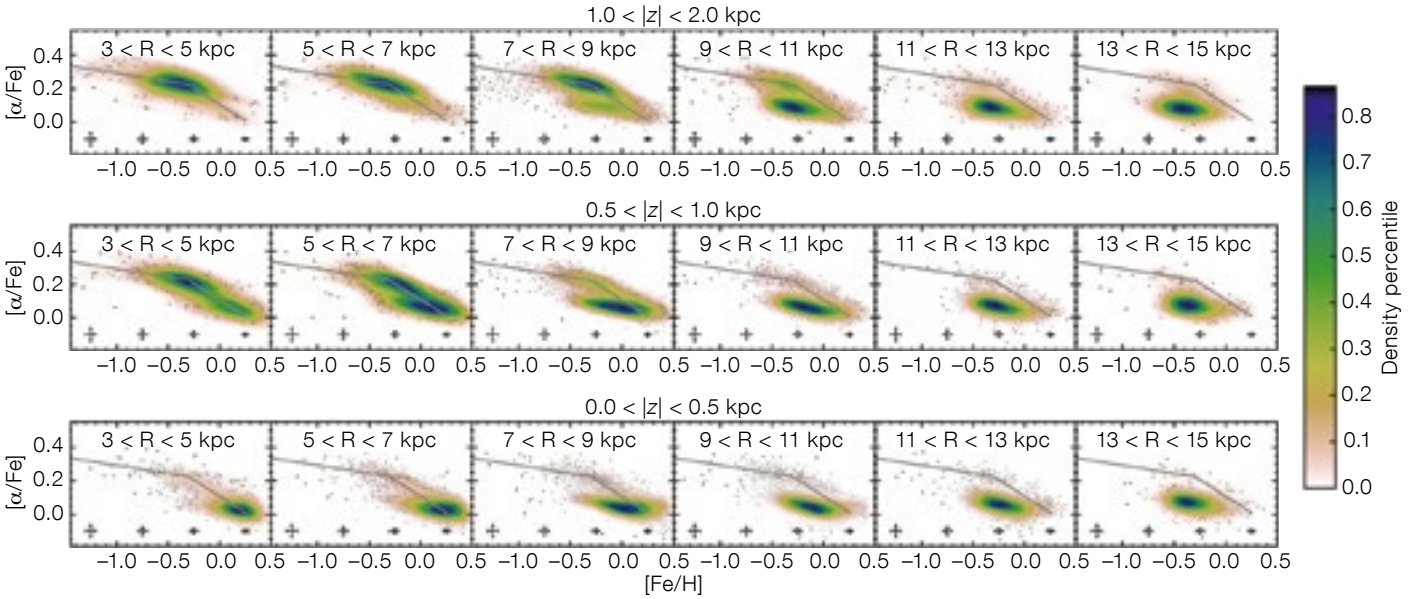

Figure 3. Chemical abundance patterns [α/Fe] *vs.* [Fe/H] across the entire Milky Way Disc from APOGEE (from Hayden et al., 2015). The high [α/Fe] sequence probes the early history of the Disc; the uniformity in the radial direction suggests a quiescent history since $z \sim 2$ with no major mergers.

Figure 4. Survey strategy for the Panchromatic Hubble Andromeda Treasury (PHAT) survey comprising 23 “bricks” each an array of 3 × 6 HST pointings. Six-filter photometry provides colour-magnitude diagrams, star formation histories and measures of dust extinction with 20 pc resolution across the entire disc.

galaxy on the Tully-Fisher relation, but is in the lowest 10 % by physical size despite its other physical properties. Wechsler described an ambitious SAGA (Strömgren survey for Asteroseismology and Galactic Archaeology) survey aimed at addressing this discrepancy in the context of securing detailed structural properties for 74 nearby isolated galaxies.

As expected, the panel discussion session was dominated by debate over the physical reality of a thick Disc component and its connection with dispersion-dominated rotating systems seen at $z \sim 2$. Several erudite participants commented that the nomenclature is unfortunate. Not everything in the Milky Way that is “thick” is lying in the so-called thick Disc, since part of the thin Disc is flaring. The debate continues...

Interfacing theory with observations

The final conference theme related to the interface between theory and observations. Numerical simulations traditionally

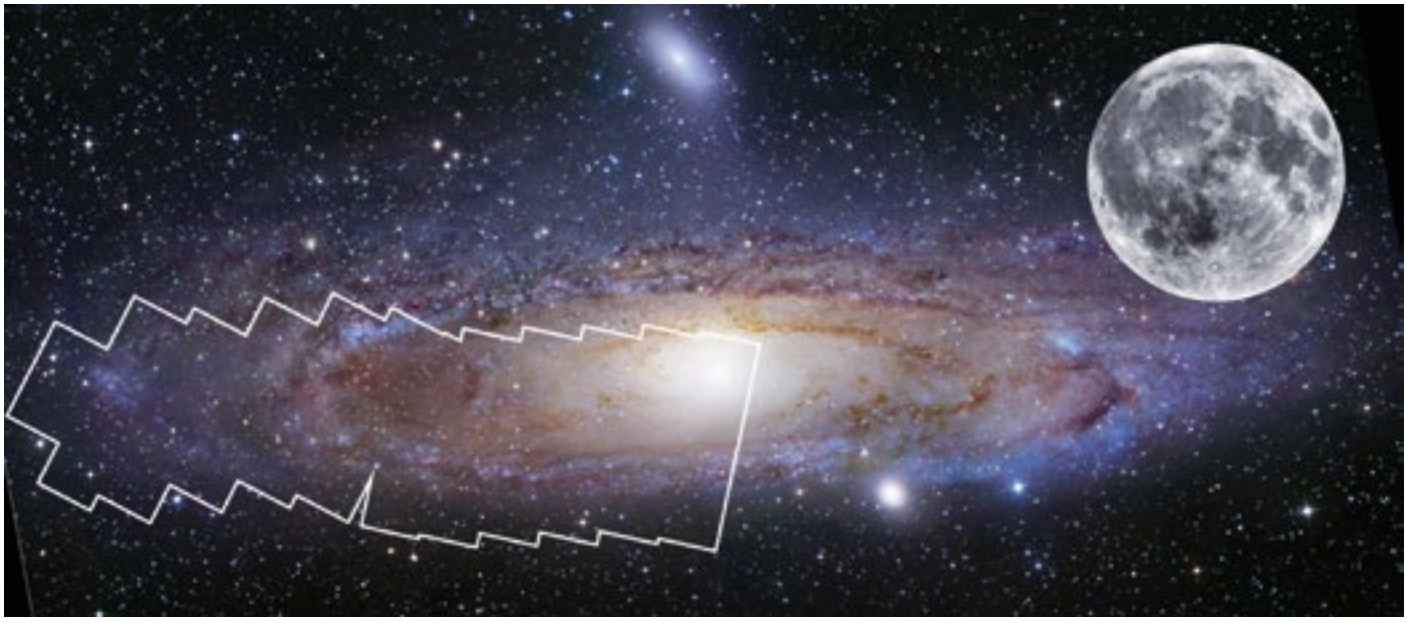

L. Cliff Johnson/Robert Gendler

had great difficulty reproducing even the most basic observational scaling relations, but recent progress has been impressive. Richard Bower summarised the results from the EAGLE project, and Shy Genel those from Illustris simulations (Figure 5). Strong feedback that declines with increasing halo mass is a key ingredient in enabling us to reproduce, for example, the relationship between the stellar specific angular momentum and galaxy mass, as well as both galaxy sizes and their angular momentum distributions. The onset of black holes is necessary for the termination of widespread star formation.

Rob Grand presented moving mesh, magneto-hydrodynamic simulations of Milky Way sized galaxies (the Auriga project). These simulations are claimed to have sufficient resolution to address important observables, such as the time-dependent velocity dispersion and the effect of spiral arms and bars on chemodynamics of galaxies. Discs grow thinner with time and outward radial migration, driven by spiral arms, decreases their velocity dispersion and leads to azimuthal metallicity enhancement signatures that can readily be tested, e.g., with MUSE observations. In a complementary approach, James Binney modelled the controlled growth of a thin disc in an isolated galaxy. Heating by giant molecular clouds seems a critical factor in establishing the vertical structure, with radial migration essential for reproducing chemical gradients. Karl Glazebrook presented a new picture of disc stability and bulge formation, illustrating how the atomic gas fraction is intimately connected to the angular momentum.

The last panel discussion focused on where the subject is moving observationally. Integral Field Unit (IFU) data is clearly a major advance in intermediate redshift studies and we can expect close synergies between observations by MUSE with adaptive optics and studies of the gaseous component with the ALMA and the Square Kilometre Array (SKA) precursors. With the first Gaia data release imminent and enabling multi-element tagging, it is questionable whether we ready for this explosion of data. Which of these numerous observational directions best test the physical processes? Many worry that

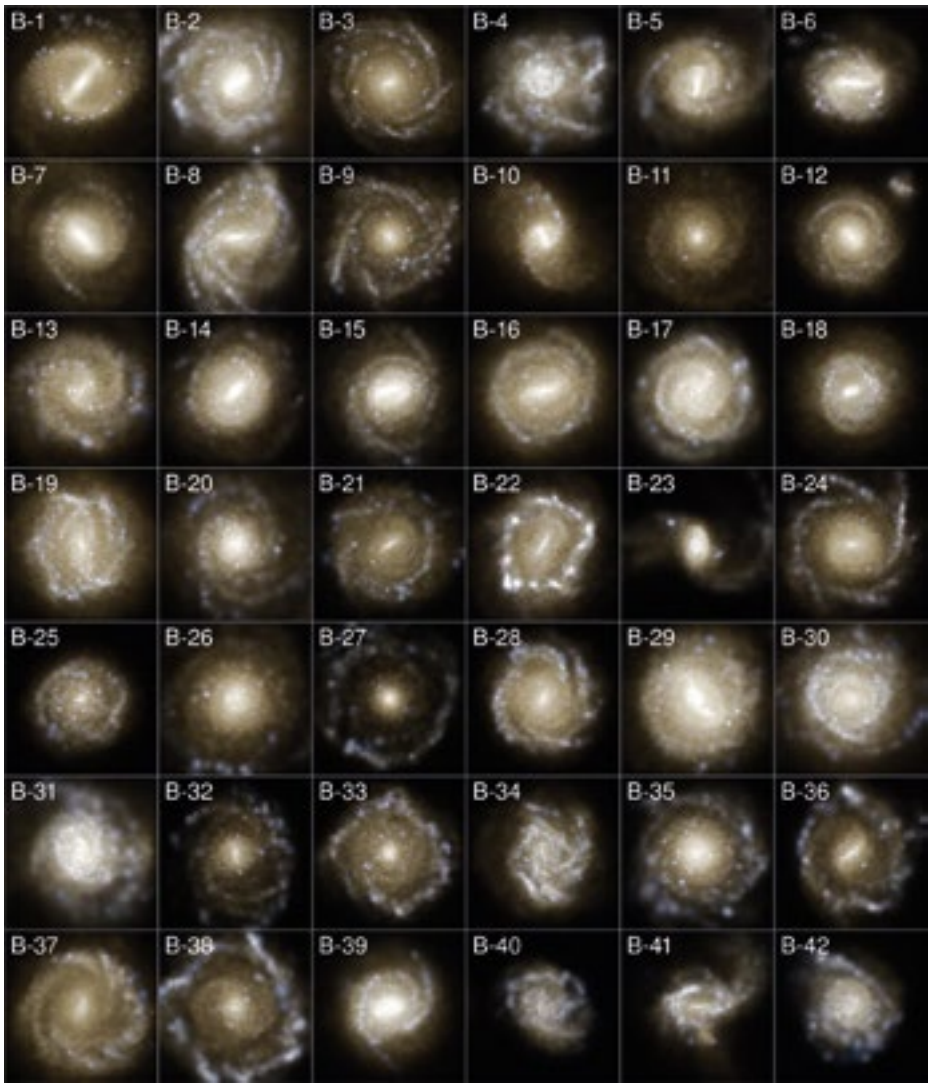

Figure 5. Simulated present-day disc galaxies in $10^{12–13} M_{\odot}$ halos from the Illustris simulation. From Vogelsberger et al. (2014).

feedback is still treated rather as a black box! Florent Renaud emphasised the importance of feedback, and how it is just as dependent on the topology of the interstellar medium as the choice of subgrid recipes; he warned of the critical need for high resolution.

As in all successful meetings, one is overwhelmed by the sheer enthusiasm of the participants, the intense level of activity and progress, as well as some outstanding puzzles. The participants were uniformly good-natured (despite the torrential downpour during the conference dinner held in a Schwabing biergarten!).

Acknowledgements

The conference was supported through the cheerful administrative assistance of Hildegarde Haems and Stella Chasiotis-Klingner (ESO). Thanks are also due to the ever-enthusiastic team of local helpers: Hannah Übler, Ken-ichi Tadaki and Rodrigo Herrera-Camus (MPE); Christine Schulz, Nicolas Guillard and Vinod Arumugam (ESO).

References

Belfiore, F. et al. 2016, MNRAS, 461, 3111
Hayden, M. R. et al. 2015, ApJ, 808, 132
Schinnerer, E. et al. 2013, ApJ, 779, 42
Vogelsberger, M. et al. 2014, MNRAS, 444, 1518

Links

[1] Workshop programme: http://www.eso.org/sci/meetings/2016/Discs2016/program.html

Report on the ESO Workshop

Active Galactic Nuclei: what's in a name?

held at ESO Headquarters, Garching, Germany, 27 June – 1 July 2016

Paolo Padovani[1]

[1] ESO

The workshop was aimed at presenting a multi-wavelength picture of active galactic nuclei. The contents of the workshop are here briefly summarised; a review article synthesising the invited reviews, presentations and discussions is in preparation.

Active Galactic Nuclei (AGN) are being discovered in ever-larger numbers over the whole electromagnetic spectrum. Different spectral bands employ different methods to identify these sources but, most importantly, they provide different windows on AGN physics. For example, the infrared band is mostly sensitive to obscuring material and dust, the optical/ultraviolet band is related to emission from the accretion disc, while the X-ray band traces the emission of a (putative) corona. Gamma-ray and (high flux density) radio samples, on the other hand, preferentially select AGN emitting strong non-thermal radiation. This has led to a proliferation of classes, which outsiders (and insiders as well!) find mesmerising. The main goal of the workshop was to paint the AGN "big picture" emerging from these multi-wavelength surveys, and to understand the truly intrinsic and fundamental properties of AGN and the physics behind them. This was addressed in discussions of the following topics:

1. the different types of AGN selected in the various spectral bands;
2. the similarities and differences they display;
3. the impact of selection effects on the interpretation of the results;
4. the physical mechanism(s) behind the emission in a given band;
5. the effective range of black hole mass and Eddington ratio probed by each selection method;
6. the possible limitations of current observations and/or facilities.

The workshop consisted of six different sessions: radio, infrared, optical, X-ray, gamma-ray, and variability. Each session was introduced by a review talk which set the scene, followed by contributed talks, by a total of eighty-six speakers. Sixty-seven posters completed the programme. A summary talk and a discussion session were held at the end of the workshop. The workshop was very well attended, with 165 participants, covering five continents and 31 different countries; 60 of the participants were students. The full workshop programme is available online[1], from where a PDF copy of most of the presentations, and some of the posters, can be downloaded. Many of the individual presentations are also available through Zenodo[2], accessible by their Digital Object Identifier (DOI).

A review paper, to be published in The Astronomy and Astrophysics Review, is currently being prepared (Padovani et al. 2017, in prep). It will summarise our knowledge of the AGN phenomenon from all angles by synthesising the review talks and the content of presentations and discussions during the workshop. This will hopefully be a useful legacy of the workshop for all AGN researchers.

Acknowledgements

I would like to thank all the members of the Scientific Organising Committee (SOC) and the Local Organising Committee (LOC): Damien Coffey (LOC), Hildegarde Haems (LOC), Evanthia Hatziminaoglou (SOC and LOC), Ryan Hickox (SOC), Bernd Husemann (LOC), Darshan Kakkad (LOC), Lisa Kewley (SOC), Vincenzo Mainieri (SOC and LOC), Allison Man (LOC), Mara Salvato (SOC and chair of the LOC), John Silverman (SOC), Torben Simm (LOC), and Sylvain Veilleux (SOC). Their contributions and practical help ensured a lively and productive workshop.

Links

[1] Workshop programme: http://www.eso.org/sci/meetings/2016/AGN2016.html
[2] Zenodo DOI platform: http://zenodo.org/

ESO/M. Zamani

Figure 1. The participants at the workshop photographed in the grounds of ESO Headquarters.

Report on the ESO/OPTICON

Instrumentation School on Use and Data Reduction of X-shooter and KMOS

held at ESO Headquarters, Garching, Germany, 9–13 May 2016

Pascal Ballester[1]
Michel Dennefeld[2]

[1] ESO
[2] Institut d'Astrophysique de Paris, CNRS, and Université P. et M. Curie, Paris, France

The NEON Archive Schools have since 1999 provided opportunities for young researchers to gain practical experience of the reduction and analysis of archive data. Twenty-four participants from 17 nationalities gathered to learn about the end-to-end cycle of observation proposal, data reduction and archive usage for X-shooter and KMOS. A brief description of the school is presented and the content of the main sessions is described.

The Network of European Observatories in the North (NEON) Archive Schools[1] provide training and practical experience for young researchers through the example of archive data. The purpose of this NEON School, jointly sponsored by ESO and OPTICON[2], was to provide the students with an introduction to the end-to-end cycle of observation proposal, data reduction and archival usage for the X-shooter and *K*-band Multi-Object Spectrograph (KMOS) instruments. These are two 2nd generation Very Large Telescope (VLT) instruments: a single-object wide-band spectrograph and a multi integral-field unit spectrograph, respectively. Additional training included proposal and observation preparation tools.

The first two days of the School were devoted to X-shooter data reduction. A general session on Wednesday addressed the topics of observation proposals, advanced data reduction and archive usage for both instruments. The last two days covered KMOS observation preparation and data reduction. A total of 24 participants, of 17 different nationalities, attended the School at ESO Headquarters (see Figure 1).

The meeting was organised around a set of computer workstations, where groups of up to four students could gather for the hands-on tutorial sessions. Ample time was reserved for discussions, and the students gave short presentations on the results obtained from their practical exercises, commenting on the tools they used in extended feedback sessions. At the end of the first session on Monday afternoon, a "Beer and Brezen" event in the garden outside the meeting room allowed the students and tutors to get better acquainted and to enjoy a sunny Bavarian evening.

X-shooter observation preparation and data reduction

Opening the first session, Joël Vernet provided insights on the optical design and performance of the X-shooter echelle spectrograph, with its emphasis on optical stability, high throughput and low background light. Sabine Möhler described the data from the instrument and the specific features of the calibration and science exposures. Andrea Modigliani described the data reduction chain and the most relevant algorithms involved in the X-shooter calibration cascade. Sabine Möhler and Wolfram Freudling then introduced the ESO Reflex scientific workflow environment[3], which was used as the processing platform for data reduction (Freudling et al., 2013).

Completing the series of X-Shooter presentations, Giacomo Beccari spoke about the preparation of X-shooter observations, and the documents and tools available to the observer: User Manual; Exposure Time Calculators; Phase 2 Proposal preparation (P2PP) system. He also covered the optimal selection of instrument setups and configuration of the templates. His main message (also valid for any other instrument) was: read the manuals! The tutors for the X-shooter hands-on data reduction sessions, Andrea Modigliani, Giacomo Beccari, Sabine Möhler, Analisa De Cia, Michael Hilker, and Valentin Ivanov, provided guidance to the students on the practical use of ESO Reflex for the calibration and data processing of three different X-shooter data sets.

From proposal preparation to Science Archive access

The general session on Wednesday opened with a talk by Gaitee Hussain on the process of proposal submission and best practice for the preparation of successful observation proposals. Marina Rejkuba presented the VLT end-to-end dataflow system with emphasis on the tools for preparation and execution of observations. Advanced topics of

ESO/M. Zamani

Figure 1. The NEON School students and organising team gathered in the precincts of the ESO Headquarters building.

ESO/M. Zamani

Figure 2. NEON School presentations were held in the Fornax room at ESO Headquarters.

ESO/M. Zamani

Figure 3. Valentin Ivanov (left) and Michael Hilker (right) provide support to NEON School students during a KMOS hands-on tutorial.

data reduction were discussed in another presentation by Sabine Möhler, on the correction of telluric lines with the molecfit tool[4], followed by a talk by Wolfram Freudling on the advanced use of ESO Reflex[3] (Freudling et al., 2013). Concluding the session, Magda Arnaboldi described the VLT Science Archive Facility (SAF[5]), and the Science Data Products made available both from external user programmes and surveys, and from in-house data reprocessing.

KMOS observation preparation and data reduction

The second half of the workshop was devoted to KMOS data reduction and observation preparation. Suzie Ramsay summarised the KMOS science drivers, its optical design, instrument modes, and the most important calibration strategies. Lodovico Coccato presented the KMOS data reduction process, with an overview of the calibration and science data, the data reduction cascade and the KMOS workflow. On the last day of the workshop, Michael Hilker presented the observation preparation for KMOS, with the specific preparation tool KARMA (Figure 2). The tutors for the KMOS hands-on tutorial, Lodovico Coccato, Anja Feldmeier-Krause, Yves Jung, and Michael Hilker, guided the students through the reduction of data sets downloaded from the SAF (Figure 3).

In summary, this NEON Instrumentation School was an excellent opportunity not only for the participants to learn about the preparation of observations and the handling of instrument data, but also for the tutors to meet directly with the users of various ESO tools. Useful feedback could thus be gathered on the practical problems that can occur when going through the whole process from data collection, reading of the documentation, to use of the data reduction tools. Issues encountered by novice users were especially obvious. It was unanimously recognised that such hands-on sessions were very useful and should be extended to other ESO instruments. This NEON Instrumentation School is thus fulfilling a wish expressed by users, and is a nice complement to the standard NEON Observing Schools, such as the one that took place in La Silla in February 2016 (Dennefeld, Melo & Selman, 2016). The slides of all talks are provided on the workshop webpage[6].

Acknowledgements

This ESO/OPTICON School would not have been so successful without the efficient work of many people: Martine Peltzer who helped with organising the meeting; ESO-Garching logistics who organised both the accommodation of the students and the configuration of the meeting; the ESO IT team who efficiently installed and configured the presentation equipment and the computers for the hands-on sessions; and Artur Szostak and Enrique Garcia who provided support for the installation of the scientific software. The financial support of ESO and of the European Commission (through the I3 OPTICON programme) was instrumental in the success of this school. We would like to gratefully acknowledge the contribution of the Scientific Organising Committee (Magda Arnaboldi, Sandra Castro, Wolfram Freudling, Marina Rejkuba and Martino Romaniello) and, last but by no means least, thanks to all the tutors for devoting their time, talents and effort to ensuring the success of the School.

References

Dennefeld, M., Melo, C. & Selman, F. 2016, The Messenger, 164, 47
Freudling, W. et al. 2013, A&A, 559, A96

Links

[1] NEON Schools: http://www.iap.fr/opticon/past_neon_schools/
[2] OPTICON: http://www.astro-opticon.org
[3] ESO Reflex: http://www.eso.org/reflex
[4] molecfit telleuric absorption correction tool: http://www.eso.org/sci/software/pipelines/skytools/
[5] ESO Science Archive Facility (SAF): http://archive.eso.org/cms.html
[6] NEON School Web Site, with list of participants: http://www.eso.org/sci/meetings/2016/garching_school2016.html

Report on the

ALMA Developers' Workshop

held at Chalmers University, Gothenburg, Sweden, 25–27 May 2016

Robert Laing[1]
Tony Mroczkowski[1]
Leonardo Testi[1]

[1] ESO

A workshop was recently held in Gothenburg to discuss the ALMA Development Programme for the period 2015–2030. The main aims were to inform the European and international communities about progress on current development projects, to solicit new ideas and to discuss priorities for the future. This contribution summarises the outcomes of the workshop.

The Atacama Large Millimeter/Submillimeter Array (ALMA) is already the world's premier facility for astronomical observations from 84 to 950 GHz, and will soon be fully operational in all of its originally planned frequency bands. Since its first observations, ALMA has routinely delivered ground-breaking scientific results in nearly all areas of astrophysics. Looking forward to 2030, the purpose of the ALMA Developers' Workshop was to ask the European and international mm/submm communities "What's next for ALMA?". The specific aims were to review previous and current development studies and projects, to discuss priorities identified by the community and to solicit new ideas for ALMA.

The workshop formed part of the programme on "Origins of Habitable Planets" of the Gothenburg Centre for Advanced Studies in Science and Technology (GoCAS), a joint endeavour between Chalmers University and the University of Gothenburg. It was held on the Chalmers campus in Gothenburg, just before the release of a new ESO Call for ALMA Development Studies. The workshop was chaired by Leonardo Testi.

The ALMA Science Advisory Committee (ASAC) has considered the way forward for ALMA over the next 15 years in its ALMA2030 documents, which cover major science themes, the landscape of major facilities, and pathways to ALMA development, respectively. Following the completion of ALMA2030, a Development Working Group has been established to draft a prioritised and roughly costed plan covering the next 5–15 years for approval by the ALMA Board in 2017. The Working Group is chaired by the ALMA Director, Pierre Cox, who opened the workshop by reporting on its activities. The main development paths recommended in ALMA2030 are:

1. Completion of ALMA as originally specified by restoring functionality deferred on grounds of cost.
2. Improvements to the ALMA Archive: enabling gains in usability and impact.
3. Larger bandwidths and better receiver sensitivity: enabling gains in speed.
4. Longer baselines: enabling qualitatively new science.
5. Increasing the instantaneous field of view and enabling more efficient mapping.

The ALMA Development budget is currently 13.6 M$/year, shared between the three regional executives (Europe, North America and East Asia). It is allocated within the regions to a mix of small studies and larger projects. The current regional development programmes were summarised by the programme scientists: Leonardo Testi (ESO), Al Wootten (National Radio Astronomy Observatory, NRAO) and Daisuke Iono (National Astronomical Observatory of Japan, NAOJ), while Nick Whyborn (Joint ALMA Observatory, JAO) outlined related activities in Chile.

Current developments

Major development projects to date have concentrated on restoring deferred capabilities. These include receiver bands and phasing for millimetre Very Long Baseline Interferometry (VLBI). Band 5 (167–211 GHz) receiver cartridges are currently being delivered by the Nederlandse Onderzoekschool voor Astronomie (NOVA) and the Group for Advanced Receiver Development (GARD), with NRAO providing the warm cartridge assemblies. The cartridges are currently being integrated into the ALMA front ends at the Operations Support Facility (OSF) in Chile. Pavel Yagoubov (ESO) described the progress of Band 5 production: 18 cartridges had been integrated at the time of the workshop and the performance comfortably meets the specification.

Approval for full production of Band 1 (35–50 GHz) was given just before the workshop to a consortium led by Academia Sinica Institute of Astronomy and Astrophysics (ASIAA). The project was described by Ted Huang. Millimetre VLBI and the ALMA Phasing Project were introduced by Eduardo Ros (Max-Planck-Institut für Radioastronomie, MPIfR), with contributions on the software from Ivan Marti-Vidal (Onsala Space Observatory, OSO) and Mark Kettenis (Joint Institute for VLBI in Europe, JIVE). These activities have resulted in VLBI with phased ALMA being offered in Cycle 4, with the first observations scheduled for March 2017.

The final receiver band originally planned for ALMA is Band 2 (67–90 GHz). This was discussed in detail at a specialised meeting held immediately before the workshop, and its conclusions were summarised by Robert Laing. Development is under way both at NRAO (where a prototype cartridge designed to meet the existing Band 2 specification is currently under test) and in Europe/Chile, where a consortium of the University of Manchester, the Science and Technology Facilities Council (STFC) Rutherford Appleton Laboaratory (RAL), Istituto Nazionale di Astrofisica (INAF) Osservatorio Astrofisico di Arcetri (OAA), INAF Istituto di Astrofisica Spaziale e Fisica Cosmica (IASF) Bologna, the University of Chile and ESO has taken the alternative approach of building a receiver designed to cover the wider frequency range between 67 and 116 GHz with an increased instantaneous bandwidth. Promising test results have been obtained by both groups for the optics and passive components and characterisation of optimised Monolithic Microwave Integrated Circuit (MMIC) amplifiers is eagerly anticipated.

New Developments

There were contributions on possible improvements to the higher-frequency receivers, which are based on superconductor-insulator-superconductor (SIS) technology, by Victor Belitsky (OSO/GARD), Andrey Baryshev (Netherlands Institute for Space Research, SRON) and Takafumi Kojima (NAOJ). Sideband separation for the two highest frequency bands (perhaps using digital techniques),

focal-plane arrays, ultra-wide-band receivers and high current density junctions are all promising approaches.

Wider instantaneous bandwidths require enhancements in digital electronics as well as new receivers. Options for faster digitisers and upgrade or replacement of the ALMA correlator were presented by Al Wootten, Benjamin Quertier (Université de Bordeaux) and Lewis Knee (National Research Council Canada, NRC), while Satoru Iguchi (NAOJ) showed plans for a spectrometer to deliver improved sensitivity, linearity and spectral dynamic range for total-power observing.

A wide variety of software upgrades was also presented, including a redesigned Observing Tool (Alan Bridger, UK Astronomy Technology Centre, UKATC), science archive development (Felix Stoehr, ESO; Sandra Burkutean and Marcella Massardi, INAF Istituto di Radioastronomia [IRA]), a new integrated alarm system (Maurizio Chavan, ESO) and high-performance computing for data reduction in CASA (Sandra Castro and Justo Gonzalez, ESO). Potential improvements in phase calibration were described by Remo Tilanus (Leiden University) and Anita Richards (University of Manchester). It was clear that phase correction using the water-vapour radiometers generally works very well, but that better could be done both in poor conditions (for example in the presence of clouds) and in the very best conditions, when the dry component of the atmosphere dominates.

ALMA and development of other facilities

The final part of the meeting concerned development at other millimetre and sub-millimetre facilities and its relevance to ALMA. Progress towards completion of the NOrthern Extended Millimeter Array (NOEMA) — which will be the most powerful mm array in the northern hemisphere — was presented by Frederic Gueth (Institut de Radioastronomie Millimétrique, IRAM). Several presentations discussed developments for single dishes, including the Atacama Submillimeter Telescope Experiment (ASTE), the Nobeyama 45-metre telescope, the descoped Cerro Chajnantor Atacama Telescope (CCAT) project and the Atacama Pathfinder EXplorer (APEX).

There is considerable interest (particularly from the ESO community) in a large survey telescope located either on the ALMA site or nearby at higher altitude. This would complement ALMA, in particular by providing a highly multiplexed survey capability. Leonardo Testi summarised the report of the ESO Single Dish Science Strategy Working Group, which had considered the options, concluding that a 40-metre class dish on the ALMA site with state-of-the-art cameras for line and continuum would be very productive in synergy with ALMA.

Conclusion

The concluding discussion at the workshop led to consensus on a number of general points. Firstly, ALMA needs a new set of top-level science requirements to replace the original version that successfully drove the construction of the array. This can then flow down to a new set of system-level technical requirements. Secondly, we need a rigorous analysis of current performance (including possible optimisations and failure rates) to act as a baseline for new developments: much of the quantitative system verification of ALMA was done when the array was incomplete. Finally, it was clear to everyone that there are far too many exciting technical possibilities to implement at once and that priorities will need to be set very carefully.

All of the presentations from the workshop are available on the workshop webpage[1].

Acknowledgements

We are grateful to GoCAS, Chalmers University (GARD, Onsala Space Observatory and the Nordic ARC Node) and ESO for financial and organisational support. We would particularly like to thank Emma Åberg, Sandra Johansson, Victor Belitsky, John Conway and Wouter Vlemmings for their help.

Links

[1] Workshop webpage: http://www.chalmers.se/en/centres/GoCAS/Events/ALMA-Developers-Workshop/Pages/Programme.aspx

P. Horálek/ESO

Some of the 50 ALMA 12-metre antennas in close configuration on the Chajnantor Plateau.

Fellows at ESO

Ruud Visser

Ruud Visser

Growing up in the densely populated Netherlands, with all of its light pollution and cloudy weather, I never had much of a clear view of the night sky as a kid. Perhaps that explains why I was never all that interested in astronomy in high school. I developed a liking for chemistry instead, and that is what I ended up studying at the Vrije Universiteit in Amsterdam.

A few years later, towards the end of my Bachelors programme, I attended a one-day symposium for chemistry students. One of the talks was on the topic of astrochemistry, where I learned that the Universe was filled with a lot more interesting stuff than stars, planets and the occasional black hole. There were molecules in space!

Although I was already set to do a Masters degree in theoretical chemistry, the notion of interstellar chemistry held such appeal that I wanted to learn more about it. I contacted the speaker, Ewine van Dishoeck from Leiden University, and she was kind enough to accept me into her group for a half-year research project as part of my Masters programme. I constructed a model of the chemistry of polycyclic aromatic hydrocarbons (PAHs) in circumstellar discs, which was used by a PhD student and a postdoc to analyse PAH observations from the Very Large Telescope (VLT) and the Spitzer Space Telescope.

After completing my Masters in Amsterdam, I returned to Leiden in September 2005 to start a PhD project on chemical evolution during low-mass star formation. My first task was to turn the research report from the PAH project into a paper for *Astronomy & Astrophysics*. During this time I accompanied another PhD student on an observing run with the VLT Imager and Spectrometer for mid-InfraRed (VISIR) on the VLT to gather more spectra of PAHs in discs. I barely had any idea what I was doing, but that just made the trip all the more useful as a hands-on introduction to astronomy. Needless to say, the night sky over Paranal was much more spectacular than anything I had ever seen back home.

The bulk of my PhD thesis work consisted of modelling the physical and chemical evolution of a molecular cloud core as it collapses to form a star and a circumstellar disc. At first I was interested only in the chemistry itself, and the physical model of a collapsing cloud merely formed the canvas onto which to paint my chemical picture. Soon, however, I began to appreciate the astrophysical aspects of this project. No longer did I feel like a chemist lost in space; I had become a proper astrochemist, and felt very much at home in an astronomy department.

Like most chemists and astronomers, I became part of an ever-growing number of international teams. My thesis project required only a small number of collaborators, but I got a taste of working in a bigger team through the “Cores to Disks” Spitzer Legacy Project. Telecons and team meetings became a part of everyday life.

Around the time that I finished my PhD, the Herschel Space Observatory started operations. I stayed in Leiden as a postdoc for one year to join Ewine’s Key Programme on water in protostars, giving me a taste of working in another team of many dozens of people spread all around the world. The first water spectra from Herschel showed booming lines in embedded protostars, but barely anything in circumstellar discs. Ancillary data on rotationally excited CO revealed widespread gas of a few hundred to a few thousand kelvins almost anywhere we looked. Frantically, the whole team got to work and cranked out a dozen letters for the *Astronomy & Astrophysics* special issue. The six months between receiving the first data and submitting the letters were as hectic as they were rewarding.

In early 2011, I moved to the University of Michigan in Ann Arbor (near Detroit) to continue working on the analysis of Herschel data and the development of my chemical models with Ted Bergin. I began to investigate the effects of luminosity outbursts from a young star on the chemical composition of the surrounding gas, eventually teaming up with researchers in Denmark to discover the first chemical evidence of such outbursts with the Atacama Millimeter/submillimeter Array (ALMA). The energy released during an outburst heats up the circumstellar gas and dust and some of that dust becomes too warm to hold on to its icy mantle, thus increasing the column densities of CO and other volatile species. This excess CO showed up as a serendipitous discovery in a collaborator’s ALMA observations. By now we have also seen excess CO in archival data from the Submillimeter Array (SMA), suggesting that luminosity bursts are a common event for embedded protostars.

When I moved to the US, some of my friends joked that I would get married there and never return. I did indeed get married in Ann Arbor, but still returned (to Europe, at least) when my wife and I both started ESO Fellowships in September 2014. The move to ESO provided an excellent opportunity to get hands-on experience with ALMA data. Although my own research continues to focus on computer simulations, I have benefitted greatly from discussions with ALMA experts at ESO on the observational tests and implications of my models.

My functional work, not surprisingly, takes place in ESO's ALMA group. I help with calibrating and imaging of newly taken ALMA data to ensure the observations meet certain quality criteria before delivery to the Principal Investigator. In April 2015, my duties took me to Llano de Chajnantor for two one-week shifts as astronomer on duty at ALMA. Working with this state-of-the-art facility was one of the high points of my career, both literally and figuratively.

People sometimes ask me if I think of myself as a chemist or an astronomer. The only possible answer is that I think of myself as an astrochemist, combining the best of both fields in an effort to unravel our own cosmic history. I may not have seen much of the stars as a kid, but trips to the VLT, ALMA, Mauna Kea and many other places around the world have more than made up for that. As I enter my third year as an ESO Fellow, I look forward to the opportunity to see more of the Universe and to explore the chemistry that takes place within it.

Linda Watson

In high school I enjoyed most of my classes without a strong preference for a particular subject. In retrospect, I see that my science and maths teachers helped me lay the foundations for my astronomy career. I am especially grateful to my Earth and Space Science teacher for devoting a couple weeks to astronomy and inspiring me to ask my first good astronomy question: are there stars between galaxies?

Linda Watson

I went to college at The University of Florida (UF), where I developed more of a science focus. I tried out classes in chemistry, engineering and physics. With the help of more fantastic teachers and mentors, I decided to major in astronomy and physics. The astronomy department at UF helped me test whether I wanted to pursue an astronomy career by allowing me to work with two professors on research projects, sending me to the Kitt Peak National Observatory to learn about observing and encouraging me to spend a summer doing research at another university.

I then went to graduate school at The Ohio State University (OSU). After studying the supermassive black holes at the centres of galaxies for a couple years, I studied the connection between gas and star formation in nearby galaxies for my thesis. I enjoyed working with data from across the electromagnetic spectrum, including optical, infrared, and radio wavelengths. I am not sure when the transition happened (first published paper? graduation?), but my mentors at OSU helped me to become an astronomer.

After receiving a PhD, astronomy encourages early-career scientists to work in short-term (2–3 year) postdoc positions, both so that newly-minted PhDs can develop more expertise and independence and because there are relatively few permanent astronomy positions. My first postdoc was at the Harvard-Smithsonian Center for Astrophysics. I worked for the Submillimeter Array (SMA), which I used to study the cold interstellar medium that contains molecules and dust and is the raw material out of which stars form.

I am now lucky to be at ESO in Chile for my second postdoc. I continue to study the cold interstellar medium and star formation in nearby galaxies. For my functional duties, I support the Atacama Large Millimeter/submillimeter Array (ALMA) by observing and processing data. I have especially enjoyed working with the telescope operators, engineers, computing experts, outreach coordinators, and astronomers that make ALMA the world-class facility that it is.

I have followed a relatively standard career path for an astronomer. However, I believe that science is better when the community has diverse backgrounds. So I look forward to continuing to work with curious and motivated individuals who have followed both standard and non-standard paths into astronomy.

Daniel Asmus

It is thanks to my father that I am now in the position to write this article about my career as a scientist. All his life he was very interested in nature and technology, in particular aeroplanes and flying. The conditions and times in which he grew up did not permit him to follow his curiosity and become a scientist himself. However, he made sure that I would have this possibility, and early on he taught me to how to understand, plan and realise things from scratch. One of my earliest memories in my childhood is of him showing me how to build a wall of LEGO bricks, with an interlocking pattern. Such a wall would be strong and would not collapse easily.

Daniel Asmus

In this spirit, I grew up with a big interest in natural sciences and technology in Bad Segeberg, a small (and boring) town in northern Germany. It turned out that I was also good at mathematics, although (even today) I am not very fond of it. As a child, I was interested in planets and space travel but it never occurred to me to use telescopes to look at the heavens, possibly because of the weather in northern Germany, or maybe because in my environment nobody knew about astronomy. It did not help either that during my school years there were too few kids interested in physics for it to be offered as a major subject in either of the high schools in town. Therefore, it was probably rather Star Wars that set the course for my path into science (fiction). While not necessarily the case today, at the age of seven it made a huge impression on me.

With only basic physics (but a major in maths), a short period of uncertainty occurred when it came to choose the career path after high school. A degree in marine engineering seemed to be the more solid choice but I was already an idealist at that time and therefore chose to study physics (at the University of Kiel). While I was struggling to understand quantum physics and thinking about a diploma thesis in dusty plasma physics (which certainly would have led me into industry), something very rare at German universities happened: a new astronomy professor arrived, and with him a new group. And they were working on black holes! Well, on accretion discs around them, but that was exciting enough for me to aim for a diploma with Wolfgang Duschl, the new professor. When I saw the rings of Saturn with my own eyes through a 15 inch telescope during a cold night on the roof top of the institute, all last doubts were extinguished, and the title of my diploma thesis became “The Inner Region of Accretion Disks around Black Holes”, a theoretical work.

Everything changed when I heard from a finishing PhD student in Wolfgang’s group about the possibility of a studentship at ESO in Chile. So I decided to abandon my hydrodynamical relaxation code and get some observing experience under the supervision of Alain Smette. Indeed, the experience started sooner than expected, namely with writing an ESO observing proposal! It had to be written even before starting the ESO studentship, while I was still part of a group of pure theoreticians. However, I was lucky: we were awarded B rank, and almost all the requested observations were executed. These observations of nearby active galactic nuclei (AGN) brought me into contact with the mid-infrared and the VLT Imager and Spectrometer for mid-InfraRed (VISIR) for the first time, the start of a long and continuing relationship, as it would turn out.

The ESO studentship in Chile was certainly one of the best experiences of my life. Not only did I experience Paranal and became an observational astronomer (although I never wanted to give up on simulations actually!), but also personally it was a mind-blowing experience. Therefore, it is probably not surprising that I returned as a Fellow to ESO Chile in 2014, after finishing my PhD on the subject of mid-infrared properties of local AGN at the University of Kiel in 2012, and a joyful two year postdoc at the Max Planck Institute in Bonn in Gerd Weigelt’s group, which led to the longest paper I will ever write (not recommendable).

My ESO fellowship started just in time to join the VISIR recommissioning activities in 2014 as instrument fellow. I enjoyed being part of the team a lot, giving me not only fundamental insights into VISIR and the observatory but also into working in (bigger) groups. When I am not working on VISIR, I am support astronomer at Unit Telescope 3 and I love to astonish visitors with the incredible adaptive optics performance of the Spectro-Polarimetric High-contrast Exoplanet REsearch instrument (SPHERE). Working in Paranal is a great experience, which I strongly recommend to (almost) everyone. I learned so much about all aspects of observational astronomy.

In my “free time”, I continue to research on active galactic nuclei and regularly meet with the fast growing community of AGN friends in Santiago. Furthermore, I am also one of two Fellow representatives in Chile.

For the future, I cannot wait to see the James Webb Space Telescope (JWST) fly and the European Extremely Large Telescope (E-ELT) being built. Both will have excellent mid-infrared instruments that I hope to be able to point into the hearts of our neighbouring galaxies to unveil the eating habits of the supermassive monsters lurking there.

ESO

European Organisation
for Astronomical
Research in the
Southern Hemisphere

ESO Studentship Programme 2016 — 2nd Call

The research studentship programme of the European Southern Observatory provides an outstanding opportunity for PhD students to experience the exciting scientific environment at one of the world's leading observatories for a period of up to two years.

ESO is the foremost intergovernmental astronomy organisation in Europe. Its approximately 110 staff astronomers, 40 Fellows and 50 PhD students conduct front-line research in fields ranging from exoplanets to cosmology, offering one of the most vibrant and stimulating scientific settings anywhere in the world.

ESO's studentship positions are open to students enrolled in a PhD programme in astronomy or related fields. Students accepted into the programme work on their doctoral project under the formal supervision of their home university, but they come to ESO to work and study under the co-supervision of an ESO staff astronomer, normally for a period of between one and two years. Studentships may be hosted either at ESO's Headquarters in Garching (Germany) or at ESO's offices in Santiago (Chile), where up to two positions per year are provided for students enrolled in South American universities.

Applicants and their home institute supervisors should agree upon and coordinate their research project jointly with their prospective ESO supervisor. For this purpose the ESO supervisor should be contacted well in advance of the application deadline (15 November 2016).

ESO Chile students have the opportunity to visit the observatories and to get involved in small technical projects aimed at giving insights into the observatory operations and instrumentation. Such involvement is also strongly encouraged for Garching students. In addition, students in Garching may attend and benefit from the series of lectures delivered in the framework of the International Max-Planck Research School on Astrophysics. ESO students are expected to contribute to the science life at ESO, participating in the activities promoted by the Offices for Science, including organisations of seminars and workshops, science gatherings, training sessions, outreach initiatives, etc.

Students who are already enrolled in a PhD programme in the Munich area and who wish to apply for an ESO studentship in Garching, should provide a compelling justification for their application.

If you are interested in enhancing your PhD experience through an extended stay at ESO, then please apply by completing the web application form available at: https://recruitment.eso.org

Please include the following documents in your application:
- a cover letter;
- a Curriculum Vitae, including a list of publications, if any;
- copies of your university transcript and certificate(s) or diploma(s);
- a summary of your master's thesis project (if applicable) and ongoing projects, indicating the title and the supervisor (maximum half a page);
- the names and contact details of your home institute supervisor and the ESO local supervisor. They will be automatically invited to submit a recommendation letter, however, applicants are strongly advised to trigger these invitations (using the web application form) well in advance of the application deadline;
- an outline of the PhD project, containing a clear timeline including the start and expected end dates of the PhD, the requested starting date and duration for the ESO studentship (recommended one page, maximum two). The candidate should highlight in the project description the advantages of coming to ESO;
- a letter from the home institute that: i) guarantees financial support (salary, health insurance and travel money) for the remaining PhD period after the termination of the ESO studentship; ii) indicates whether the prerequisites to obtain the PhD degree at the home institute have already been met.

All documents should be typed in English (but no translation is required for the certificates and diplomas).

There are two application rounds each year (May and November): the closing date for applications for this 2nd round is 15 November 2016. Review of the application documents, including the recommendation letters, will begin immediately. Incomplete or late applications will not be considered.

Candidates will be notified of the results of the selection process during December 2016. Studentships will normally begin between January and June 2017.

Further information

For more information about the studentship programme please see:
http://www.eso.org/sci/activities/FeSt-overview/ESOstudentship.html

For a list of current ESO staff and fellows, and their research interests, please see: http://www.eso.org/sci/activities/personnel.html

A list of PhD projects currently being offered by ESO staff can be found at:
http://www.eso.org/sci/activities/thesis-topics.html

Details on the employment conditions and benefits are available at:
http://www.eso.org/public/jobs/conditions/students/

For any additional questions, please contact:
For Garching: Eric Emsellem, Tel.: +49 89 32006914,
email: eric.emsellem@eso.org
For Chile: Claudio De Figueiredo Melo, Tel.: +56 2 4633032,
email: cmelo@eso.org

Although recruitment preference will be given to nationals of ESO Member States (Austria, Belgium, Brazil, the Czech Republic, Denmark, Finland, France, Germany, Italy, the Netherlands, Poland, Portugal, Spain, Sweden, Switzerland and United Kingdom), and, for Chile, to students enrolled in a South American university, no nationality is in principle excluded.

The post is equally open to suitably qualified female and male applicants.

Personnel Movements

Arrivals (1 July–30 September 2016)

Europe	
Bachmaier, Christine (DE)	Programme Assistant
Barr, David (UK)	Control Engineer
Cavaller Marquès, Lluís (ES)	Mechanical System Engineer
Circosta, Chiara (IT)	Student
Díaz Cano, Carlos (ES)	Software Test and Integration Engineer
Khan, Ahmed Mubashir (PK)	Software Test Engineer
Klitsch, Anne (DE)	Student
Kolwa, Sthabile Namakau (ZA)	Student
Lampater, Ulrich (DE)	Control Engineer
Milakovic, Dinko (HR)	Student
Palacio Valenzuela, Juan Carlos (CL)	Mechanical Construction Engineer
Peest, Peter Christian (DE)	Student
Turner, Owen James (UK)	Student
Williams, Andrew (UK)	International Relations Officer
Yen, Hsi-Wei (TW)	Fellow
Zuluaga Ramírez, Pablo (ES)	Mechanical Engineer

Chile	
Bolmer, Jan (DE)	Student
Desbordes, Christine (FR)	Head of Logistics Paranal
Herrero-Illana, Ruben (ES)	Fellow
Meister, Alexander (DE)	Optical Engineer
Messias, Hugo (PT)	Fellow
Pantoja, Blake (US)	Student
Rodler, Florian (AT)	Operation Staff Astronomer
Sánchez-Portal, Miguel (ES)	ALMA Deputy Program Manager
Vinet, Andrés (CL)	Head of IT Group Chile

Departures (1 July–30 September 2016)

Europe	
Alvarado Gomez, Julian David (CO)	Student
Arab Salmani, Maryam (IR)	Student
Baade, Dietrich (DE)	Deputy Director for Science
Berger, Jean-Philippe (FR)	VLTI Programme Scientist
Bonnefond, Sylvain (FR)	Student
Cabrera Ziri Castro, Ivan (VE)	Student
Deiries, Sebastian (DE)	Technician
Dhawan, Suhail (IN)	Student
Ginsburg, Adam (US)	Fellow
Gray, Peter Murray (AU)	Programme Engineer
Hess, Guy (FR)	Senior Mechanical Designer
Hubert, Georgette (DE)	Secretary/Assistant
Husemann, Bernd (DE)	Fellow
Krause, Anja (DE)	Student
Lavail, Alexis (FR)	Student
Madsen, Claus (DK)	Senior Advisor International Relations
Nicholson, Belinda Annette (AU)	Student
Patt, Ferdinand (DE)	Electronics Engineer
Tazzari, Marco (IT)	Student
Voggel, Karina Theresia (DE)	Student

Chile	
Aladro, Rebeca (ES)	Fellow
Carraro, Giovanni (IT)	Operation staff Astronomer
Gesswein, Rodrigo (CL)	Data Handling and System Administrator
Gutiérrez Avendaño, Claudia Patricia (CO)	Student
Kaminski, Tomasz (PL)	Fellow
Mueller, Andre (DE)	Fellow
Palacio, Juan Carlos (CL)	Mechnical Engineer
Sedaghati, Elyar (IR)	Student
Taylor, Matthew (CA)	Student

Left: Webcam view of recent construction progress on the ESO Supernova Planetarium & Visitor Centre (http://supernova.eso.org/), due to open in late 2017.

Following two page spread: A spectacular and informative wide-field (39 × 27 degree) image of the Magellanic Cloud System taken by small robotic telescopes at the La Silla Observatory with a Baader Luminance filter (passband 4000–7500 Å). The Large Magellanic Cloud (LMC) is located towards the upper left (north-east) and the Small Magellanic Cloud (SMC) to the lower right (south-west), with the Milky Way globular cluster 47 Tucanae just west of the SMC; tidal interactions between the Magellanic Clouds are evident. Colour images of the LMC and SMC have been inserted for reference. Full details are presented in Besla et al. 2016 (ApJ, 825, 20); see also Picture of the Week potw1630. Credit: Y. Beletsky (LCO), D. Martinez-Delgado/ESO

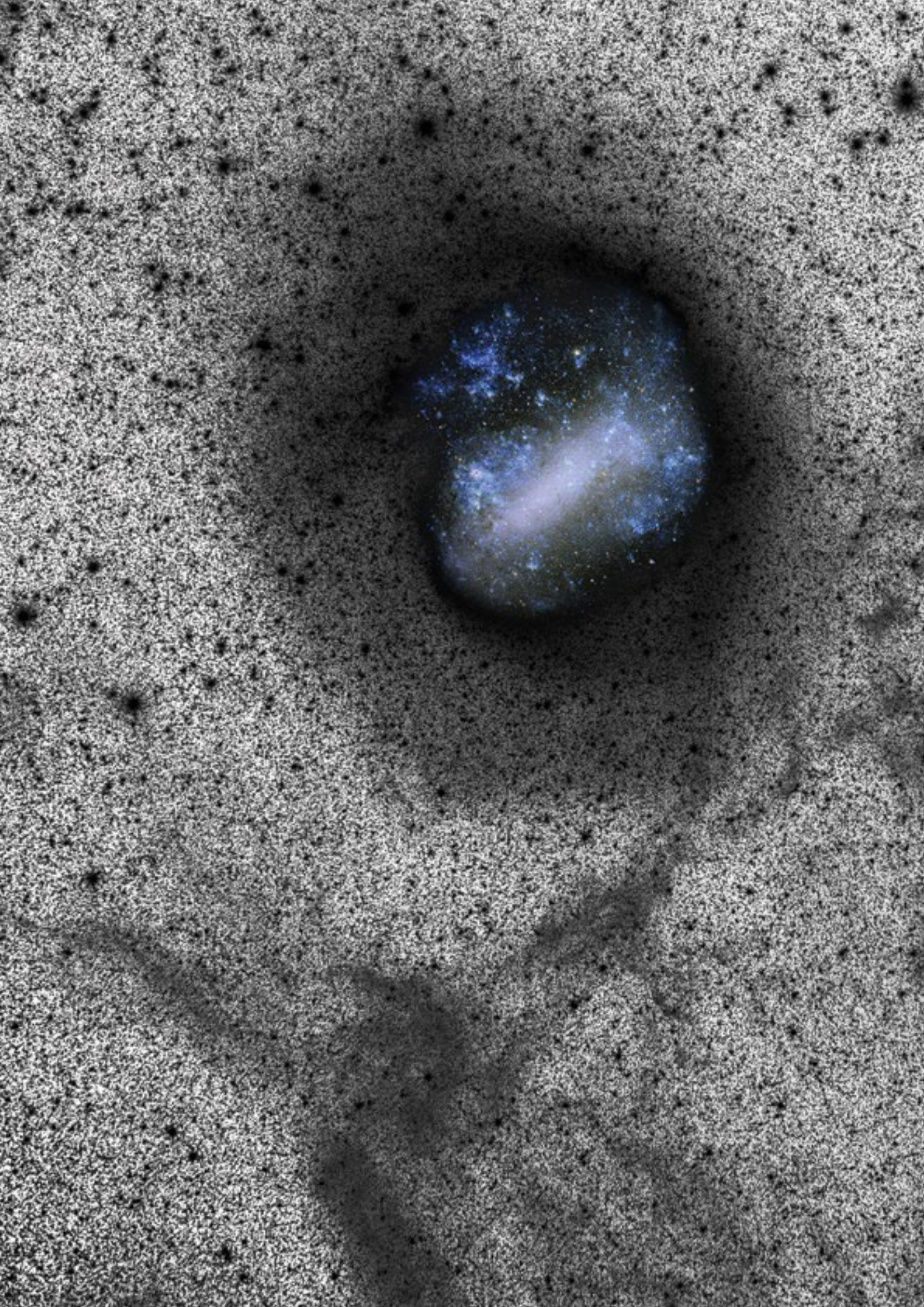

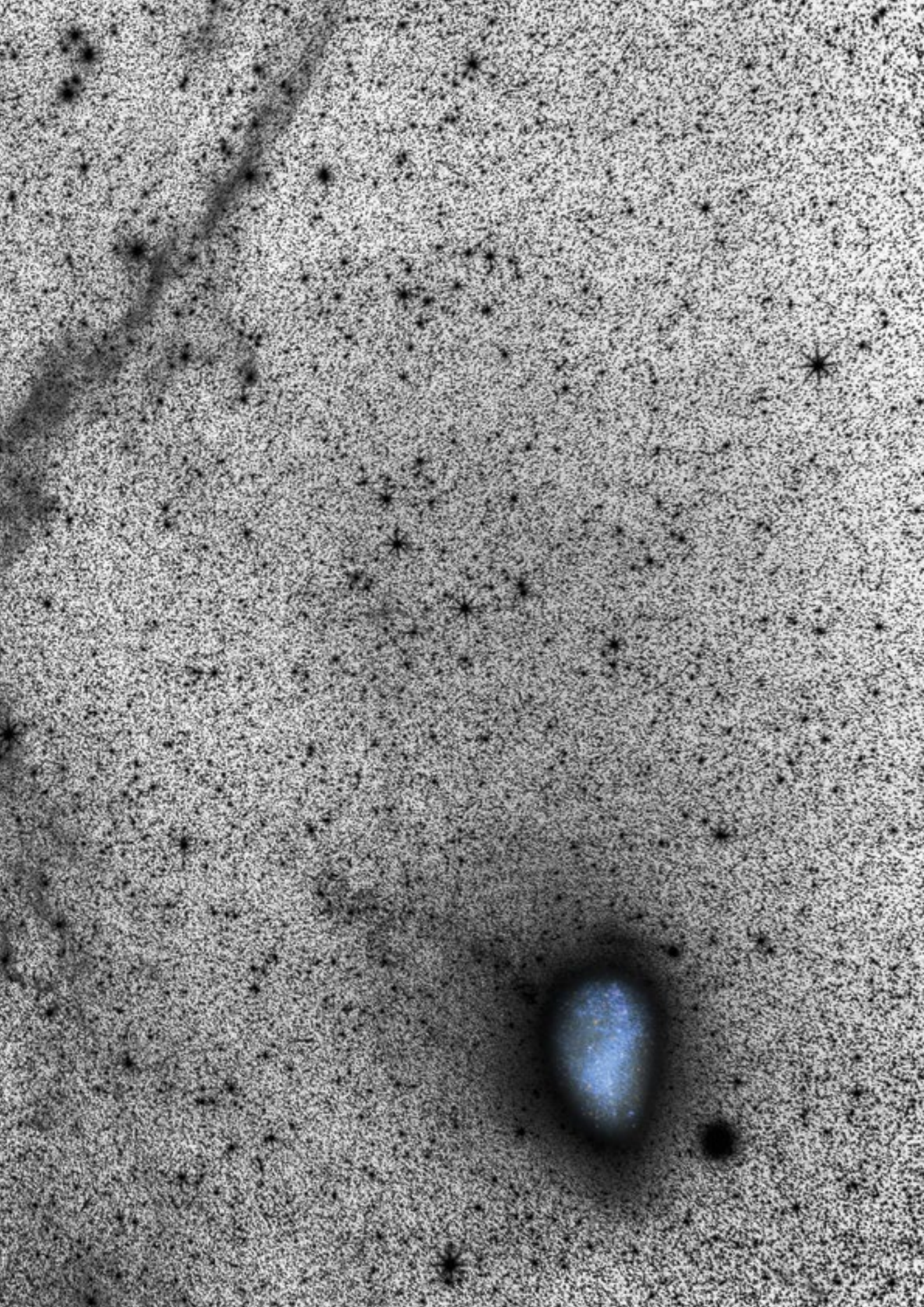

ESO, the European Southern Observatory, is the foremost intergovernmental astronomy organisation in Europe. It is supported by 16 countries: Austria, Belgium, Brazil, the Czech Republic, Denmark, France, Finland, Germany, Italy, the Netherlands, Poland, Portugal, Spain, Sweden, Switzerland and the United Kingdom. ESO's programme is focused on the design, construction and operation of powerful ground-based observing facilities. ESO operates three observatories in Chile: at La Silla, at Paranal, site of the Very Large Telescope, and at Llano de Chajnantor. ESO is the European partner in the Atacama Large Millimeter/submillimeter Array (ALMA). Currently ESO is engaged in the construction of the European Extremely Large Telescope.

The Messenger is published, in hard-copy and electronic form, four times a year: in March, June, September and December. ESO produces and distributes a wide variety of media connected to its activities. For further information, including postal subscription to The Messenger, contact the ESO education and Public Outreach Department at:

ESO Headquarters
Karl-Schwarzschild-Straße 2
85748 Garching bei München, Germany
Phone +49 89 320 06-0
information@eso.org

The Messenger:
Editor: Jeremy R. Walsh;
Design, Production: Jutta Boxheimer;
Layout, Typesetting: Mafalda Martins;
Graphics: Joanna Law.
www.eso.org/messenger/

Printed by FIBO Druck und Verlags GmbH, Fichtenstraße 8, 82061 Neuried, Germany

ISSN 0722-6691

Contents

Front cover: Deep near-infrared (*J*-, *H*- and *Ks*-band composite) colour image of the Orion Nebula Cluster (M43 and M42) taken with the High Acuity Wide field *K*-band Imager (HAWK-I). The image has size 14 by 19 arcminutes (1.7 × 2.3 pc for a distance of 414 pc). The HAWK-I imaging led to the detection of many faint brown dwarfs and isolated planetary mass objects, described in Drass et al. (MNRAS, 461, 1734, 2016), and providing important evidence for bimodality at the low mass end of the initial mass function. See Release eso1625 for details. Credit: ESO/H. Drass et al.